2013

Preparation and evaluation of oil-in-water self-nanoemulsifying systems with potential for pulmonary delivery

Ashish Kalra
The University of Toledo

A Thesis

entitled

Preparation and Evaluation of Oil-in-Water Self-Nanoemulsifying Systems with Potential for Pulmonary Delivery

by

Ashish Kalra

Submitted to the Graduate Faculty as partial fulfillment of the requirements for the Master of Science Degree in Pharmaceutical Sciences with Industrial Pharmacy Option

_____
Jerry Nesamony, Ph.D., Committee Chair

_____
Sai Hanuman Sagar Boddu, Ph.D.,
Committee Member

_____
Surya M. Nauli, Ph.D., Committee Member

_____
Patricia R. Komuniecki, Dean
College of Graduate Studies

The University of Toledo

May 2013

An Abstract of

Preparation and Evaluation of Oil-in-Water Self-Nanoemulsifying Systems with Potential for Pulmonary Delivery

by

Ashish Kalra

Submitted to the Graduate Faculty as partial fulfillment of the requirements for the Master of Science Degree in Pharmaceutical Sciences with Industrial Pharmacy Option

The University of Toledo
May 2013

Self-Nanoemulsifying Drug Delivery Systems (SNEDDS) are mixtures of oil, surfactant and cosolvent/cosurfactant, which emulsify under conditions of gentle agitation. SNEDDS can drastically improve absorption of poorly water soluble drugs by keeping it in solubilized form at the site of absorption. The objective of the study was to develop a formulation to increase the solubility of poorly water soluble drugs and carbamazepine was selected as a model drug. The solubility of carbamazepine was tested in the formulation components. Formulation development and screening of oil-in-water nanoemulsions was done based on results obtained from an evaluation of self-emulsification time, phase diagram domains, and characteristics of resultant nanoemulsions. The optimized formulation was found to contain Cremophor RH 40 as the surfactant, PEG 400 as the co-surfactant and Labrafil M 2125 CS as the oil.

Oil-in-water nanoemulsions were evaluated for clarity, precipitation, zeta potential, and droplet size distribution. Nanoemulsions were characterized using dynamic light

scattering, electrophoretic light scattering, transmission electron microscopy and differential scanning calorimetry. The droplet size analysis was done using Dynamic Light Scattering (DLS) and Transmission Electron Microscopy (TEM). Nanoemulsions were nebulized into a mist using a commercial pediatric nebulizer and characterized using laser diffraction and transmission electron microscopy (TEM). An aseptic method was developed and validated for preparing sterile SNEDDS. The biocompatibility of the formulation was evaluated on NIH3T3 cell lines using MTT assay. SNEDDS were also loaded with a fluorescent dye (Sudan IV) in order to study its permeation characteristic through porcine lung tissue using histological analysis.

Nanoemulsions showed a droplet size of less than 20 nm with a neutral zeta potential. Nebulized SNEDDS were able to retain the physiochemical properties of liquid SNEDDS. The mist showed a droplet size of less than 5 μm. Sterility testing and cell toxicity results validated that the method is capable of formulating microorganism free nanoemulsion that was biocompatible. In vitro permeability tests indicated penetration of oil droplets intracellularly through biological membranes.

Thus SNEDDS developed in this study demonstrated good stability and has the potential to deliver poorly water soluble drugs.

Acknowledgements

I would like to thank Dr. Jerry Nesamony for providing me an opportunity to be a part of his research group and for his mentoring and guidance throughout these past two years of my research. He provided me with the resources that allowed me to succeed in this Masters program, while always encouraging me to think innovatively. I would like to thank Dr Sai Boddu for providing me with continuous guidance and suggestions and for being part of my defense committee.

I thank Dr. Curtis Black and Dr. Kenneth Alexander for providing me a wonderful TA experience in their labs. I thank Dr. Surya Nauli and Maki for their help with histological analysis and for being member on my thesis committee. I thank Dr. Rose Jung for helping me with sterility testing. I thank Dr. Joseph Lawrence at CMSC, UT for his help with the DSC and SEM. I would also like to thank Dr Andrew Ditto for his assistance with my research. I thank Dr Sanko Nguyen for helping me with thesis writing.

I would also like to thank my fellow labmates and classmates for their continuous support and providing me with some wonderful memories.

Finally, I thank my family and friends for their encouragement and support.

Table of Contents

List of Tables

List of Figures

List of Abbreviations

ANOVA – Analysis of Variance

BCS – Biopharmaceutical Classification System

CBZ – Carbamazepine

CFU – Colony Forming Unit

DAPI – 4',6-Diamidino-2-phenylindole

DI Water– De-ionized Water

DLS – Dynamic Light Scattering

DMEM – Dulbecco's Modified Eagle Medium

DMSO – Dimethyl Sulfoxide

DNA – Deoxyribonucleic Acid

DPIs – Dry Powder Inhalers

DSC – Differential Scanning Calorimetry

EDTA – Ethylenediaminetetraacetic Acid

ELS – Electrophoretic Light Scattering

FBS – Fetal Bovine Serum

FDA – Food and Drug Administration

FTM – Fluid Thioglycollate Medium

GRAS – Generally Regarded As Safe

He-Ne – Helium-Neon

HLB – Hydrophile-Lipophile Balance

HPLC – High Performance Liquid Chromatography

IR – Infra-Red

LD_{50} – Lethal Dose causing death in 50% of test animals

MDIs – Metered Dose Inhalers

MH Agar – Müller-Hinton Agar

MS – Mass Spectroscopy

MTT – (3-(4, 5-Dimethylthiazol-2-yl)-2,5-diphenyltetrazolium bromide

NMR – Nuclear Magnetic Resonance

O/W – Oil-in-Water

OCT – Optimal Cutting Temperature

PBS – Phosphate Buffered Saline

PDA – Photodiode Array

PEG – Polyethylene Glycol

P-gP – P-Glycoprotein

QELS – Quasi-Elastic Light Scattering

RT – Respiratory Tract

SCD – Soybean Casein Digest

SEDDS – Self-Emulsifying Drug Delivery System

SME – Self-Nanoemulsifying

SNEDDS – Self-Nanoemulsifying Drug Delivery System

TE – Transmission Electron

TEM – Transmission Electron Microscope

UV-Vis – Ultraviolet-Visible

W/O – Water-in-Oil

Chapter 1 – Introduction

The field of drug discovery is rapidly expanding with the increasing availability of newer drug molecules. In recent years, most of the drug molecule synthesis has been based on receptor structural characteristics. This receptor guided synthesis has regularly resulted in development of polycyclic compounds which are usually hydrophobic. These large molecular weight compounds present formulators with marked formulation challenges with their slow dissolution rates. To solve this problem, formulators have started using lipid excipients to solubilize the drugs prior to administration.

1.1 Lipid based drug delivery systems

Lipid based drug delivery system is a broad field and allows for the formulation of drug in a variety of different forms. Formulation of a drug in a lipid based delivery system can be in the form of a simple solution, suspension, emulsion, nanoemulsion, self-emulsifying drug delivery system (SEDDS) or dry emulsion. The success of a lipid based drug delivery system revolves around the selection of appropriate vehicles and a logical design of the delivery system. According to the biopharmaceutical classification system (BCS), poorly water soluble drugs are classified either under class II (high permeability,

low solubility) or class IV (low permeability and solubility). Lipid based delivery systems often involves solubility enhancement of class II drugs where drug bioavailability is governed by dissolution properties [1]. Lipid formulations may contain mono-, di- and triglycerides, lipophilic surfactants, hydrophilic surfactants and cosurfactants or cosolvents. Table 1.1 shows a broad classification of lipid systems along with their compositions and characteristics [2].

Table 1.1: Classification of lipid based drug delivery systems

TYPE I		
Excipients	**% (w/w)**	**Characteristics**
Oils	100	Non-dispersing
TYPE II		
Excipients	**% (w/w)**	**Characteristics**
Oils	40-80	SEDDS without water-soluble components
Water-insoluble surfactants (HLB<12)	20-60	
TYPE III A		
Excipients	**% (w/w)**	**Characteristics**
Oil	40-80	SEDDS/SNEDDS with water-soluble components
Water-soluble surfactants (HLB>12)	20-40	
Hydrophilic cosolvents	0-40	
TYPE III B		
Excipients	**% (w/w)**	**Characteristics**
Oil	<20	SNEDDS with water-soluble components and low oil content
Water-soluble surfactants (HLB>12)	20-50	
Hydrophilic cosolvents	20-50	

TYPE IV		
Excipients	**% (w/w)**	**Characteristics**
Water-insoluble surfactants (HLB<12)	0-20	Oil-free formulation based on surfactants and cosolvents
Water-soluble surfactants (HLB>12)	30-80	
Hydrophilic cosolvents	0-50	

1.2 Self-emulsifying/nanoemulsifying drug delivery systems (SEDDS/SNEDDS)

SEDDS are mixtures of oil, surfactant and cosolvent/cosurfactant, which emulsify or nanoemulsify (SNEDDS) under conditions of gentle agitation as provided by digestive motility of the stomach and intestine [3]. The difference between emulsions and nanoemulsions is that emulsions may exhibit excellent kinetic stability but they are thermodynamically unstable and will eventually phase separate, unlike nanoemulsion which are thermodynamically stable. Another difference can be seen in their appearance as emulsions are cloudy while nanoemulsions are clear or translucent [4].

SEDDS and SNEDDS can be differentiated based on the droplet size. SEDDS having droplet size less than 100 nm are termed as SNEDDS. Hydrophobic drugs can be dissolved in SEDDS and be delivered in a variety of dosage forms. SNEDDS when dispersed in water or other bodily fluids inside the body, forms droplets of nearly the same size range as those observed in nanoemulsion systems. After getting dispersed these systems behave *in vivo* like oil-in-water (O/W) nanoemulsions. The hydrophobic drug remains in solution throughout its transit across the body and the dissolution step, which

is the rate limiting step in the absorption of such drugs, can be bypassed. SEDDS promote drug solubilization and drug release at the absorption site providing more consistent absorption of the hydrophobic drug and hence better bioavailability [3]. Figure 1-1 shows the three types of nanoemulsions that can be encountered depending on their composition.

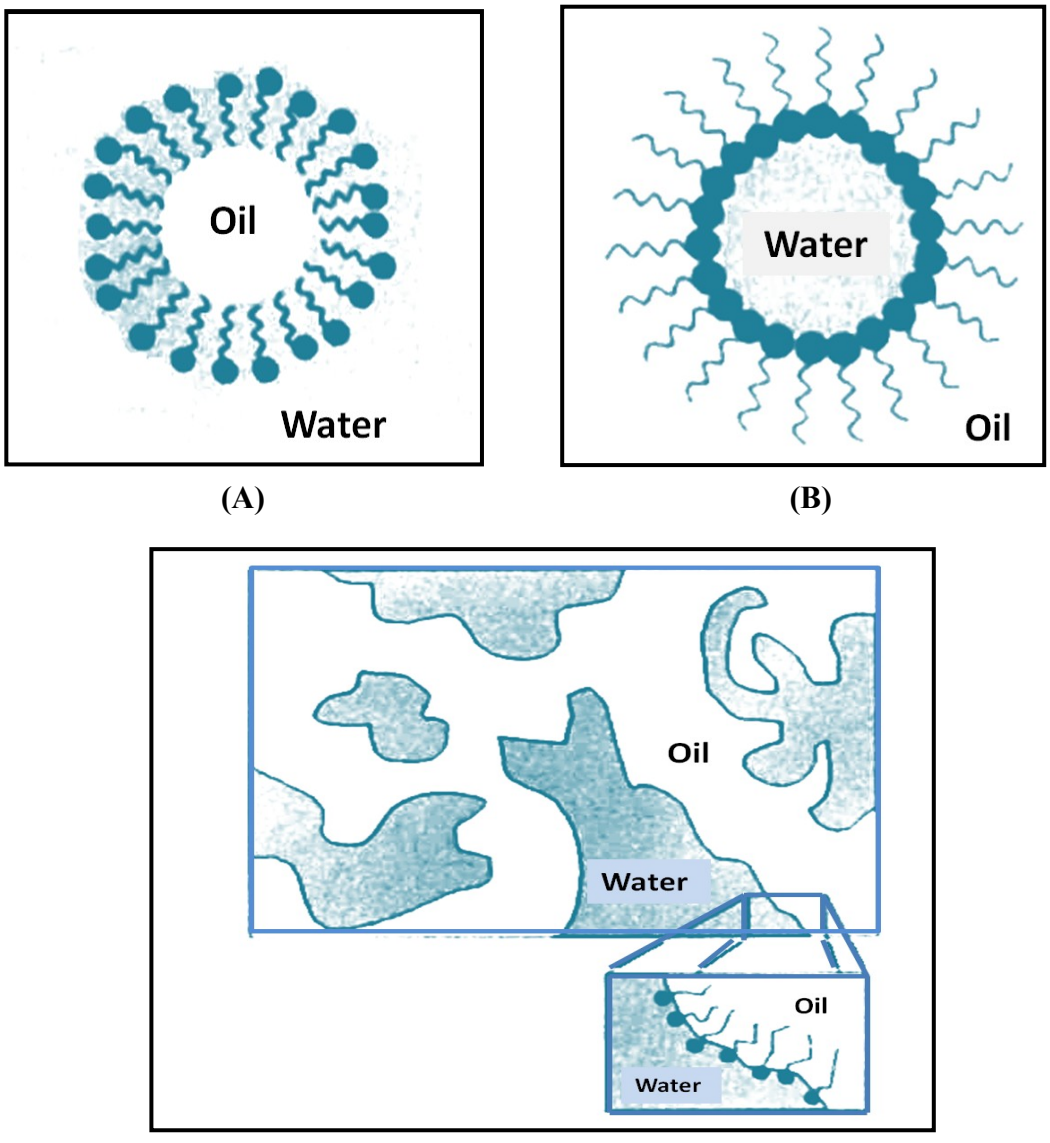

Figure 1-1: Schematic illustration of three types of nanoemulsions: (A) oil in water (B) water in oil and (C) bicontinuous nanoemulsion

Although all three structures are quite different, an interfacial surfactant monolayer separating the oil and water can be seen in all of them. O/W nanoemulsion droplets will be present in a nanoemulsion system having low oil fraction while water-in-oil (W/O) droplets are likely to be present in a nanoemulsion with low water fraction. The bicontinuous nanoemulsion may result when water and oil fractions are similar rendering a continuously fluctuating surfactant stabilized interface [5].

1.3 Theory of nanoemulsion formulation

Many theories have been proposed for nanoemulsion formulation with the three most common theories being: interfacial film theory [6], solubilization theory [7] and thermodynamic treatment theory [8]. The thermodynamic theory is the most accepted theory and is discussed in detail. According to the thermodynamic rationalization free energy of nanoemulsion formation can depend on the extent to which surfactant lowers surface tension of the oil-water interface and the change in entropy of the nanoemulsion system according to Equation 1.1

$$\Delta G_f = \gamma \Delta A - T \Delta S \qquad \text{(Equation 1.1)}$$

where, ΔG_f is the free energy of formation, γ is the surface tension of the oil-water interface, ΔA is the change in interfacial area on nanoemulsification, ΔS is the change in entropy of the system or dispersion entropy, and T is the temperature. In case of nanoemulsions, ΔA is very large due to the large number of small droplets present. γ is

very small positive value and is offset by the entropic component. The mixing of one phase with the other in the form of large number of small droplets results in very large value for dispersion entropy (ΔS). Other favorable entropic contributions are also present arising from processes like surfactant diffusion in the interfacial layer. Hence, a negative free energy of formation is seen when large reductions in surface tension are coexistent with significant favorable entropic changes, leading to a spontaneous and thermodynamically stable nanoemulsification [5].

1.4 Excipient selection

Excipient selection is normally based on the application of the nanoemulsion along with toxicity considerations. The formulation of W/O or O/W nanoemulsion usually involves a combination of three or more components which are, oil, water, surfactant, cosurfactant and electrolyte [9]. Whether the formation will result in a W/O or O/W nanoemulsion is dependent on the properties of the oil and surfactant along with the oil-to-water ratios. Hydrophile-lipophile blanace (HLB) is a very useful tool in selecting surfactants for nanoemulsions [10]. HLB values for ionic surfactants normally ranges from 20-45, while for non-ionic surfactants the values are usually lower (1-20). The HLB range for surfactants forming W/O nanoemulsion is 3-8, while for those forming O/W nanoemulsion is from 8-18. Non-ionic surfactants are generally considered more suitable for pharmaceutical applications as they are less affected by pH and ionic changes. In addition, they are generally less toxic [11].

Normally, water soluble cosolvents/cosurfactants are used to formulate nanoemulsions. Cosurfactants are usually alcoholic by nature and help to dissolve large quantities of hydrophilic surfactant in the oil and increse the solvent capacity of the drug. They can also enhance the stability of nanoemulsion by squeezing themselves between the surfactant molecules. Some of the commonly used cosurfactants include: polyethylene glycol (PEG), glycerol and propylene glycol.

The oil play an important role in successful formulation of drug loaded SNEDDS as they are responsible for solubilization of the lipophilic drug. Furthermore, they can increase the lymphatic transport of the drug *in vivo*, thus, increasing drug bioavailability [12]. Medium-chain glycerides derived from coconut oil are of particular interest in formulating orally active nanoemulsions as they are food grade products. Table 1.2 shows some of the commonly used oils in the formulation of SNEDDS.

Table 1.2: Oils used in SEDDS/SNEDDS formulation

Type of oil	**Examples**
Triglyceride vegetable oils	olive oil, soybean oil
Vegetable oils derivatives	Cutina HR, Lubritab®
Mixed partial glycerides	Capmul MCM, Peceol
Polyoxyglycerides	Labrafil 1944CS, Labrafil M 2125 CS
Ethoxylated glycerides	Cremophor RH40, Cremophor EL
Polyalcohol esters of fatty acids	Capryol, Mirj

1.5 Drug incorporation

In order to select a suitable nanoemulsion system for drug solubilization and delivery, preformulation work, such as drug solubility characteristics and oil/water partition, is required [13]. To design an efficient nanoemulsion system for a specific drug, computational modeling along with physiochemical studies of the drug and the nanoemulsion systems are often necessary. In case of O/W nanoemulsions, the drug is solubilized in the oil and the oil-surfactant blend, while in W/O nanoemulsions the drug is solubilized in the aqueous phase. The amount of drug that can be incorporated into a given nanoemulsion system depends on its solubility in various components which is governed by oil/water partition coefficient or log P values. All the necessary physiochemical parameters of the nanoemulsion system should be re-evaluated after drug incorporation. If the drug itself is surface active, it can significantly affect the nanoemulsion properties [9]. Table 1.3 lists the various BCS classes along with the appropriate nanoemulsion system and the respective benefits.

Table 1.3: BCS classes of drug along with suggested nanoemulsion systems and their benefits [9, 14]

BCS Class	Aqueous Solubility	Membrane Permeability	Type of Nanoemulsion System	Drug Delivery Benefits
I	High	High	W/O	Stabilization and hydrolysis protection
II	Low	High	SEDDS, O/W	Improved solubilization/dissolution and increased bioavailability
III	High	Low	W/O	Stabilization, hydrolysis protection and increased bioavailability
IV	Low	Low	SEDDS, O/W	Improved solubilization/dissolution and increased bioavailability

1.6 Pulmonary delivery

Pulmonary delivery, as an alternative route of administration for systemic action of drugs, has attracted much attention due to the growing emphasis on improving the quality of the patient's life as it offers a non-invasive route for drug delivery. Lungs possess a well developed vascular system together with extremely thin walled alveolus. The major advantages it offers over oral route is the relatively low activity of drug-metabolizing enzymes and the avoidance of first pass metabolism [15]. In addition, lungs provide an extremely large area for drug absorption making mucosal permeation of drug molecule relatively easy. Rapid drug absorption in the lungs permit systemic delivery through this route possible [16].

1.6.1 Mechanism of drug absorption through lungs

Airborne drug particles enter the lung via the trachea and travels through a branching system of airways comprising of bronchi and bronchioles leading to the alveoli [17]. Figure 1-2 shows the anatomy of the human lung. The airways are covered with 30-40μm thick columnar epithelium, roughly similar to that of the nose and GI tract, and is virtually impermeable to large molecules like proteins. Although it is easy for air to flow to the alveoli, the branched airway acts like an impaction filter for inhaled particles. The particle size is, thus, a major factor in the delivery of drugs to the lungs [18]. The alveoli

are in such close contact with blood capillaries that they provide an absorption surface area of 50 to 100 m^2 [19].

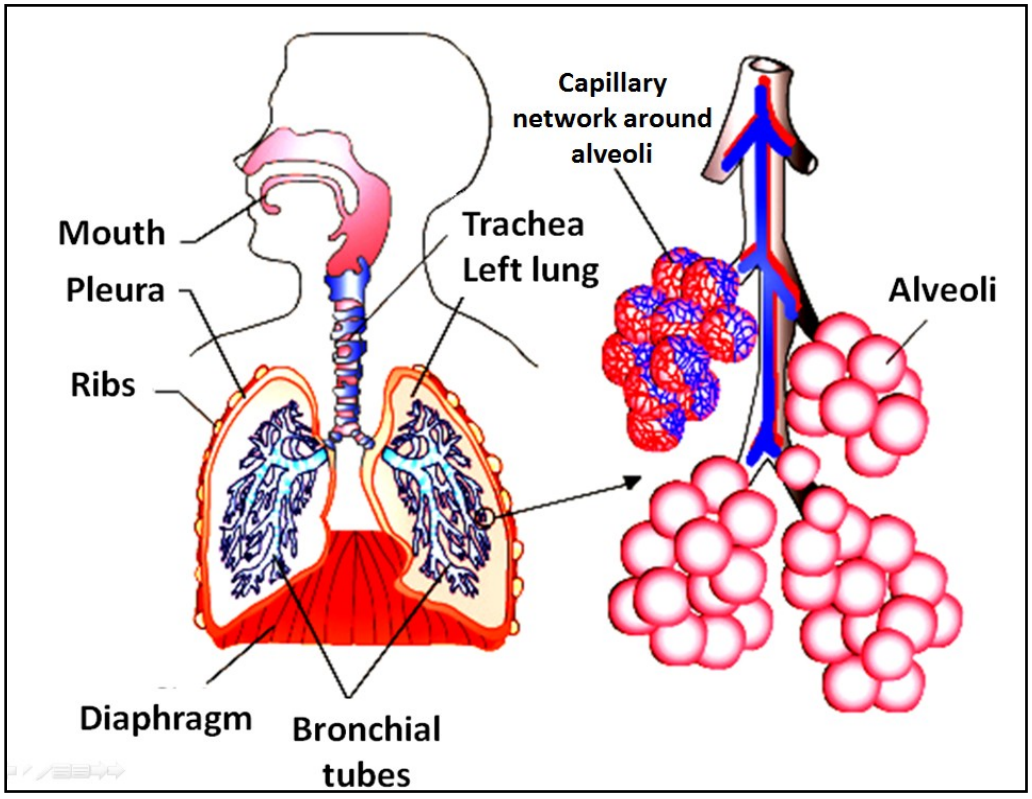

Figure 1-2: Anatomy of the human lung showing vascularity of the alveoli [20]

Apart from drug diffusion through the alveoli, drug absorption can occur through aqueous pores, by carrier-mediated transport and phagocytosis of the insoluble particles. The lung pH of 5.7 – 7.5 makes drug delivery of acid labile compounds possible [21].

The site and efficiency of deposition of particles in the respiratory tract (RT) is governed by particle size (aerodynamic diameter) and size distribution, their shape and density

[22]. The maximum alveolar deposition occurs with particles of diameter 1.5 to 2.5μm with breath holding and 2.5 to 4μm without breath holding [23].

The deposition of aerosolized drug in the RT involves processes like inertial impaction, sedimentation and diffusion [24]. The inertial impaction is responsible for the deposition of particles of around 5μm in the upper airways. Particles larger than 5μm cannot travel beyond upper airways. Particles of size ≤ 3μm undergo sedimentation under gravity and deposit in the lower airways. Longer residence time combined with low velocities in the lower airways favors the deposition of sub-micron sized particles by the process of diffusion. The efficiency of deposition to RT is also dependent upon breathing pattern, the depth of inhalation and the degree of pulmonary disease. The retention of drug particles in the lung is influenced by clearance by the host-defense mechanism [25].

1.6.2 Pulmonary drug delivery devices

The overal goal of pulmonary drug delivery devices is to offer greater control and reproducibility over pharmacological and therapeutic actions. It has been proved that appropriate selection of drug delivery device can increase the delivery to lungs by up to 90% [26]. There are a variety of pharmaceutical inhalation devices available today for the delivery to the RT. These devices can be divided into three major categories: nebulizer inhalers, metered dose inhalers (MDIs) and dry powder inhalers. Nebulizers are further classified into two types based on the method of production of the aerosol/mist: air jet

nebulizers and ultrasonic nebulizers. The air jet nebulizers produce a stream of high velocity air to convert the liquid into a mist while ultrasonic nebulizers utilize high frequency vibrations to form the mist. A schematic illustration of an air jet type nebulizer is shown in Figure 1-3

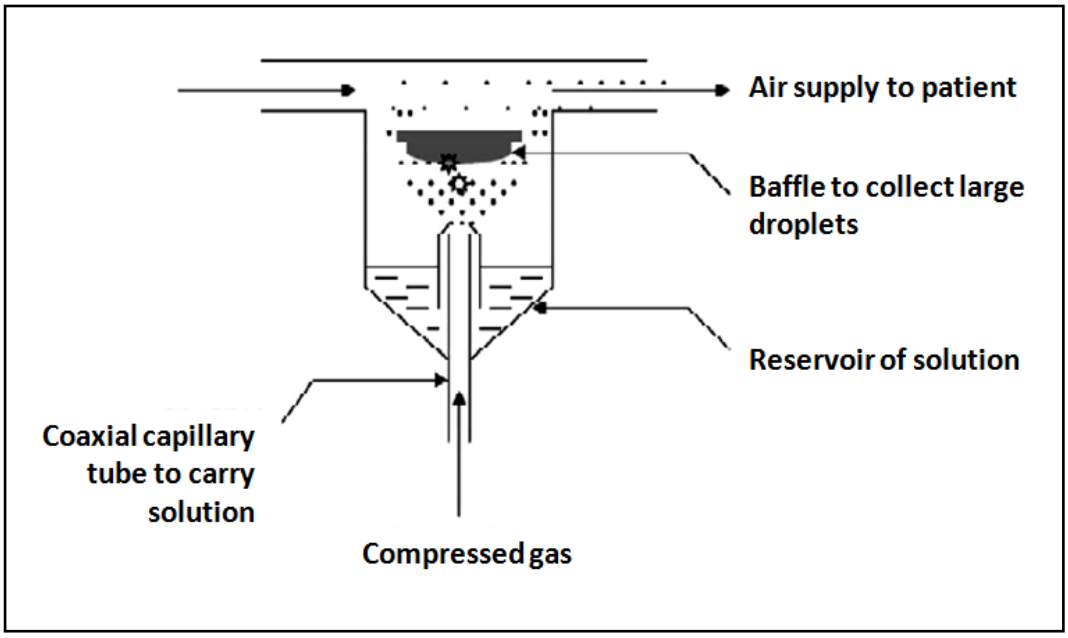

Figure 1-3 Schematic illustration of an air jet type nebulizer [27]

The major advantage offered by nebulizers over other inhalation devices is the production of very small sized droplets which can easily penetrate the small airways [25]. Figure 1-4 shows the difference in deposition of particles by MDIs and nebulizers.

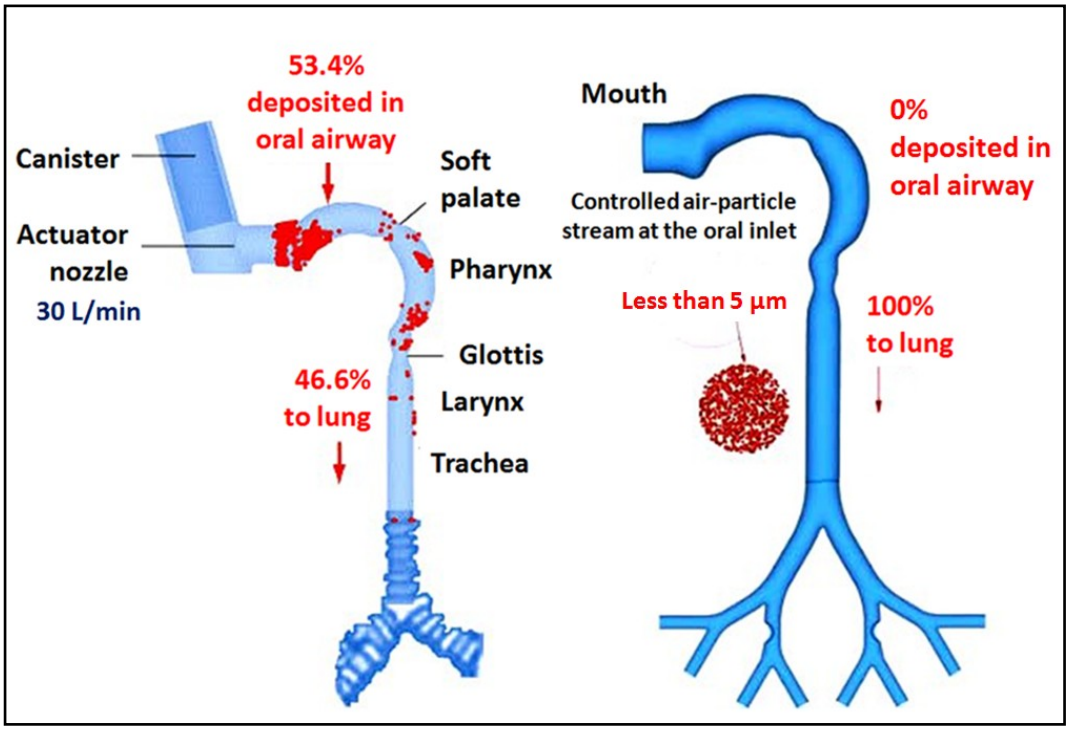

Figure 1-4: The deposition of particles by MDIs and nebulizers: (left) incomplete delivery to lungs by a MDI, (right) 100% delivery to the lungs achieved by a nebulizer system [28].

MDIs represent traditional pharmaceutical aerosols, comprising of formulation packed under pressure with a propellant. Their operation is controlled in a way that pre-determined volume of liquid is discharged per actuation. A schematic illustration of a MDI is shown in Figure 1-5.

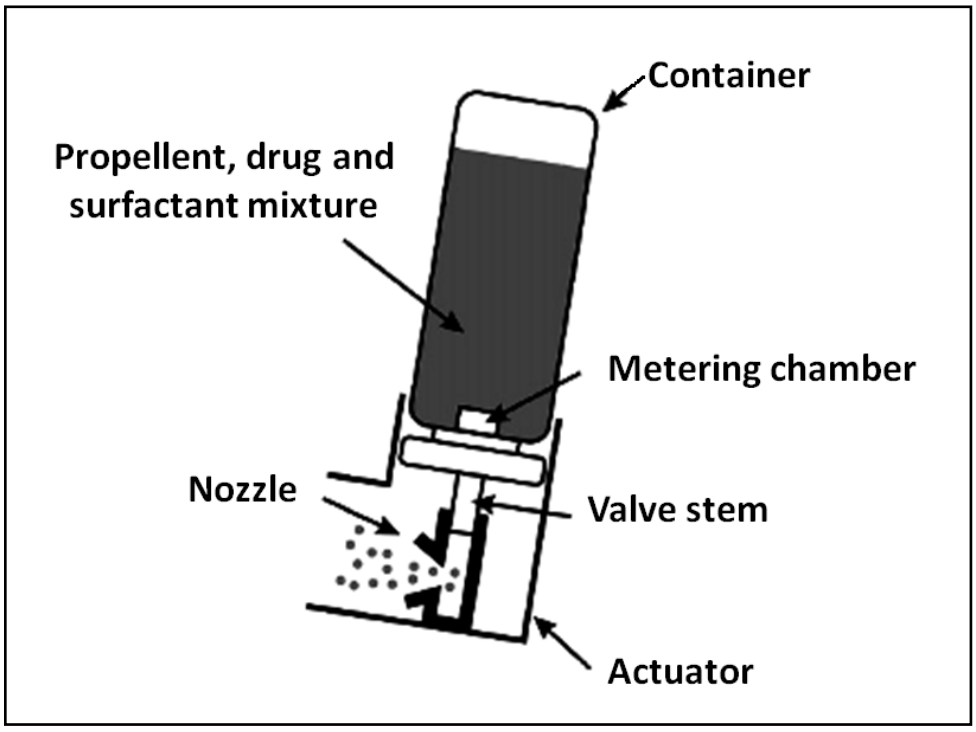

Figure 1-5 Schematic illustration of a metered dose inhaler(MDI) [29]

An improved variant of MDIs is the breath-actuated MDI known as the Autohaler®. Autohalers® are similar to normal MDIs except the that their dose delivery is triggered by user's breathing cycle [25].

Dry powder inhalers (DPIs) were the next addition to the RT drug delivery devices. The DPIs provide a reservoir of free flowing powder which is taken up by the patient's inspiratory air-stream. Figure 1-6 shows a schematic illustration of a DPI.

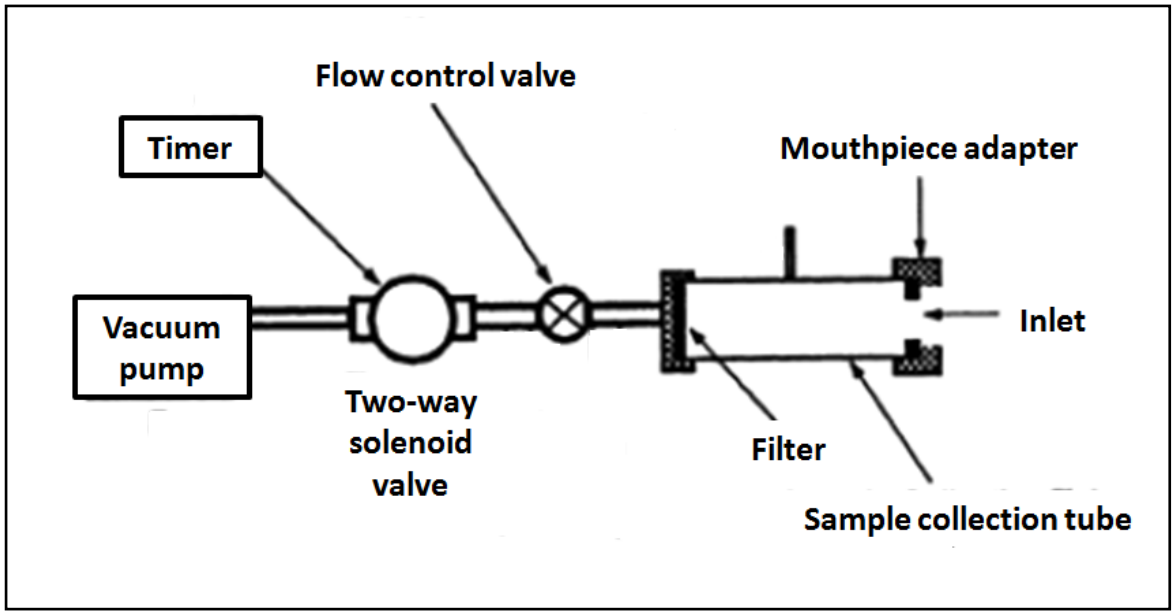

Figure 1-6: Schematic illustration of a dry powder inhaler (DPI) [30]

The next advancement in DPI technology was Spinhaler®, first introduced in 1970s [31]. Spinhaler® contains the drug inside a capsule which is pierced prior to delivery. When the patient inhales, the propeller blades rotate which in turn rotates the capsule, projecting the drug particles centrifugally into the air-stream. One the most sophisticated DPI currently in market is the Turbuhaler® which can meter a known quantity of terbutaline sulfate [32].

The goal of the current research was to develop a formulation to increase the solubility of poorly water soluble drugs. Various lipid excipients were tested and a SNEDDS formulation was formulated and optimized. The optimized liquid SNEDDS was nebulized to check its potential for pulmonary delivery and its permeation characteristics were studied through a porcine lung tissue.

Chapter 2 – Instrumentation

2.1 Dynamic light scattering

Dynamic light scattering (DLS) or quasi-elastic light scattering (QELS) is an important technique for the determination of size distribution of sub-micron particles, especially those dispersed in a solvent (colloidal suspensions and nanoemulsions).

2.1.1 Principle

The instrument utilizes principles of light scattering theory and Brownian motion of particles to measure particle size. Brownian motion is the random thermal, translational, and rotational motion (diffusion) of the particles in the solution. Kinetic theory suggests that molecules are constantly translating and rotating (Brownian motion) thus fluctuating the instantaneous dielectric constant of a given sub region of a solution. Since the fluctuations in the dielectric constant depends on the position and orientation of the molecules, it gives rise to light scattering [33]. When particles come in the path of laser light, the light gets scattered with varying intensities depending on the particles' molecular weight, size, shape, and refractive indices of the surrounding solvent. Intensity

versus time profile is generated by recording these variations. The goal of the DLS technique is to find out the diffusion coefficient, D, of the particles from the fluctuating light scattering signals. The autocorrelator of the instrument creates a correlation function by comparing the signal with a time-delayed version of itself [34]. The particle radius, R, can be calculated from the diffusion coefficient using the Stokes-Einstein relation:

$$D = kT/6\pi\eta R \qquad \text{(Equation 2.1)}$$

where D is the diffusion coefficient, k is the Boltzman constant, T is the temperature in Kelvin scale, η is the viscosity of the medium and R is the hydrodynamic radius of the particle [35].

2.1.2 Instrumentation

A conventional DLS instrument consists of a light source, focusing lens, sample holder, detector and an autocorrelator (Figure 2-1). A vertically polarized monochromatic laser emitted from He-Ne lamp is often used as a light source. A focusing lens is used to direct the laser beam to the sample holder which holds the sample contained in a glass cuvette. The scattered light collecting optics can collect the scattered light at a specific angle ranging from $30^0 – 150^0$. A photodiode detector or photomultiplier tube converts the light signals into electrical impulses. The autocorrelator converts the electrical signals into correlation functions which is used to extract the diffusion coefficient and ultimately the particle size [36].

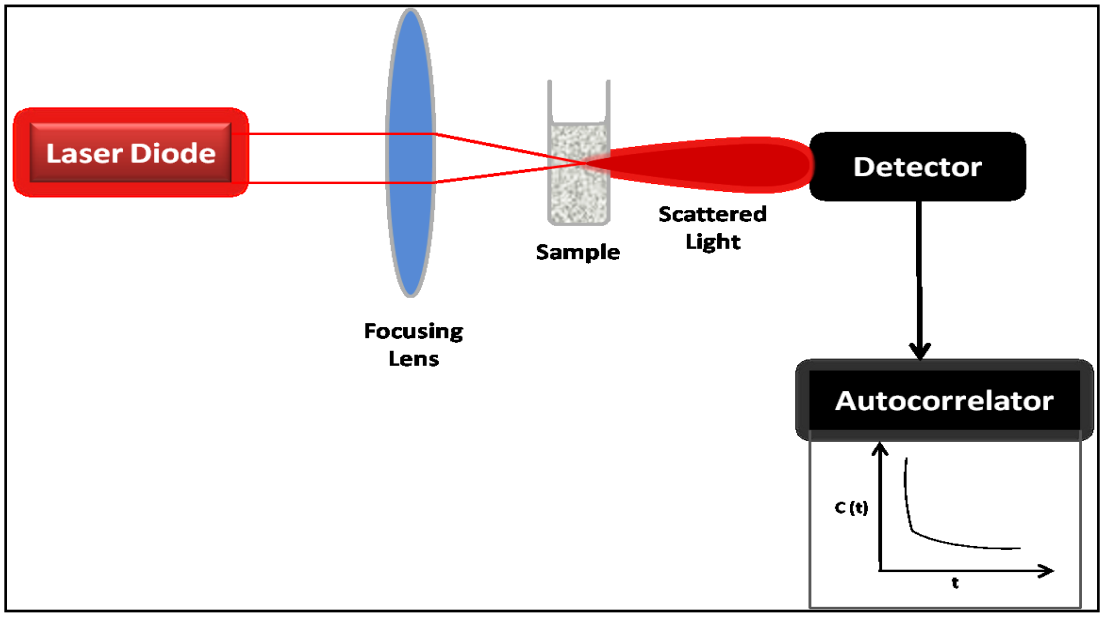

Figure 2-1: Schematic illustration of a Dynamic Light Scattering (DLS) instrument

2.1.3 Sample preparation

There are several factors that need to be carefully considered to make a precise DLS analysis. Some of the factors that can affect the correct determination of particle size are viscosity and refractive index of the solvent and sample temperature. Correct values are manually entered into the software by the user which information is used to calculate the particle size [37]. DLS requires sample to be in a very dilute state to suppress interparticulate interactions. Air bubbles can greatly affect the analysis by scattering the light in a manner similar to actual particles. Ultrasonication can be used to remove air bubbles from the sample.

2.1.4 Application

DLS is the most common particle size determination technique as it is a non-destructive technique requiring only a very small volume of sample (50µl – 2ml). Particle size distribution along with polydispersity index can be measured for proteins, polymers, colloidal dispersions, emulsions and nanoemulsions [37]. DLS can also be used to conduct stability studies. Periodic DLS measurements of a sample can reveal whether particles remain dispersed or tend to aggregate over time [38].

2.2 Electrophoretic light scattering

Electrophoretic light scattering (ELS) is a technique that can provide a quantitative measure of the charge on colloidal, dispersed particles. Surface charge or zeta potential of the colloids is a useful parameter in evaluating the stability of the colloidal dispersions.

2.2.1 Principle

The mobility of charged particles towards an anode or a cathode is directly proportional to their zeta potential. Zeta potential is the difference in potential between the surface of the tightly bound layer or shear plane and the electro-neutral region of the solution [39]. Figure 2-2 shows zeta potential as a function of distance from the charged surface of a suspended particle.

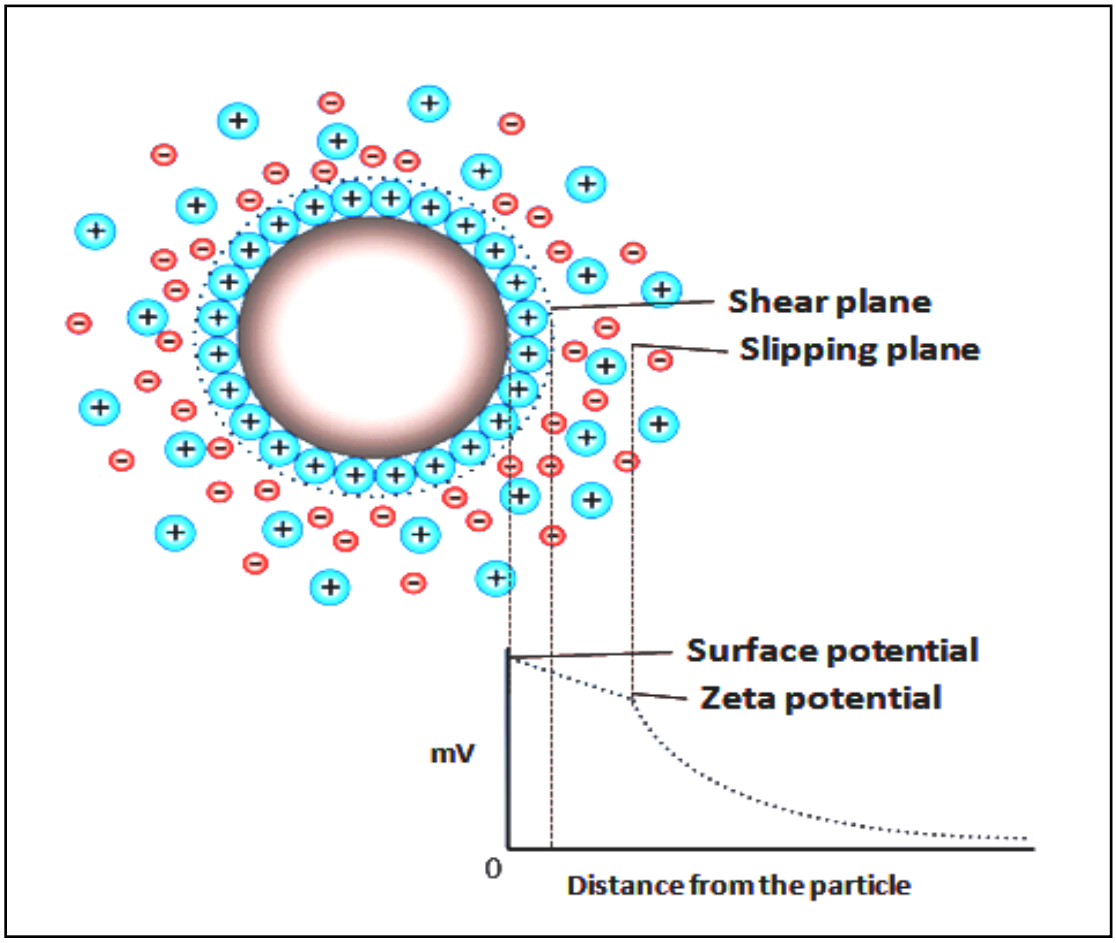

Figure 2-2: The zeta potential of a dispersed particle.

A colloid, dispersed in a liquid media can acquire charge by either absorption of ions present in the solution or due to the difference in the dielectric constants of particles and the surrounding medium [40]. ELS measures the electrophoretic mobility of charged particles under the influence of an electric field. When a laser light is focused on charged particles, electrophoretic mobility causes the light to scatter. Mobility of the charged particle can be used to calculate the zeta potentials using Smoluchowski's equation:

$$\mu = \zeta \varepsilon / \eta \qquad \text{(Equation 2.2)}$$

where μ is the electrophoretic mobility of particles, ζ is the zeta potential, ε is the electric permittivity and η is the viscosity of the surrounding medium [35].

2.2.2 Instrumentation

ELS works on the same principles as DLS and, thus, its instrumentation is similar to that of DLS. Major components of ELS include a laser light source, beam splitter, focusing lens, sample holder, receiving lens and a photomultiplier tube detector. Figure 2-3 shows a typical assembly of an ELS instrument. The beam splitter divides the monochromatic laser into two beams of equal intensity. These beams are focused by the lens to cross each other and the crossing point is known as the measurement volume. The velocity of the mobile charged particles is measured at this crossing point. The scattered light is then collected by the detector [41].

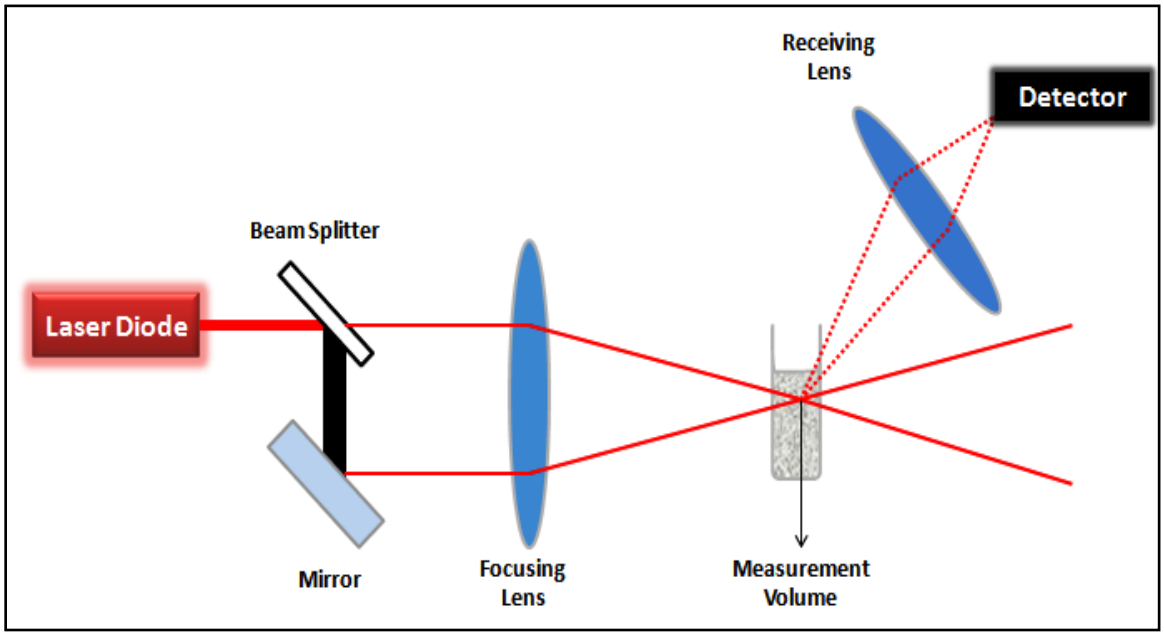

Figure 2-3: Schematic illustration of Electrophoretic Light Scattering (ELS) instrument

2.2.3 Sample Preparation

Sample preparation and requirements are similar to that of DLS (Section 2.1.3).

2.2.4 Application

ELS measures the zeta potential which is an indicator of repulsive and attractive forces between particles suspended in a colloidal system, and can be used to determine long term stability of colloids [42]. The zeta potential can also be used to determine the

absorption characteristics and cellular uptake of a colloidal formulation by predicting the nature of charged interactions between cell membrane and drug molecule [43].

2.3 Transmission electron microscope

Transmission electron microscope (TEM) is a type of light microscope which uses a beam of electrons instead of light to visualize specimens. Due to the small De Broglie wavelength of electrons, TEM offers very high resolution images (down to 0.1 nm) [44].

2.3.1 Principle

TEM relies on the interaction of an electron beam with the object under observation for image formation. The image contrast obtained in TEM is a result of elastic scattering of electrons. Electrons are produced by heating a tungsten filament at voltages ranging from 60,000 to 100,000 volts. As electrons are charged particles, their interaction with air can greatly distort the beam. Hence, air must be evacuated from the TEM before examining the sample. Furthermore, since electrons are negatively charged particles, they are not capable of passing through lenses made of glass. Therefore, powerful electromagnets are used as lenses in TEM instead. By varying the strength of these lenses, different magnifications of the image can be obtained [45]. Various contrast modes can also be used to improve the quality of the image by changing illumination conditions, action of objective lens and arrangement of apertures. Some of these modes are phase contrast mode, diffraction contrast mode and bright and dark field contrast mode [44].

2.3.2 Instrumentation

Principle components of TEM include a high voltage source, electron gun, condenser lens, objective lens, projector lens, sample stage, detectors, data output device and a vacuum system. A schematic representation of a transmision electron microscope is shown in Figure 2-4.

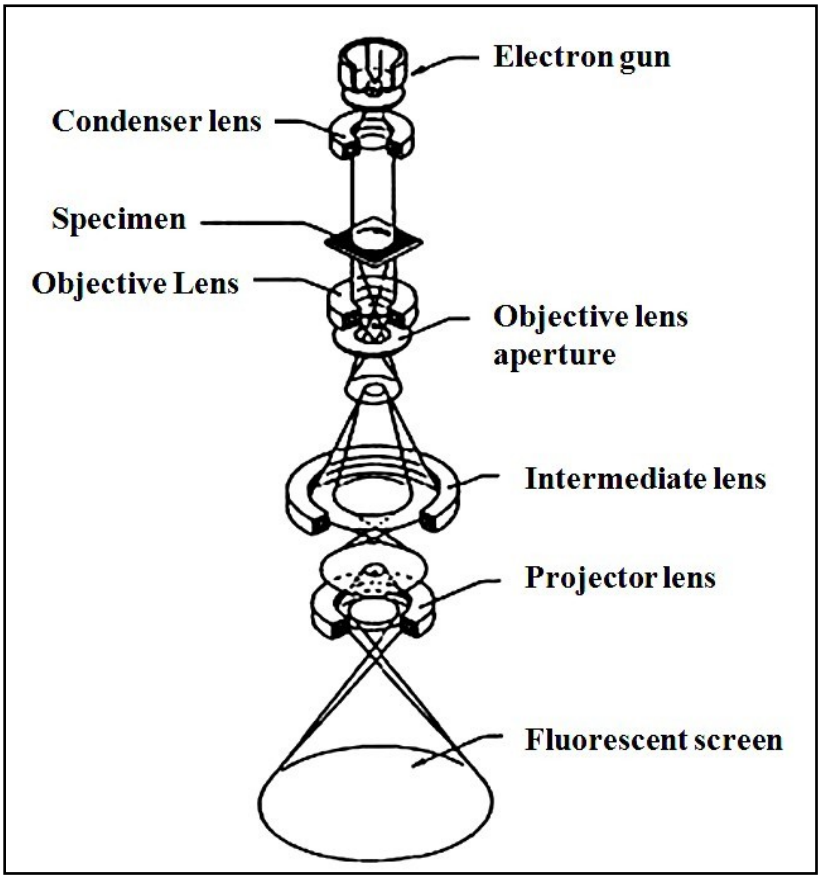

Figure 2-4: Schematic illustration of a Transmission Electron Microscope (TEM) [46]

The electron gun usually consists of a heated tungsten filament and is the emission source for electrons. The electromagnetic lenses together with the apertures control the size of the beam and focus it on the specimen. The incident electron beam interacts with the sample and gets scattered depending on the density of the sample [47]. Higher number of electrons gets blocked at the denser region of the sample resulting in a darker image and vice versa. The electrons that pass through the sample hit a phosphorescent/fluorescent screen and produce an image. The interior of the TEM is maintained in vacuum to minimize scattering of electrons by air [48].

2.3.3 Sample preparation

A support mesh known as grid is used to hold the sample. If it is a solid sample then it has to be dissolved or dispersed in a solvent before it can be deposited on the grid. A grid is made of metals like copper, gold or platinum and is usually less than 3 mm in diameter with a 5-400 mesh size. Generally, very small amount of dilute sample is deposited on the grid and is dehydrated before visualizing it under the microscope.

2.3.4 Application

TEM is capable of displaying magnified images of very thin specimens with magnifications in the range of $10^3 – 10^6$ X. TEM can provide topographical, morphological and compositional information. Furthermore, TEM can provide

crystallographic information which can be very useful in analyzing properties of crystalline specimens [49].

2.4 Ultraviolet - Visible spectrophotometry

Ultraviolet - visible (UV-Vis) spectroscopy is an absorption spectroscopy that uses the ultraviolet and visible region of the electromagnetic spectrum for qualitative and quantitative analyses of samples. UV-Vis spectroscopy is carried out in the wavelength region of 200-400nm (UV) and 400-800nm (Visible) [50].

2.4.1 Principle

UV/Vis spectroscopy is based on the absorption of UV-Visible radiations by certain compounds called chromophores. Generally, chromophores are conjugated molecules such as alkenes, aromatics, conjugated dienes etc. When chromophores are exposed to UV-Vis radiation, their valence electrons get excited and undergo an electronic transition from the highest occupied molecular orbital (HOMO) to the lowest unoccupied molecular orbital (LUMO). UV-Vis region only involves transitions from $\mathbf{n}\rightarrow\boldsymbol{\pi}^*$ and $\boldsymbol{\pi}\rightarrow\boldsymbol{\pi}^*$ as UV-Vis radiations have sufficient energy for only these electronic transitions (Figure 2-5) [50].

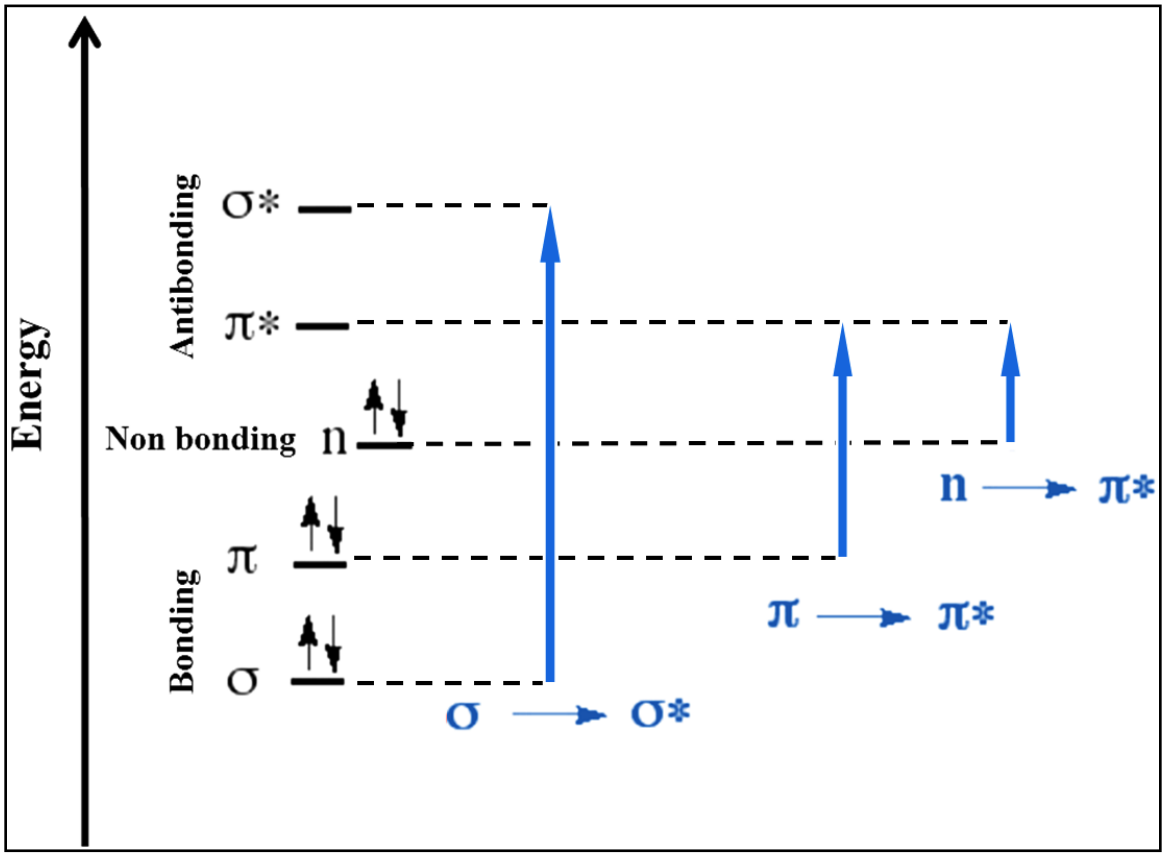

Figure 2-5: Energy diagram showing electronic transitions

The absorption of UV-Visible light results in broad bands due to the involvement of vibrational and rotational energy levels along with electronic transitions [50].

The absorption of UV-Vis radiations by chromophores obey Beer's-Lambert law (Equation 2.3) which states that absorption by a chromophore in solution is directly proportional to the concentration of the absorbing species in the solution and the path length.

$$A = -\log (I/I_0) = \varepsilon\, c\, L \qquad \text{(Equation 2.3)}$$

where A is the absorbance of the sample, I is the intensity of transmitted light, I_0 is the intensity of incident light, ε is the molar absorptivity of the absorbing species, c is the concentration of the absorbing species and L is the pathlength of light. Thus, for a fixed pathlength, concentration of the chromophore in a solution can be determined [51].

2.4.2 Instrumentation

A UV-Vis spectrophotometer consists of a light source (often deuterium or tungsten-halogen lamps), dispersion element (prism, grating monochromator, and interferometer), sample compartment and sample cells (cuvette, 96 well plates), detector (photomultiplier tubes, photodiode array, charge-coupled device cameras) and a computer for data acquisition. There are two types of UV-Vis spectrophotometers: single beam or dual beam [51]. A single beam UV-Vis spectrophotometer was used during current research. In a single beam instrument (Figure 2-6), the absorbance/transmittance of the sample and reference has to be measured separately [50].

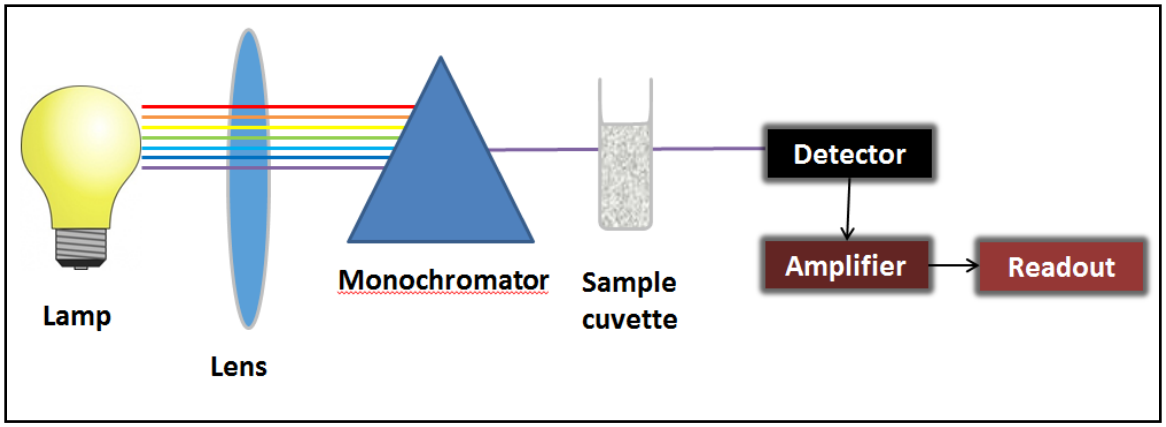

Figure 2-6 Schematic illustration of a single beam UV-Vis spectrophotometer

In a dual beam instrument (Figure 2-7), the light beam is split into two beams of equal intensity. Thus, in dual beam spectrophotometer both the sample as well as the reference transmittance can be measured simultaneously [50].

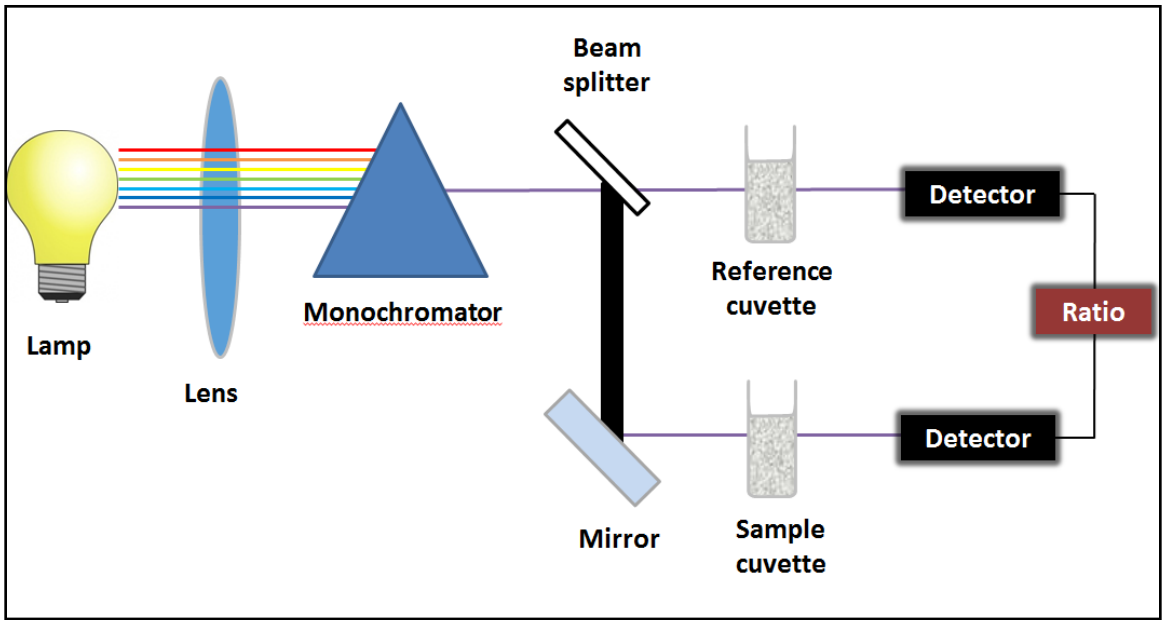

Figure 2-7 Schematic illustration of a dual beam UV-Vis spectrophotometer

2.4.3 Sample preparation

UV-Vis spectroscopy requires samples to be in solution form. Solvents that are used to dissolve solid samples usually have their absorbance maximums below 200nm to avoid erroneous results. Some of the commonly used solvents along with their wavelength cutoffs are listed in Table 2.1.

Table 2.1: Solvents used in UV-Vis spectroscopy

Solvent	Wavelength cutoff (nm)
Acetonitrile	190
Water	191
Cyclohexane	195
Methanol	201
Ethanol	204
Methylene chloride	220

Liquid samples are placed in a transparent cuvettes. The cuvettes are usually made of silica, quartz or plastic in order to avoid absorbance of UV-Vis light by the cuvettes themselves [50].

2.4.4 Application

UV-Vis spectroscopy is routinely used for quantitative estimation of organic and inorganic compounds. It offers a detection limit of 10^{-4} to 10^{-5} M with good accuracy. Qualitative applications of UV-Vis spectroscopy involve detection of functional groups. UV-Vis results are usually combined with NMR, IR and MS for determination of complete chemical structure of compounds [52]. Derivative spectroscopy is another extension of UV-Vis spectroscopy which can quantitatively determine a compound in a mixture of two or more compounds having close absorption maxima. The technique helps in improving the resolution of overlapping peaks by reducing the background absorption [53].

2.5 Differential scanning calorimetry

Differential scanning calorimetry (DSC) is one of the most commonly used thermo-analytical techniques because of its rapidity and ease of operation. DSC measures the heat flow associated with transitions in materials with respect to time and temperature and compares it with a reference standard.

2.5.1 Principle

The DSC instrument measures the difference in the heat flow between a reference and the sample. It measures the difference in the amount of heat required to raise the temperature of a sample and reference while maintaining both at nearly same temperature. The analysis is designed to cause a linear increase in the temperature of the sample holder as a function of time. Heat results in physical transformation like phase transitions in the sample. The amount of heat required to flow through the sample pan as compared to reference pan to maintain same temperature will depend on whether the process of physical transformation is exothermic or endothermic. The reference pan is usually an empty sample pan or is filled with an inert material [54].

2.5.2 Instrumentation

DSC systems can be classified into two categories: power-compensated DSC and heat-flux DSC. A power-compensated DSC was used for current study. In a power-compensated DSC, the temperature of the reference and sample are compared as shown in Figure 2-8.

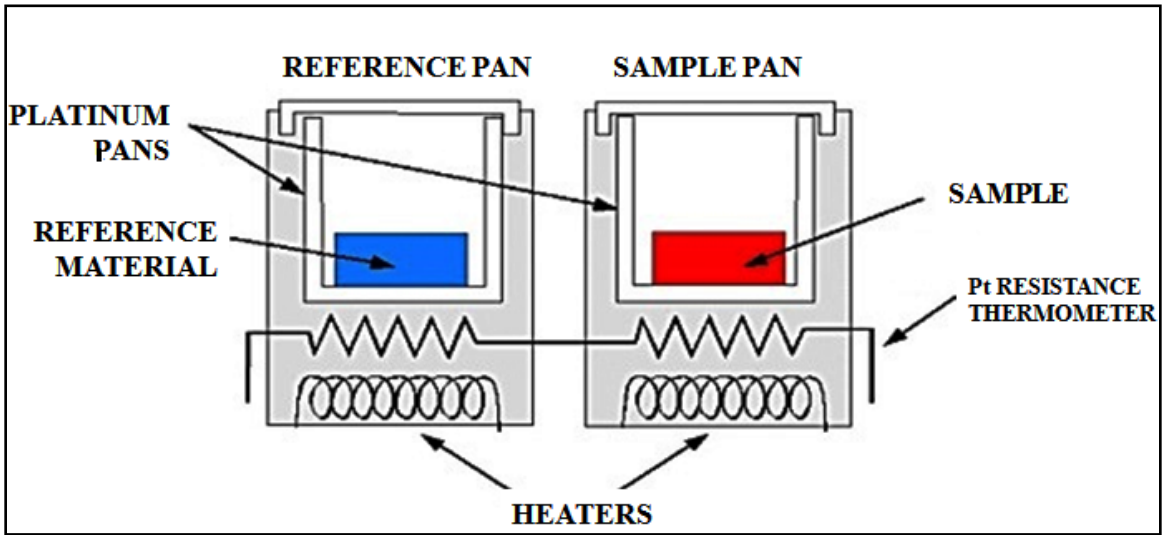

Figure 2-8: Schematic illustration of power-compensated Differential Scanning Calorimeter (DSC) [55]

In power-compensated DSC, power is applied to the sample to adjust the temperature to be similar as the temperature in the reference [51]. Amount of power applied is depending on the amount of difference in observed temperature in sample and reference. Heat can be supplied to either of the pans based on the nature of the enthalpy event. In exothermic reactions heat is supplied to the reference, whereas in endothermic reactions heat is supplied to the sample pan. The change in power is directly correlated to the heat flow into or out of the pan and results in a peak in the thermogram [56].

In heat-flux DSC, a single heating element is used to heat both the sample as well as the reference pan. Both the pans are placed on a thermocouple as shown in Figure 2-9 [51].

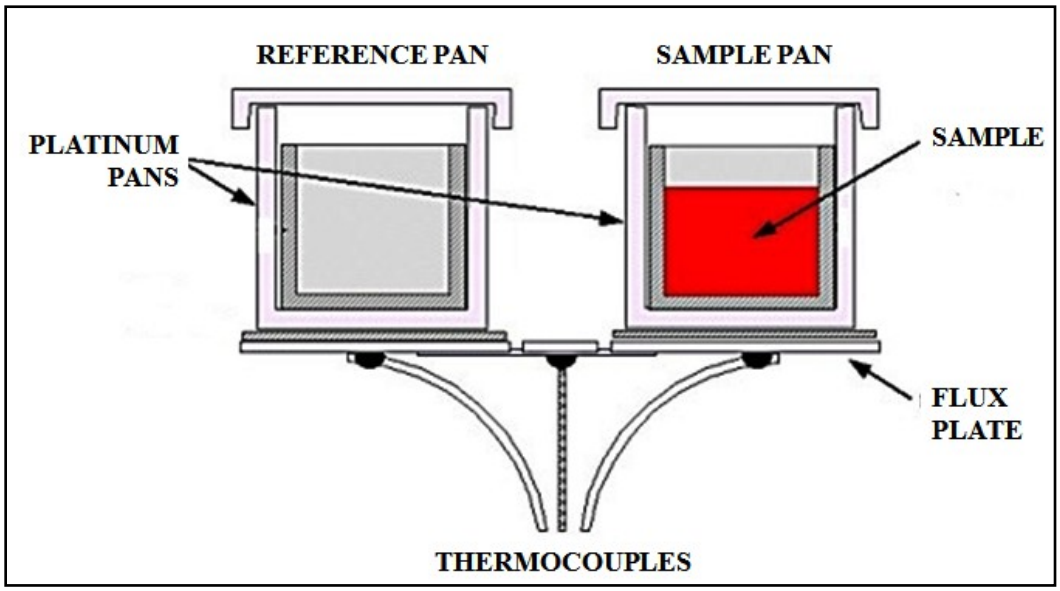

Figure 2-9: Schematic illustration of a heat-flux Differential Scanning Calorimeter (DSC) [55]

The thermocouple measures the temperature differential which is then converted into a heat flow signal through a calibration procedure [56].

2.5.3 Sample preparation

The sample is placed in a metal pan made of platinum or aluminum, and is inserted into the sample holder. The pans can be left open or sealed based on the nature of the sample being analyzed. Sealed pans can be pin-holed to avoid high pressure building up inside the pan. A reference pan identical to the sample pan is inserted into the reference holder. Reference pan is usually left empty but can be filled with a material that does not show

transition in the temperature range of interest. A very small amount of sample is required for analysis so it is very important that the portion of sample being analyzed must be representative of the total sample. Ideally, less than 5mg of sample is enough for analysis but certain polymers may require up to 10mg of sample. For best results sample weight should be accurate to ± 1%.

2.5.4 Application

DSC is regularly used in the pharmaceutical industry for characterization of drugs and excipients. The thermodynamic properties obtained by DSC can be used to study additives added to polymeric systems to increase flowability or to improve oxidative stability. DSC is often used in quality control of pharmaceutical excipients to examine lot-to-lot variability. Determination of glass transition and melting point are important for the qualitative analysis by DSC. DSC can also be used to conduct quantitative analysis such as determination of bound water in a molecule. Other applications of DSC include heat capacity determinations, crystallinity and crystallization rate determinations, reaction kinetic studies and polymer degradation determination [51].

2.6 High performance liquid chromatography

High Performance Liquid Chromatography (HPLC) is a form of liquid chromatography used to separate and quantify components in complex liquid mixtures. By choosing the

appropriate combination of detector and column, HPLC is capable of detecting and quantifying variety of compounds ranging from small organic and inorganic molecule to high molecular weight proteins.

2.6.1 Principle

Chromatographic separation can be achieved for compounds that migrate at different speeds through a column based on their different affinities to the stationary phase. In HPLC, the mobile phase is a liquid solvent and the stationary phase consists of a colulmn filled with solid particles. HPLC can be of two types based on the nature of the mobile and stationary phases. First type is known as normal-phase HPLC and consists of a polar stationary phase operated by a mobile phase of low polarity. Second type is known as reversed-phase HPLC and involves a non-polar stationary phase operated by an aqueous-organic mobile phase. A reversed-phase HPLC technique was used for current research.

Separation of individual compounds from a mixture is based on migration of analytes at different speeds through the column. The migration velocity is given by equation 2.4:

$$\mu_i = \mu_0 [1/(1+ki)c] \qquad \text{(Equation 2.4)}$$

where, μ_0 is the average migration velocity of the mobile-phase components, and k_i is the retention factor of the considered component which is equal to the distribution coefficient of compound between stationary and a mobile phase [57].

2.6.2 Instrumentation

HPLC instrument consists of a mobile phase reservoir, a mixing chamber, a pump, an injector, a separation column and a detector. Figure 2-10 shows a schematic illustration of an HPLC system.

Solvents of the mobile phase used must be degassed to eliminate formation of bubbles. A degasser removes dissolved gasses from the solvents and the degassed solvents are then mixed in the desired ratios with the help of a programmable quaternary pump. The pump then pushes solvents through the column in a steady and non pulsating manner. The liquid sample is introduced through the sample loop which injects the sample into the stream of mobile phase. The mobile phase carrying the sample enters the column and analytes are eluted out of the column and detected at different rates depending on their individual retention on the column.

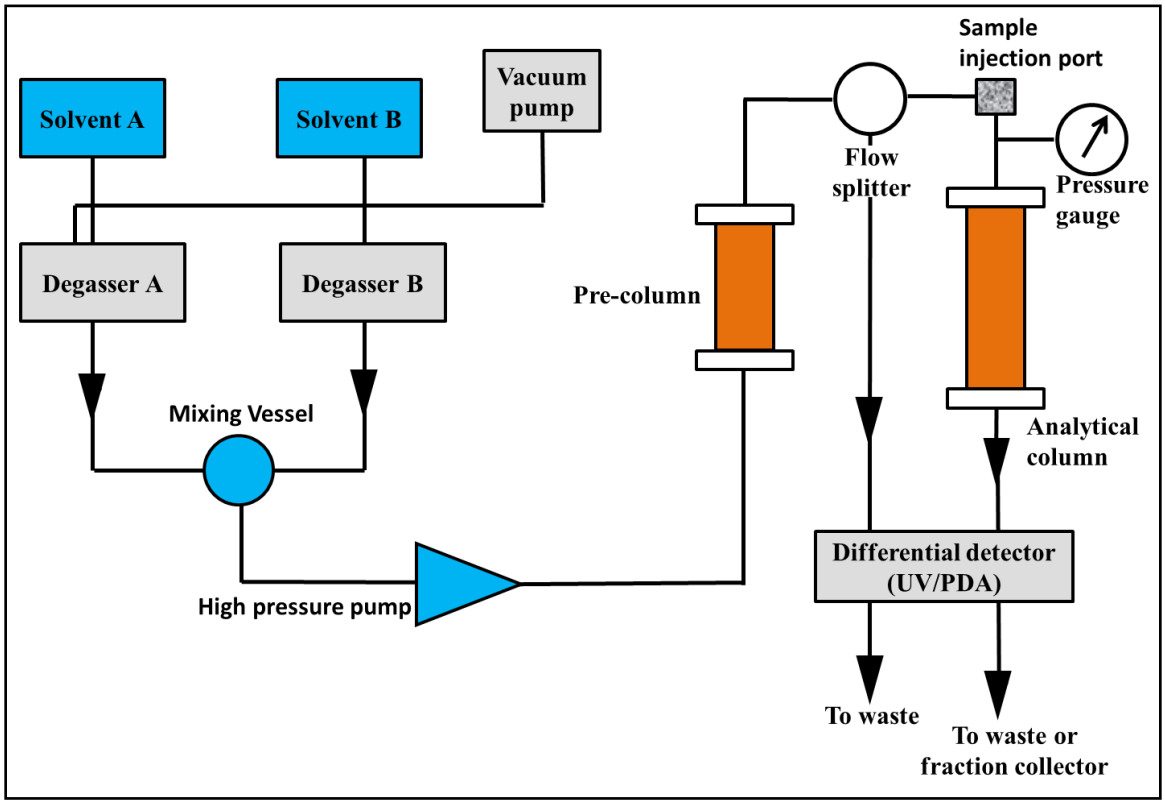

Figure 2-10: Schematic illustration of a High Performance Liquid Chromatography (HPLC) instrument.

The detector converts the data into electrical signals and generates a chromatogram. Various detectors, such as UV-Vis, mass spectrometers and fluorometers, can be used based on the type of information required from the HPLC separation [58].

2.6.3 Sample preparation

Sample preparation is a critical step in the analysis of pharmaceutical products. The samples to be analyzed can come in a variety of forms requiring simple to complex preparation procedures. Regardless of the complexity, the final sample which is ready for

injection into the HPLC should be an accurate representation of the original sample. As HPLC requires samples to be dissolved in a solvent before injection, care should be taken to use a solvent that is part of the mobile phase or at least is compatible with the mobile phase. All sample solutions need to be filtered to remove particulates that can alter the results or may even damage the HPLC column. The concentration of the sample solution should also be carefully considered based on the method of detection [59].

2.6.4 Application

HPLC is an important analytical technique for the qualitative as well as quantitative analysis of a variety of chemical compounds. HPLC has been extensively used for analyzing complex mixtures, purifying chemical compounds, isolating natural products and predicting physical and chemical properties of compounds. HPLC continues to be a very popular analytical technique for the analysis of drugs in biological samples. It is a very important tool in chiral pharmaceutical analysis and for the separation of enanatiomers of drugs. It also has application in food and nutritional analysis for the detection and separation of carbohydrates, lipids, vitamins, and polyphenols [57].

2.7 Fluorescence microscopy

A fluorescent microscope is an optical microscope that uses fluorescence and phosphorescence to generate a fluorescent image. In fluorescent microscopy, the sample

itself is the light source and can only be used to study specimens that can be made to fluoresce.

2.7.1 Principle

In a fluorescent microscope, the sample is irradiated with a light close to its absorption maximum, and the resulting fluorescence at a particular emission wavelength is measured. Figure 2-11 shows an energy diagram for fluorescence.

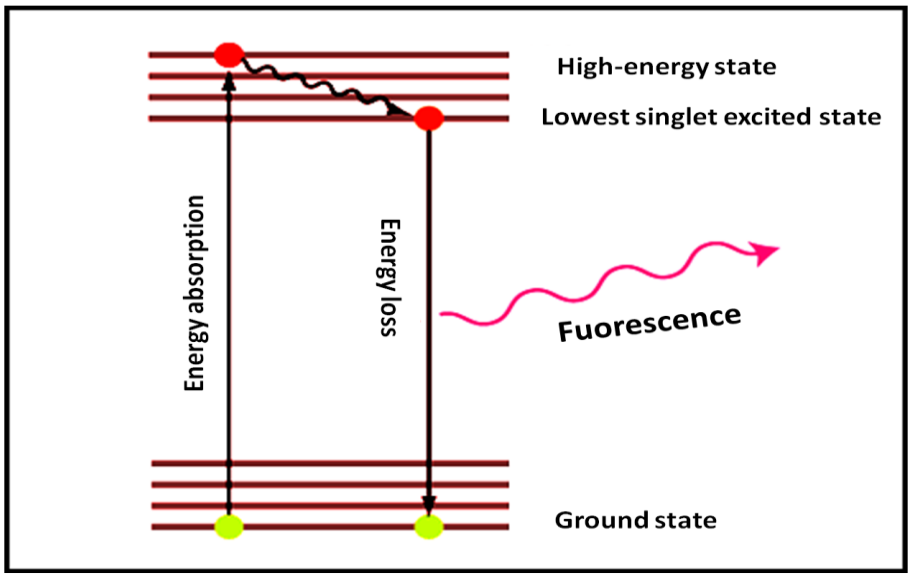

Figure 2-11 An energy diagram for fluorescence (Jablonski diagram) [60]

When a substance absorbs light, the molecules excite from ground state to a higher energy state and subsequently return back to the ground state by losing energy. In special compounds known as fluorophores, the energy absorbed can be reemitted as radiation by

a process known as fluorescence. Usually fluorophores contain delocalized electrons present in conjugated double bonds.

Any fluorescence process can be characterized by a quantum yield, which is the efficiency of the fluorescence process. Quantum yield is the ratio of intensity of the fluorescent light to the exciting light. It can be determined by comparing the sample against a substance of known quantum yield (standard) at a similar wavelength [61].

2.7.2 Instrumentation

A typical fluorescent microscope consists of a light source, an objective lens, a dichroic mirror, excitation and emission filters, and a detector. Figure 2-12 shows a schematic illustration of a fluorescent microscope.

Normally a mercury arc lamp is used as the light source to produce the light with correct wavelengths for excitation. The fluorophores/fluorochromes emit light upon excitation. To visualize this light, filtering components are required. The filters isolate the excitation and emission wavelengths of the fluorophore. A dichoroic mirror then reflects shorter wavelengths of light and allows longer wavelengths to pass towards the objective lens. The excitation light is reflected by the surface of the dichroic mirror into the objective while the fluorescence emission passes through the dichroic mirror to the detector system [62, 63].

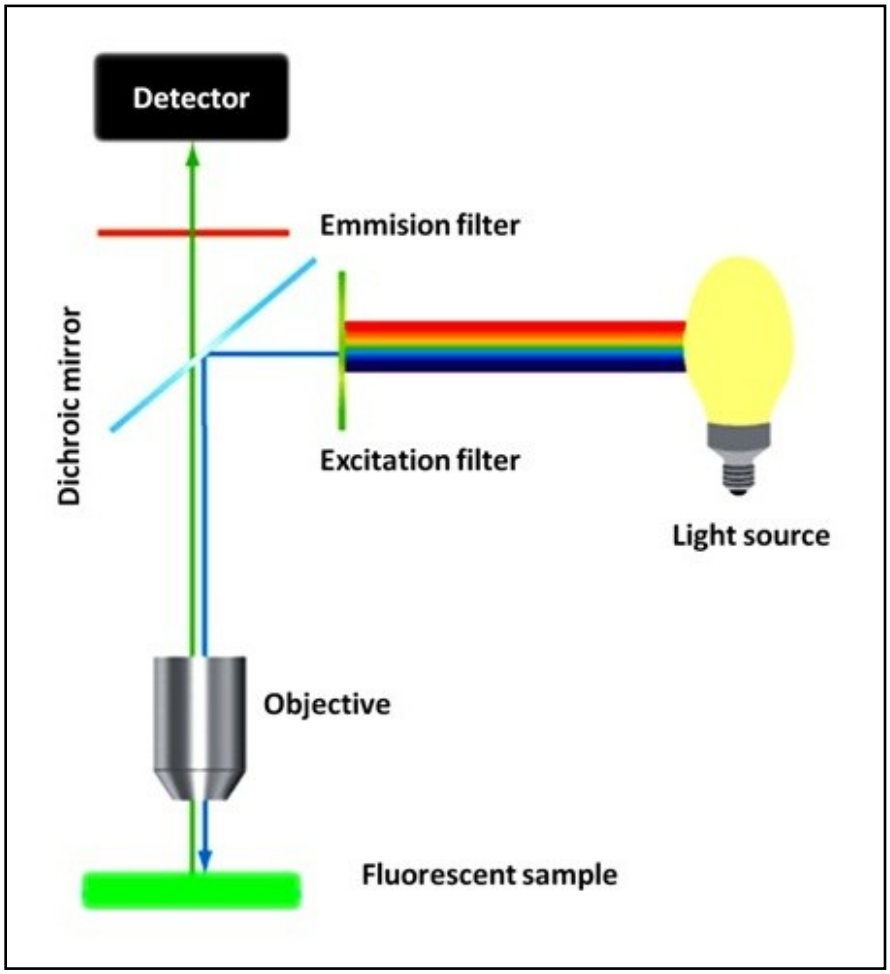

Figure 2-12: Schematic illustration of a fluorescent microscope [60]

2.7.3 Sample preparation

The most important requirement for a sample to be visualized under a fluorescent microscope is that it should fluoresce. If the sample does not possess inherent fluorescent properties, it can be made fluorescent by labeling with fluorescent stains. If the sample is of biological origin, the expression of a fluorescent protein can render the sample fluorescent [64]. Another consideration is that samples of low absorbance should be used

due to inner filter effects. Alternatively, calibration curves of fluorescence against absorbance may be used to quantify sample for a particular system [62].

2.7.4 Application

Fluorescence microscopy is an important imaging tool having applications in various fields of science, particularly in medical sciences. It has been used to generate high resolution images of structural components of small specimens like cells. It has also been used to visualize the genetic material inside the cells (DNA and RNA). Fluorescent microscopes are used for routine diagnosis and inspection in the medical field including anti nuclear antibody test and herpes virus infection test. It has been proved very useful in the field of neuroanatomical tract tracing [62]. Neuronal populations according to their anatomical connections have been studied using in vivo labeling with fluorescent dyes [65]. It has been extensively used to study drug permeability and diffusion characteristics through biological membranes as well cellular uptakes [66].

Chapter 3 - Materials and Methods

3.1 Materials

3.1.1 Cremophor RH 40

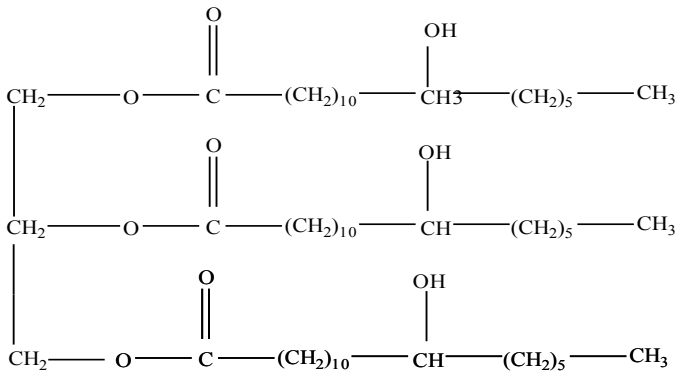

Figure 3-1**:** Chemical structure of hydrogenated castor oil

Physiochemical properties:

Source: BASF Chemicals, CAS #61788-85-0

Chemical name: Polyethoxylated castor oil

Physical state: white semisolid paste at 20^0C

pH: 6.0 – 7.0 (20^0C)

Melting Range: 160 – 260^0C

Density: 1.03 g/cm^3

Acute oral toxicity (LD_{50}/Rat): 20000 mg/kg

Solubility: Soluble in water and organic solvents

Polyoxyethylene castor oil derivatives are complex mixtures of various hydrophobic and hydrophilic components. These are nonionic surfactants used in oral, topical and parenteral formulations along with cosmetics and animal feeds. Cremophor RH 40 has an HLB range of 14-16 and can be used to solubilize various vitamins and drugs. The addition of cremophor RH 40 increases the solubility of propellants in the aqueous phase in aerosols. It is an essentially non-toxic and non-irritant material based on acute and chronic toxicity tests conducted in animals [67, 68].

3.1.2 Tween 80

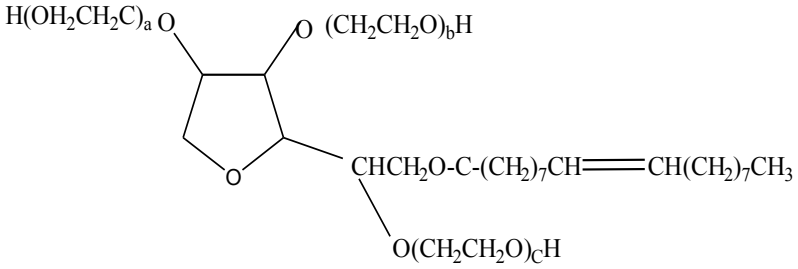

Figure 3-2**:** Chemical structure of Tween 80

Physiochemical properties:

Source: Spectrum Chemicals, CAS# 156-27-1

Chemical name: Polyoxyethylene 20 sorbitan monoleate

Molecular Formula: $C_{64}H_{124}O_{26}$

Molecular weight: 1310 g/mole

Physical state: Clear amber yellow liquid.

pH: 7 (1% solution in water)

Boiling Point: >100°C

Melting Point: - 20.556°C

Specific Gravity: 1.06 - 1.10 g/cm^3

Acute oral toxicity (LD_{50}): >36000 mg/kg [Rat]

Solubility: Soluble in hot/cold water, methanol, and corn oil; insoluble in mineral oil

Polysorbates are partial fatty acid esters of sorbitol and its anhydrides copolymerized with ethylene oxide. Tween 80 belongs to the category of hydrophilic nonionic surfactants (HLB 15) that has been widely used as emulsifying and solubilizing agent for oils and oil soluble vitamins [67]. It has been found useful in improving the oral bioavailability of drug molecules that are substrates for p-glycoprotein [69]. Tween 80 is included in the FDA Inactive Ingredients Guide.

3.1.3 Labrasol

(Chemical structure not available)

Physiochemical properties:

Source: Gattefosse, CAS # 61791-29-5

Chemical name: Caprylocapryol polyoxyl-8 glycerides

Physical state: Colorless oily liquid

Specific gravity: 1.060 – 1.070 g/cm^3

Boiling range: > 250^{0}C

pH value: 4 – 7 (10%)

LD_{50} (oral): 22000 mg/kg (Rat)

Solubility: Soluble in water

Labrasol is a non-ionic dispersible surfactant comprising of well-characterized PEG esters, a small glyceride fraction and free PEG. Labrasol has an HLB of 14. It is a solubilizing and wetting agent capable of improving the solubility of active pharmaceutical ingredients *in vitro* and *in vivo*. Labrasol also exerts a bioavailability enhancing activity which can be associated with strong inhibition of the enterocytic efflux transporter (P-gP inhibition). It has been found suitable for use in hard and soft gelatin capsules, topical ointments, nanoemulsions, gels and in transdermal patches.

3.1.4 Polyethylene Glycol 400

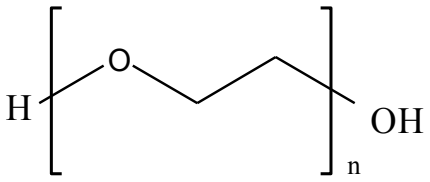

n=8.2-9.1

Figure 3-3: Chemical structure of PEG 400

Physiochemical properties:

Source: Spectrum Chemicals, CAS# 25322-68-3

Chemical name: α-Hydroxy-ω-hydroxy-poly(oxy-1,2-ethanediyl)

Chemical formula: $C_{2n}H_{4n+2}O_{n+1}$

Molecular weight: 380-420 g/mole

Physical state: Viscous clear liquid

Specific gravity: 1.1254 g/cm^3

pH: 4.0-7.0 (5% w/v solution)

Acute oral toxicity (LD_{50}): 28.9 g/kg (Mice)

Solubility: soluble in hot and cold water, aromatic hydrocarbons and slightly soluble in aliphatic hydrocarbons

Polyethylene glycols (PEGs) are widely used in a variety of pharmaceutical formulations including parenteral, topical, oral, ophthalmic and rectal preparations. PEG 400 is a stable hydrophilic substance which can be used as a suspending agent since it can increase the viscosity and consistency of other suspending vehicles. It can also stabilize emulsions in combination with other emulsifiers. A 30% v/v solution has been used as a vehicle for parenteral preparations [67]. It can be used to enhance aqueous solubility or dissolution characteristics of poorly water soluble drugs by forming solid dispersions and self-emulsifying mixtures [70].

3.1.5 Capryol 90

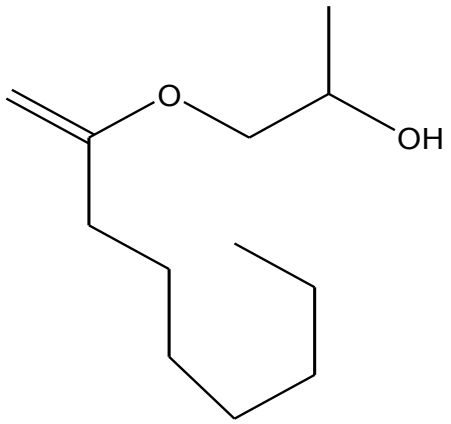

Figure 3-4: Chemical structure of Capryol 90

Physiochemical properties:

Source: Gattefosse, CAS # 85883-73-4

Chemical name: Propylene glycol monocaprylate

Chemical formula: $C_{11}H_{22}O_3$

Molecular weight: 202.29 g/mole

Physical state: Light yellow oily liquid

Specific gravity: 0.935-0.955 g/cm^3

Boiling Point: >120^{o}C

Solubility: Soluble in organic solvents and insoluble in water

Propylene glycol monocaprylate is a mixture of the propylene glycol monoesters and diesters of fatty acids, composed predominately of caprylic acid. Capryol 90 is a water insoluble surfactant (HLB 6) commonly used in self-emulsifying lipidic formulations. It

has been categorized as a bioavailability enhancer due to its inhibitory action on CYP3A4 enzyme [71].

3.1.6 Transcutol P

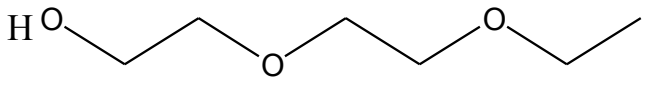

Figure 3-5: Chemical structure of Transcutol P

Physiochemical properties:

Source: Gattefosse, CAS # 111-90-0

Chemical name: Diethylene glycol monoethyl ether

Chemical formula: $C_6H_{14}O_3$

Molecular weight: 134.17 g/mole

Physical state: Colorless limpid liquid

Specific gravity: 0.985-0.991 g/cm^3 (20^{0}C)

LD_{50} (Rat): 5500 µl/kg

Transcutol P is a high purity solvent and solubilizer for poorly water soluble drugs. When formulated as topical ointments and emulsions, it has been associated with improved drug

permeation and a drug depot effect. It is used as a stabilizer for W/O emulsions and co-solvent in formulation of self-nanoemulsifying systems [67].

3.1.7 Labrafil M 2125 CS

(Chemical structure not available)

Physiochemical properties:

Source: Gattefosse, CAS# 61789-25-1
Chemical name: Linoleoyl polyoxyl-6 glycerides
Physical state: Yellow viscous liquid
Boiling point: >150°C
Specific gravity: 0.935-0.955 g/cm^3
Solubility: Insoluble but dispersible in water and soluble in organic solvents

Labrafil M 2125 CS is a water dispersible surfactant (HLB 4) comprising of a well-characterized PEG-esters and a glyceride fraction. It has the ability to self-emulsify on contact with aqueous media forming a coarse dispersion (emulsion) and when combined with other suitable surfactants it can form a fine dispersion (nanoemulsion). Thus, it can function as a lipid vehicle for poorly water soluble drugs. Labrafil M 2125 CS has been found to demonstrate bioavailability enhancing capabilities as well. Increase in oral bioavailability can be attributed to the long chain triglyceride composition and selective

absorption of highly lipophilic drugs by the lymphatic transport system reducing hepatic first-pass metabolism [72].

3.1.8 Carbamazepine

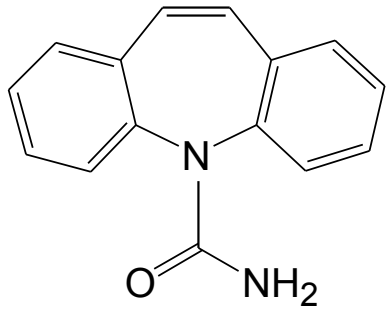

Figure 3-6: Chemical structure of carbamazepine

Physiochemical properties:

Source: PCCA, Lot # C134615, CAS # 298-46-4

Chemical name: 5H-Dibenz[b,f]azepine-5-carboxamide

Chemical formula: $C_{15}H_{12}N_2O$

Molecular weight: 236.27g/mole

Physical state: White powder

Log P value: 2.3

Melting Point: 191-192^{o}C

Solubility: Insoluble in water and soluble in ethanol and propylene glycol

Carbamazepine (CBZ) is an antiepileptic agent. It has limited aqueous solubility and is absorbed slowly and erratically after oral administration [73]. It appears to exert its anticonvulsant effect by slowing the rate of recovery of voltage-sensitive sodium channels responsible for action potential generation and enhancing inhibitory synaptic transmission at synapses that uses GABA as a neurotransmitter [74]. CBZ is now the primary drug for treatment of trigeminal and glossopharyngeal neuralgias. It has also found use in the treatment of bipolar affective diorders [6].

Marketed Products: Carbatrol®, Equetro®, Tegretol®, Biston®, Calepsin®, Epitol®, Stazepine®

Dosage Forms: Tablets, ER Tablets, Chewable Tablets, Suspensions

Dose: 200 mg b.i.d. (400mg/day) in case of Epilepsy and 100 mg b.i.d. (200mg/day) in Trigeminal neuralgia.

3.1.9 Sudan IV

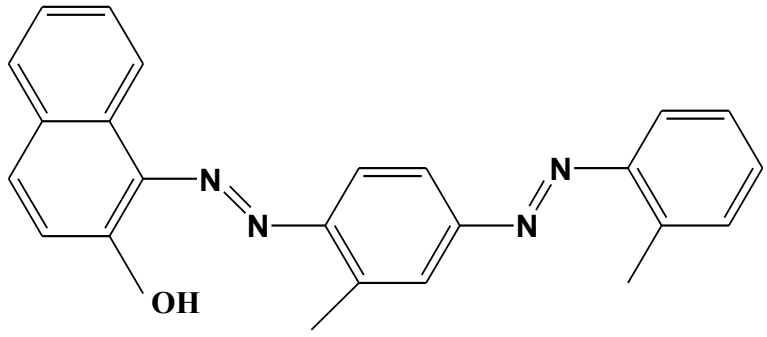

Figure 3-7: Chemical structure of Sudan IV

Physiochemical properties:

Source: Fisher Scientific, CAS# 85-83-6

Chemical name: 1-(2-methyl-4-(2-methylphenyldiazenyl) phenyl) azonapthalen-2-ol

Chemical formula: $C_{24}H_{20}N_4O$

Molecular weight: 380.1662 g/mole

Physical state: Dark red to brown powder

Log P value: 6.657

Melting Point: 181.1^0C

Solubility: Insoluble in water and soluble in fats and lipids

Sudan IV is a fat soluble dye having very high Log P value. It is commonly used for demonstrating triglycerides in frozen sections [75]. Its industrial application involves coloring nonpolar substances like oils, fats, waxes, greases and acrylic emulsions. Sudan IV is a carcinogen which prohibits its use in the food and pharmaceutical industry.

3. 2 Methods

3.2.1 Drug selection

Carbamazepine was selected as a model drug for incorporation into the nanoemulsions. The most important criterion for the selection of CBZ as the model drug for the study was its low aqueous solubility. CBZ belongs to the class II drugs of BCS, having very low solubility but high permeability. Thus, CBZ was a perfect candidate for the incorporation of drug into a lipid based drug delivery system.

3.2.2 Drug solubility determination

The solubility of carbamazepine in various excipients (surfactant, co-surfactant and oil) was determined from a calibration curve of carbamazepine in methanol using reverse phase HPLC (Waters e2695 separation module), plotted over a range of concentrations (0.01 – 2.5 mg/ml). 500mg of carbamazepine was added to 4ml of each excipient in a micro centrifuge tube and vortexed for 5 minutes. Drug-excipient mixtures were heated to 40°C in a water bath to facilitate solubilization followed by continuous shaking on a nutating mixer for 48 hours at ambient room temperature (~ 25°C). The mixtures were centrifuged at 3000 rpm for 20 min. Aliquots of supernatants were prepared and diluted using methanol and the drug content was quantitatively determined using HPLC. The method was carried out on a C_{18} reverse phase column (Symmetry C_{18} column - 3.5µm, 4.6×75 mm) and a mobile phase comprising water/methanol/acetonitrile (60/20/20) at a

flow rate of 1.0 ml/min were operated. The absorbance measurement was performed at 285 nm using PDA detector connected to the HPLC separation module.

3.2.3 Selecting excipients for self-nanoemulsification

The unique property of self-nanoemulsion is exhibited by only certain combinations of surfactant, co-surfactant and oil in specific amounts. In the present study, excipients shown in Table 3.1 were evaluated for possible self-emulsification tendencies:

Table 3.1: Lipid excipients used in SNEDDS

Surfactant	Cosurfactant	Oil
Cremophor RH 40	PEG 400	Labrafil M 2125 CS
Tween 80	Transcutol P	
Labrasol	Capyrol 90	

The excipients listed in Table 3.1 resulted in nine different self-emulsifying mixtures, which were evaluated:

I. Cremophor RH 40 - PEG 400 - Labrafil M 2125 CS

II. Cremophor RH 40 - Transcutol P - Labrafil M 2125 CS

III. Cremophor RH 40 - Capryol 90 - Labrafil M 2125 CS

IV. Tween 80 - PEG 400 - Labrafil M 2125 CS

V. Tween 80 - Transcutol P - Labrafil M 2125 CS

VI. Tween 80 - Capryol 90 - Labrafil M 2125 CS

VII. Labrasol - PEG 400 - Labrafil M 2125 CS

VIII. Labrasol - Transcutol P - Labrafil M 2125 CS

IX. Labrasol - Capryol 90 - Labrafil M 2125 CS

These nine combinations were prepared in the ratios of oil:(surfactant/cosurfactant) as 1:1, 1:2, 1:3, 1:4, 1:5, 1:6 and 1:7. The surfactant/cosurfactant ratios also known as k_m ratios of 1:1, 2:1 and 3:1 were evaluated. The different combinations were prepared by weighing appropriate amount of surfactant and cosurfactant and vortexed for 30 minutes to produce homogenous mixtures. The oil (Labrafil M 2125 CS) was then added and vortexed for further 5 minutes to form self - emulsifying mixtures. The above ratios resulted in mixtures containing 25-66% of surfactant, 12-44% of cosurfactant and 12-50% of oil. Thus, a total of 189 (9 combinations × 7 ratios × 3 k_m ratios) different combinations containing varying amounts of the surfactants, cosurfactants and oils were evaluated.

3.2.4 Evaluation of self-nanoemulsifying properties of SME mixtures

A test for self-emulsification was conducted on all nine SME mixtures according to a method developed by Craig et al [76]. 0.6 ml of each of the 189 possible combinations was added to 400 ml of DI water under gentle agitation using a magnetic stirrer. Emulsification time, clarity of the emulsion, and apparent stability were evaluated. The

combinations that resulted in clear, transparent nanoemulsion with no signs of instability for 24 hours were represented on a ternary phase diagram using SigmaPlot software version 12.0. After examining the phase diagrams, the most optimal formulation was selected for drug loading.

3.2.5 Drug loading of nanoemulsion

The combination consisting of Cremophor RH 40 (50%) – PEG 400 (25%) – Labrafil M 2125 CS (25%) was selected for drug loading based on an evaluation of the nanoemulsifying properties of the SME mixtures. The model drug, CBZ was added to the SME mixture and vortexed till it was completely solubilized. Nanoemulsion was formed from the SME mixture as described in section 3.2.4. The drug loading capacity was determined based on solubility data. A maximum drug loading capacity was found by observing SME mixtures containing varying concentrations of drug for 48 hours for any signs of drug precipitation or nanoemulsion phase separation. Table 3.2 shows the composition of the selected formulation.

Table 3.2: Composition of the selected formulation

Constituent	Quantity (mg)
Carbamazepine	100
Cremophor RH 40	2500
PEG 400	1250
Labrafil M 2125 CS	1250

3.2.6 Droplet size and zeta potential measurements

Droplet size and zeta potential of the optimal nanoemulsion (with and without drug) were determined using dynamic light scattering (DLS) instrument (Nicomp 380 ZLS). Volume weighted diameter was measured by placing disposable Durex borosilicate glass culture tubes containing the nanoemulsion(undiluted) in the path of a He-Ne laser having a wavelength of 658 nm at scattering angles of 60^0, 90^0 and 120^0 at 23^0C. using a visconsity value of 0.9333 cP and referactive index value of 1.333.

The measurements were done in triplicates. The droplet size was also determined after filtering the nanoemulsion through 0.2 μm Nalgene® syringe filter (25 mm surfactant free cellulose acetate membrane) attached to a syringe.

The zeta potential was measured using the same instrument but in electrophoretic light scattering (ELS) mode. Samples were measured in standard 1 cm wide, square glass cuvette and readings were taken at an angle of 14.1^0C at 23^0C. The zeta potential for each nanoemulsion was measured in triplicates.

3.2.7 Thermodynamic properties

Thermal behavior of the formulation and physical state of the incorporated drug was determined using a differential scanning calorimeter (Diamond DSC, PerkinElmer) equipped with an intercooler 1P. The data was analyzed using Pyris Manger 1.3 software. Samples of about 3-5 mg of SME mixture, both with and without drug, were placed in

standard 20 µl aluminum pans. Nitrogen was used as an effluent gas at a flow rate of 20 ml/min. The samples were analyzed for a temperature range of 0^0C to 250^0C with a ramp speed of 10^0C/min.

3.2.8 Transmission electron microscopy of SNEDDS

Transmission electron microscopy (TEM) was used to study the morphology of the nanoemulsion droplets. TEM helps to visualize the internal matrix and the shape of the individual droplets. Hitachi HD-2300 scanning transmission electron microscope was used in transmission electron mode to collect individual droplet images. One drop of the nanoemulsion was placed on a holey carbon 400 mesh copper grid (Ted Pella, CA). Excess sample was removed using a lint free wipe and the sample was left overnight for drying before examining under TEM. The images were captured and optimized using Quartz PCI version 8 software.

3.2.9 Sterility testing

The final nanoemulsion formulation was checked for sterility to verify that the method for nanoemulsion formulation is capable of producing a microorganism free nanoemulsion. The testing procedure was carried out in aseptic conditions under a laminar airflow hood. The glassware used was autoclaved before being placed under the hood. Non-autoclavable materials were thoroughly wiped with isopropyl alcohol to make

them microbe free. Blank formulation (i.e. without drug) was filtered through a 0.2 µ? Nalgene® syringe filter (25 mm surfactant free cellulose acetate membrane) attached to a syringe. The sterility of the filtered formulation was tested using plate as well as direct/tube inoculation method. *Staphylococcus aureus* (ATCC 25923) was used for positive control and was cultured on a Mueller-Hinton (MH) agar plate and incubated at 35^0C for 24 hours. The bacteria from the plate were passed on to a fresh agar plate by the streaking technique to isolate a pure strain of the bacteria (Figure 3-8).

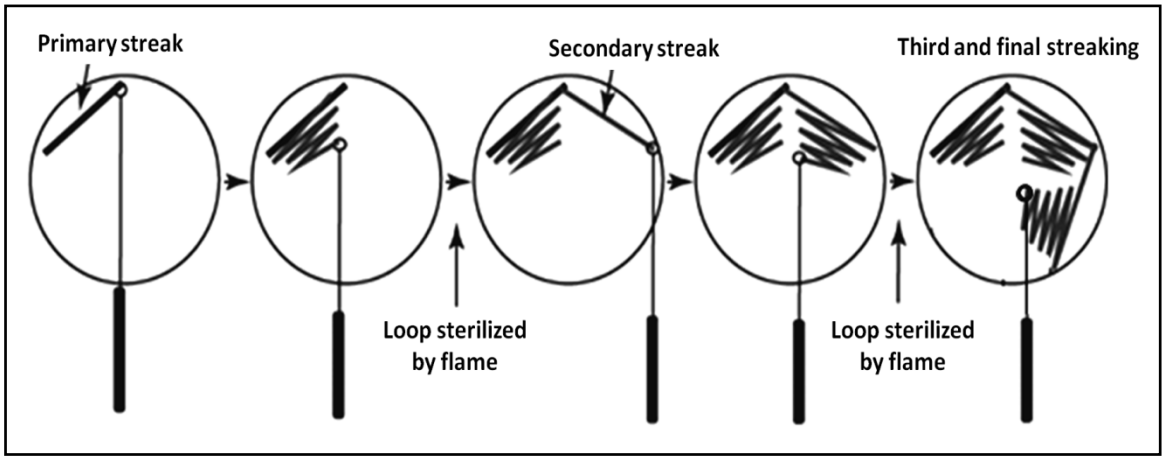

(A)

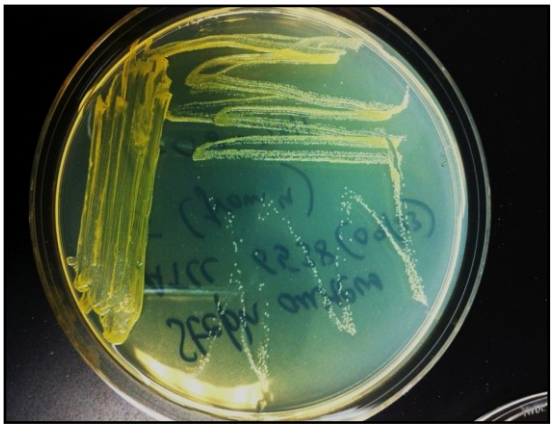

(B)

Figure 3-8: (A) The streaking procedure, (B) image of an agar palate showing isolated bacterial colonies

Bacterial colonies from the third passage were swabbed and placed into a test tube containing 5 ml of sterile water (autoclaved). The concentration of the bacteria was determined with the help of a Spectronic 20 Genesys spectrophotometer at 625nm. By using sterile water as a blank, the sample absorbance was compared to 0.5 McFarland standard having a concentration of (1.5×10^8) CFU/ml. The standard showed an absorbance range of 0.08-0.10 at $10 - 10^2$ CFU/ml concentration. Serial dilutions of the McFarland standard were performed to get a dilution of $10 - 10^2$ CFU/ml (Figure 3-9).

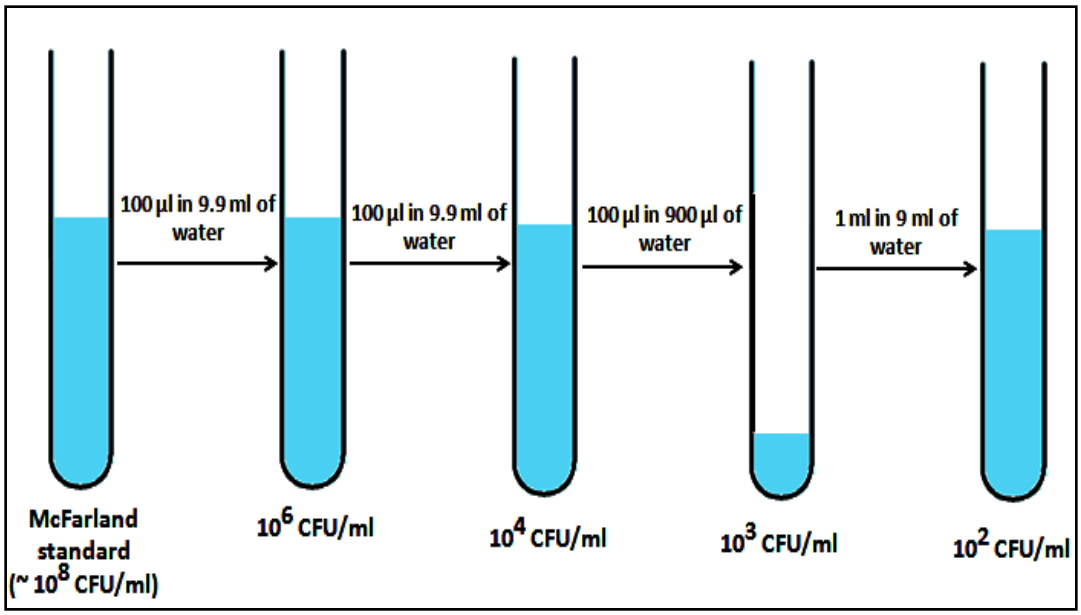

Figure 3-9: Serial dilution of McFarland standard.

Three sets of control and sample tubes were prepared for tube/direct inoculation. Table 3.3 summarizes the composition of control and sample tubes used for the direct inoculation method. The set of eight test tubes(4x2) containing fluid thioglycollate medium (FTM) were used to check the presence of anaerobe bacteria in the formulation. To avoid oxygen exposure, water, bacteria and samples were all placed at the bottom of

the tubes with minimum disturbance of the media. Soybean casein digest medium(SCD) was used for the detection of fungi and aerobes [77, 78]. Eight SCD tubes stored at 35°C mimicked temperatures similar to body temperature which promoted the growth of aerobic bacteria. Eight tubes stored at room temperature (20°C) were used for the detection of fungi [77]. All 24 test tubes were incubated at 35^0C for 24 hours to speed up the growth of the bacteria.

Table 3.3: Composition of control and sample tubes in the direct inoculation method. All tubes were prepared and tested in duplicates.

Medium	Negative control	Positive control	Positive sample control	Sample
FTM	9 ml of the medium + 1 ml of sterile water	9 ml of the medium + 1 ml of sterile water + 10-100 CFU bacteria	9 mL of the medium + 1 mL of sample with 10-100 CFU bacteria	9 mL of the medium + 1 mL of sample
SCD 30-35°C	9 mL of the medium + 1 mL of sterile water	9 mL of the medium + 1 mL of sterile water + 10-100 CFU bacteria	9 mL of the medium + 1 mL of sample with 10-100 CFU bacteria	9 mL of the medium + 1 mL of sample
SCD 20°-25C.	9 ml of the medium + 1 ml of sterile water	9 ml of the medium + 1 ml of sterile water + 10-100 CFU bacteria	9 ml of the medium + 1 ml of sample with 10-100 CFU bacteria	9 ml of the medium + 1 ml of sample

For the plate method, MH agar plates were prepared by dissolving the powdered agar in DI water followed by autoclaving. After autoclaving, it was cooled down just enough to facilitate easy handling while still being flowable. 20 ml of this solution was poured into pre-sterilized monoplates aseptically. The plates were allowed to cool to get rid of the vapors and to solidify agar. Agar plates were in the refrigerator. Before use, the plates were equilibrated to room temperature for 30 minutes. A total of 24 plates consisting of three sets of 4 plates each similar to tube inoculation method were tested in duplicates. 400 µl of sample was withdrawn from all 24 tubes listed in Table 3.3 on day 0, 7 and 14 and placed in pre-sterilized micro-centrifuged tubes. These were then spiro-plated onto the agar plates using SpiralBiotech Autoplate 4000. The machine stylus took the samples from manually held micro-centrifuged tubes and deposited them spirally on the plates. After each plate, the stylus underwent a washing cycle of bleach followed by two wash cycles of water. All 24 plates were incubated at 35^0C for 24 hours to speed up the growth of the bacteria before observing them visually at 25^0C.

3.2.10 Cell toxicity analysis

In vitro toxicity of the formulation (without drug) was tested on NIH 3T3 cell lines (ATCC # CRL-1658, mouse embryonic fibroblast tissue). The cells were subcultured in Dulbecco's Modified Eagle Medium (DMEM) containing 5% Fetal Bovine Serum (FBS) and 1% Penicillin – streptomycin solution. The cells were passed two more times with 48 hours time between each passage. The cells were detached from the plate for counting, by

adding 0.05% trypsin and 0.53 mM EDTA. The cells were then counted using a Beckman Z2 Particle Size Coulter Counter and a final cell count of 647,000 cells/ml was achieved by diluting with DMEM with 5% FBS. 100 µl of the above cell containing media was added to all the wells of a 96 well plate (except the negative control wells), to get a concentration of ~10,000 cells/well. The plate was then incubated at 37^0C in 5% CO_2 environment for 24 hours to facilitate attachment of cells to the plate. After 24 hours of incubation, media from the wells was carefully removed by slightly tilting the plate without disturbing the adherent cells. 100 µl of fresh DMEM containing 5% FBS was added to all the wells. The 96 well plate consisted of 4 wells of negative control containing 100 µl DMEM with 5%FBS in wells devoid of cells, 4 wells of positive control containing 100 µl DMEM with 5%FBS in wells with cells attached to the walls, and a set of 4 cell containing wells of each sample concentration tested (11%, 5.5%, 0.5%, 0.25% and 0.125%). These sample concentrations were obtained by diluting the samples with the media by serial dilution. Figure 3-10 shows the scheme of sample (microemulstion) dilution.

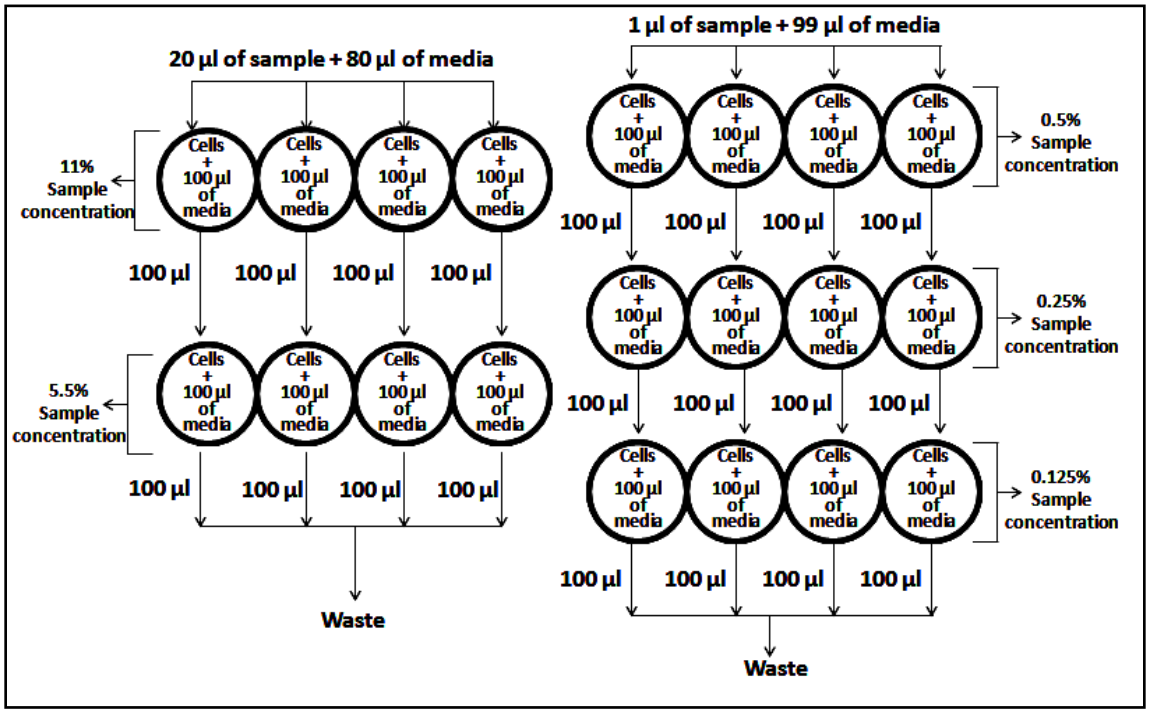

Figure 3-10: The sample dilution scheme for cell toxicity analysis.

After 48 hours of incubation, 10µl of MTT reagent was added to all the wells, carefully mixed and the plates were incubated for another 4 hours. The well plate was checked for absorbance using BioRad absorbance plate reader with wavelength set at 580 nm. Finally one way ANOVA test was used to compare the absorbance of sample containing wellsagainst the control wells.

In addition, three petri dishes were also prepared at the same time for the purpose of microscopic examination of the cells. First petri dish contained 5ml of positive control. Second petri dish contained 25 µl of sample in 5 ml of cell containing media rendering a final sample concentration of 0.5%. The third petri dish contained 0.55 ml of sample in 5

ml of cell containing media rendering a sample concentration of 11%. The petri dishes were incubated at 37^{o}C for 48 hours before being examined under a light microscopic.

3.2.11 Nebulization of nanoemulsion

Nanoemulsions with and without drug were nebulized to examine their potential for pulmonary delivery. Nebulization was achieved using a pediatric micro mist jet-type nebulizer attached to a piston compressor (PulmoNeb® Compressor Nebulizer System) (Figure 3-11). The nebulizer was capable of producing mist of droplet size smaller than 5μm at a maximum pressure of 35 psi and compressor flow rate of 9 l/min. 3 ml of the nanoemulsion was loaded in the medication cup of an aerosol type mask, fitted to an air-compressor. Compressed air from the compressor unit vaporized the sample in the nebulizer cup creating a fine mist.

Figure 3-11: PulmoNeb® compressor nebulizer system [79]

3.2.12 Droplet size determination of the mist

Droplet size distribution of the mist was determined using a particle size analyzer (Microtrac Aerotrac SPR 7340) equipped with a 1mW He-Ne laser. The wavelength of the light used to observe laser light diffraction phenomena was 632.8 nm. The data was collected at a focus length of 100 mm and a background collect time of 0.3 seconds. LDSA Win 6.21 software was used to interpret the data.

3.2.13 Transmission electron microscopy of the mist

The morphology of the nanoemulsion droplets in the mist was studied using a transmission electron microscope (Hitachi HD-2300 STEM) in TE mode. A holey carbon grid of 400 mesh (Ted Pella, Inc.) was held in a stream of nanoemulsion mist for about 10 seconds with the help of a self-locking tweezer. The grid was then left to dry overnight before it was finally analyzed under the microscope.

3.2.14 Histological analysis

Histological analysis was carried out to visualize the localization of the nanoemulsion (without drug) inside a porcine lung. Sudan IV was used as a fluorescent marker to aid in detection of the nanoemulsion under fluorescent microscope.

3.2.14.1 Dye solubility determination

The solubility of Sudan IV in various excipients was determined using a calibration curve of Sudan VI in dimethyl sulfoxide (DMSO) using UV-Vis spectrometer (Agilent UV spectrophotometer 8453). Excess amount (~500mg) of Sudan IV was added to 4ml of each excipient in a microcentrifuge tube and vortexed for 5 minutes. The mixture was then heated to 40°C in a water bath which decreased the viscosity of the excipients to facilitate mixing and solubilization. Then the mixture was finally kept at ambient room temperature (~ 25°C) on a nutating mixer under continuous shaking for 48 hours. The mixtures were centrifuged at 3000 rpm for 20 min to separate out a clear supernatant. Aliquots of supernatants were prepared and diluted using DMSO and the dye content was quantitatively determined using a UV-Vis spectrometer.

3.2.14.2 Dye incorporation of nanoemulsion

The formulation consisting of Cremophor RH 40(50%) – PEG 400(25%) – Labrafil M 2125 CS (25%) was loaded with Sudan IV. 50 mg of the dye was solubilized in 1g of oil (Labrafil M 2125 CS) based on the results from the solubility studies. The nanoemulsion was prepared as previously described under section 3.2.4 using the dye containing oil to aid in the detection of fluorescence.

3.2.14.3 Droplet size and Zeta Potential of Dye loaded Nanoemulsions

Droplet size and zeta potential of the dye containing nanoemulsion was determined using a DLS instrument (Nicomp 380 ZLS) in a manner similar to the procedure mentioned under section 3.2.6. These observations were made at scattering angles of 90^0.

3.2.14.4 Histological assay

Porcine lung from a freshly sacrificed pig was obtained from a nearby slaughterhouse for visualizing the entrapment of nanoemulsion inside the lung tissue and its diffusion through it. Approximately 1.3 mm thick sections were cut and washed several times with phosphate buffered saline (PBS) of pH 7.4. The washed lung sections were placed between the donor and receptor chamber of a 15ml Franz diffusion cell (Figure 3-12A) and equilibrated for 45 minutes at 40^0C in a water bath before adding samples to the donor chambers. Six cells were used for the study comprising of one positive control cell, one negative control cell and four sample cells containing 2 ml of the dye (Sudan IV) incorporated nanoemulsions (Figure 3-12B). The positive control consisted of 2ml of nanoemulsion devoid of the dye in the donor chamber while the negative control consisted of 2ml of PBS (pH 7.4). After an hour the tissue was removed from the assembly and stored at -80^0C until analyzed. Franz diffusion cells were only used as stands to hold the tissues and expose them to samples for specified amount of time.

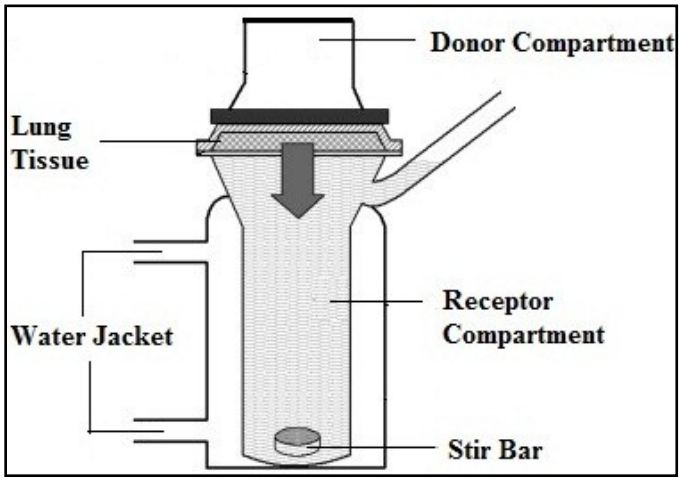

(A)

(B)

Figure 3-12: (A) An illustration of a typical Franz diffusion cell and (B) a photo of the actual assembly of the Franz diffusion cells used during the study.

A section of the frozen tissue was placed in a plastic mold containing cryo optimal cutting temperature (OCT) compound. More cryo OCT gel was placed over the frozen tissue in the mold and the mold was frozen to form a solid block. The square solid block of OCT. compound containing the tissue was removed from the mold and was mounted over a metal chuck using OCT compound as the glue (Figure 3-13A). The metal chuck containing the tissue was frozen by placing it over a block of dry ice before it was placed inside a cryostat (Bright OTF 5000 cryostat) for sectioning. The cryostat fitted with a rotary microtome was used to cut 30µm thick sections of the tissue (Figure 3-13B).

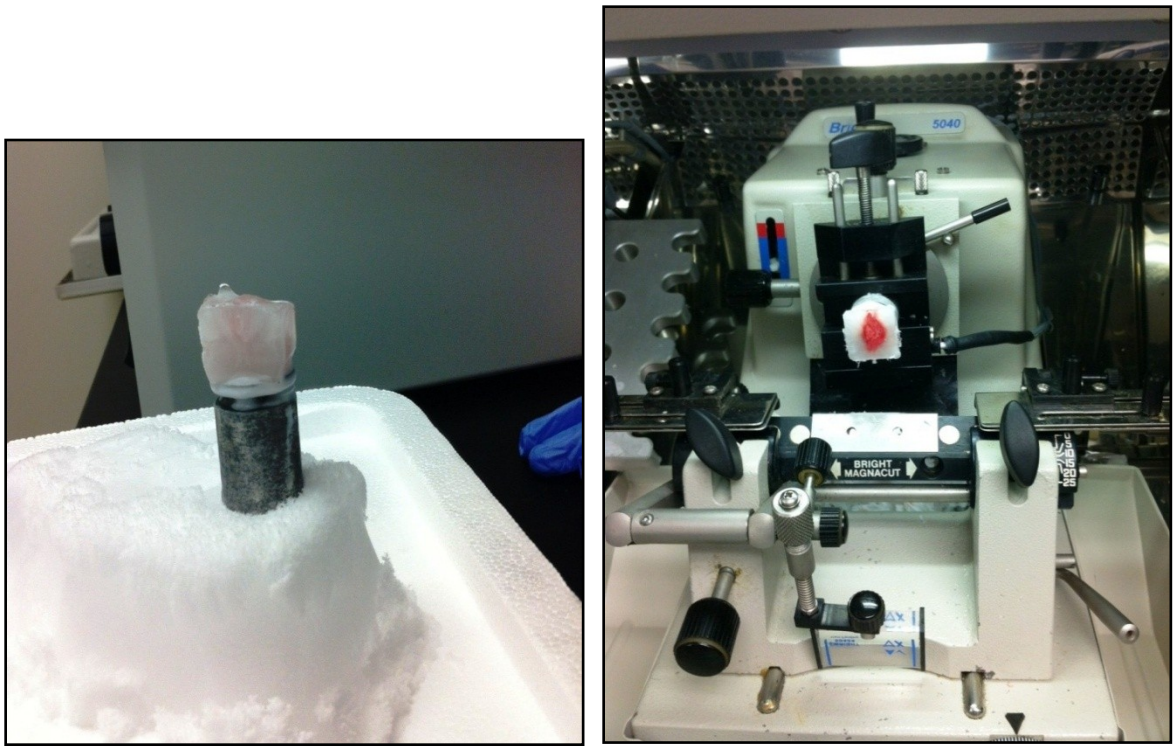

(A) (B)

Figure 3-13: (A) OCT embedded tissue mounted on a metal chuck and (B) metal chuck containing frozen tissue placed in a microtome inside a cryostat

The sections were mounted on a glass slide and a drop of DAPI (4', 6-diamidino-2-phenylindole) was added to stain the tissue before placing the cover slip on the slide. The slides were dried overnight in the dark and then were observed under a 10X objective in a Nikon TiU microscope coupled with photometric Coolsnap EZ 20 MHz camera (Photometrics, Tuczon, AZ). All images were acquired and processed using the Metamorph software (version 7.6.5.0). An excitation wavelength of 325 to 375 nm and a blue filter was used when DAPI stain was visualized while Sudan IV was analyzed at an excitation wavelength of 460 to 500 nm and a FITC filter was chosen to process the image.

Chapter 4 - Results and Discussions

4.1 Drug solubility determination

Carbamazepine is a lipophilic, poorly water-soluble compound which belongs to the class II drugs of BCS [80]. One way of increasing solubility of BCS Class II drugs involves incorporating them in lipid based formulations. An increase in the bioavailability of such drugs has been achieved by fastening the dissolution process and keeping the drug dissolved throughout its transit in the GI tract [81]. In an O/W nanoemulsion, the solubility of the drug in the oil governs the drug carrying capacity of the nanoemulsion system.

HPLC was used to find the solubility of CBZ in various excipients. CBZ had a retention time of approximately 4.9 minutes when solvent system comprised of water: methanol: acetonitrile (60:20:20). Figure 4-1 shows the quality of peak obtained in the HPLC run for one of the concentrations (0.6 mg/ml).

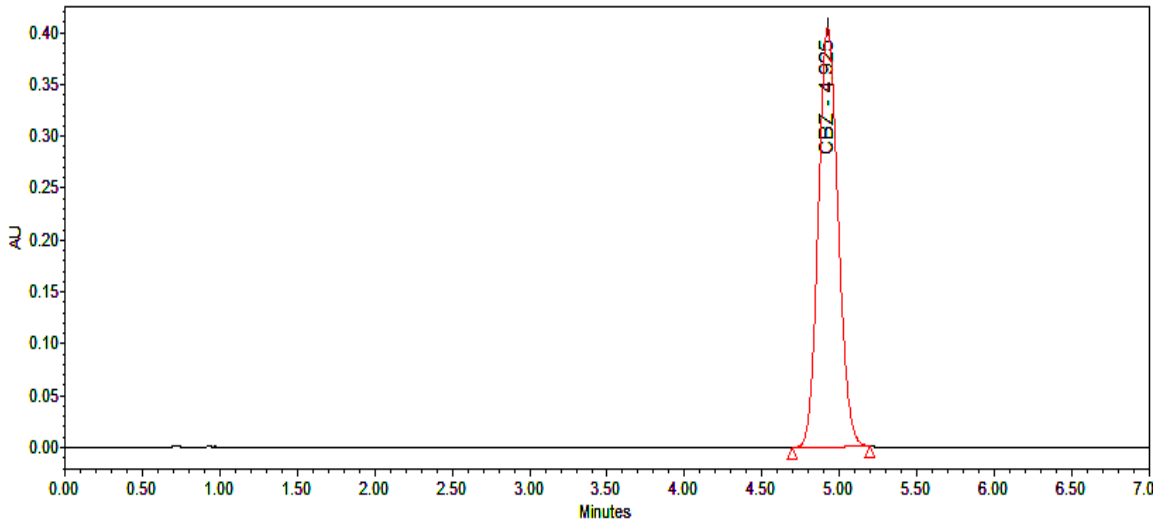

Figure 4-1: HPLC chromatogram of 0.6mg/ml carbamazepine.

A calibration curve for carbamazepine was plotted over a concentration range of 0.01-2.5mg/ml. The linear fitting line of the data was found to be:

Y = 2920000 **X** – 58300 with R^2 = 0.999352

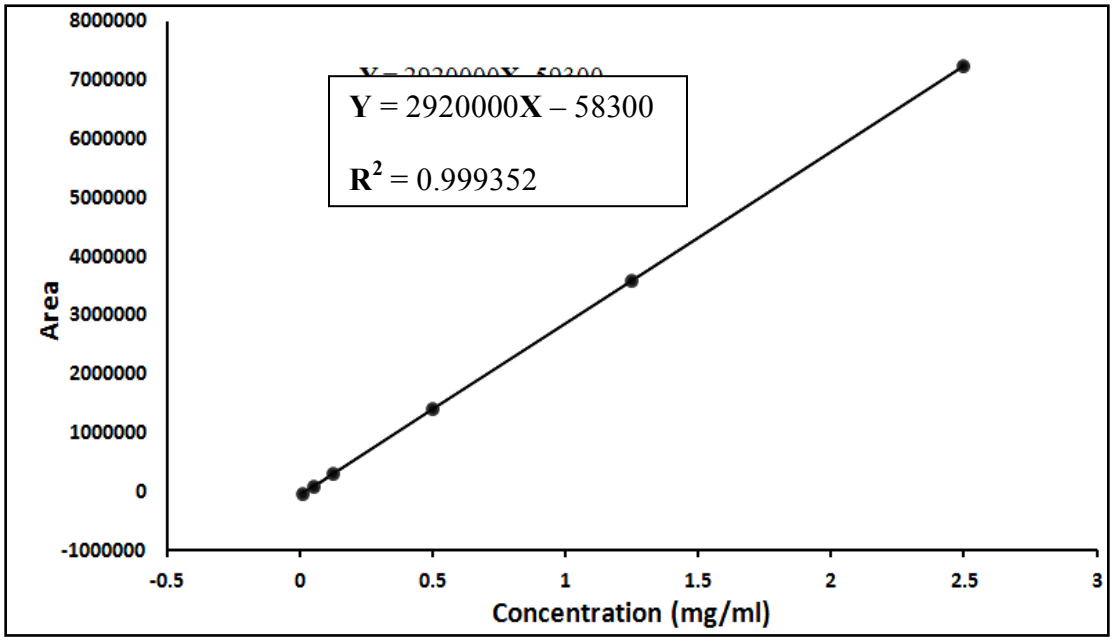

Figure 4-2: Calibration curve for solubility studies of CBZ

CBZ exhibited maximum solubility in the oil Labrafil M 2125 CS among the various oils tested and hence, surfactants and cosurfactants were selected based on their ability to form SNEDDS with this oil. Carbamazepine showed highest solubility in PEG 400 among all the cosurfactants tested. Table 4.1 lists the solubility of CBZ in various excipients tested.

Table 4.1: Solubility of carbamazepine in various excipients

Type of Excipient	**Excipient**	**Solubility (mg/ml)**
Oil	Labrafac PG	10.05 ±1.02
	Labrafil M 2125 CS	38.125 ± 0.92
	Labrafac Lipophile WL 1349	7.525 ± 0.97
	Isopropyl myristate	6.375 ± 0.62
Surfactant	Cremophor RH 40	26.25 ± 0.53
	Labrasol	143.2 ± 3.8
	Tween 80	85.5 ± 1.77
Cosurfactant	PEG 400	291.75 ± 13.61
	Capryol 90	101.975 ±2.67
	Transcutol P	151 ± 5.9
Solvent	Methanol	211.75 ± 10.43
	Water	Practically insoluble [82]

Although the drug showed greater solubility in Tween 80 and Labrasol between all the surfactants tested, Cremophor RH 40 was selected in the final formulation as it formed the most stable nanoemulsion in shortest amount of time when used with Labrafil M 2125 CS.

4.2 Selection of excipients

Selection of the appropriate excipients determines the success of the formulation. For SNEDDS, the selected excipient mixture should self-microemulsify upon aqueous dilution in GIT in shortest possible time [83]. The SME mixture should be able to solubilize a given amount of drug without harming its physical and chemical stability. The concentration of excipients used to solubilize given dose of a drug should not be toxic. Thus, as far as possible, pharmaceutically accepted surfactants, cosurfactants and oils should be employed [84]. Nine combinations of various lipid excipients were analyzed to select the optimal mixture for drug delivery. All the excipients used in the study are included in FDA's list of Generally Regarded As Safe (GRAS) materials. Following nine combinations were tested for emulsification properties:

I. Cremophor RH 40 - PEG 400 - Labrafil M 2125 CS
II. Cremophor RH 40 - Transcutol P - Labrafil M 2125 CS
III. Cremophor RH 40 - Capryol 90 - Labrafil M 2125 CS
IV. Tween 80 - PEG 400 - Labrafil M 2125 CS
V. Tween 80 - Transcutol P - Labrafil M 2125 CS
VI. Tween 80 - Capryol 90 - Labrafil M 2125 CS
VII. Labrasol - PEG 400 - Labrafil M 2125 CS
VIII. Labrasol - Transcutol P - Labrafil M 2125 CS

The nine possible combinations were added to water under mild agitation to visually test their self-nanoemulsifying tendencies. The combinations were screened based on

emulsification time, clarity at emulsion and apparent stability. SME mixtures containing drug were first examined for self-emulsification times. Table 4.2 summarizes the time taken by various combinations to form a clear nanoemulsion.

Table 4.2: Time taken by mixtures (I – IX) to self-microemulsify

K_m ratio	**Surfactant (%w/w)**	**Co - surfactant (%w/w)**	**Oil (%w/w)**	**Time (sec) I**	**Time (sec) II**	**Time (sec) III**	**Time (sec) IV**	**Time (sec) V**
1:1	25	25	50	No ME	No ME	No ME	No ME	No ME
	33.3	33.3	33.3	100	No ME	No ME	No ME	No ME
	37.5	37.5	25	95	No ME	No ME	No ME	No ME
	40	40	20	85	180	No ME	No ME	60
	41.6	41.6	16.6	80	160	280	No ME	70
	42.8	42.8	14.2	54	155	250	No ME	55
	43.7	43.7	12.5	50	120	240	No ME	65
2:1	33.3	16.6	50	No ME	No ME	No ME	No ME	No ME
	44	22	33.3	80	No ME	No ME	No ME	No ME
	50	25	25	40	No ME	No ME	No ME	No ME
	53.3	26.6	20	36	170	250	No ME	No ME
	55.5	27.7	16.6	25	150	230	+300	No ME
	57.1	28.5	14.2	20	120	175	240	110
	58.3	29.16	12.5	35	110	117	54	62
3:1	37.5	12.5	50	No ME	No ME	No ME	No ME	No ME
	49.5	16.5	33.3	90	No ME	No ME	No ME	No ME
	56.2	18.7	25	50	No ME	250	No ME	No ME
	60	20	20	40	No ME	180	No ME	No ME
	62.5	20.8	16.6	35	48	60	+300	No ME
	64.2	21.4	14.2	30	45	57	120	No ME
	65.6	21.8	12.5	28	44	50	100	No ME

K_m ratio	Surfactant (%w/w)	Co - surfactant (%w/w)	Oil (%w/w)	Time (sec) VI	Time (sec) VII	Time (sec) VIII	Time (sec) IX
1:1	25	25	50	No ME	No ME	No ME	No ME
	33.3	33.3	33.3	No ME	No ME	No ME	No ME
	37.5	37.5	25	No ME	No ME	No ME	No ME
	40	40	20	No ME	No ME	No ME	No ME
	41.6	41.6	16.6	No ME	No ME	No ME	No ME
	42.8	42.8	14.2	No ME	No ME	No ME	No ME
	43.7	43.7	12.5	No ME	No ME	No ME	No ME
2:1	33.3	16.6	50	No ME	No ME	No ME	No ME
	44	22	33.3	No ME	No ME	No ME	No ME
	50	25	25	No ME	No ME	No ME	No ME
	53.3	26.6	20	No ME	No ME	No ME	No ME
	55.5	27.7	16.6	No ME	No ME	No ME	No ME
	57.1	28.5	14.2	No ME	No ME	No ME	No ME
	58.3	29.16	12.5	No ME	No ME	No ME	No ME
3:1	37.5	12.5	50	No ME	No ME	No ME	No ME
	49.5	16.5	33.3	No ME	No ME	No ME	No ME
	56.2	18.7	25	No ME	No ME	No ME	No ME
	60	20	20	No ME	No ME	No ME	No ME
	62.5	20.8	16.6	+300	No ME	No ME	No ME
	64.2	21.4	14.2	+300	No ME	No ME	No ME
	65.6	21.8	12.5	+300	No ME	No ME	No ME

The test of self-emulsification visually assessed the dispersions and they were categorized as either nanoemulsion or macroemulsion/emulsion. The visually clear emulsions were deemed as nanoemulsion while the turbid and milky emulsions were categorized as macroemulsion/emulsion, some of which immediately phase separated (Figure 4-3).

(A) (B)

Figure 4-3: (A) A visually clear nanoemulsion and (B) a turbid and milky emulsion.

A drug can alter SME performance by penetrating into the surfactant monolayer surrounding the oil droplet causing disturbances at the interface [85]. To test the effect of drug incorporation in SME mixtures on self emulsification properties CBZ loaded mixtures were also subjected to the self-emulsification test [86]. In the present study, CBZ did not considerably change the properties of the drug loaded nanoemulsions when compared with the blank nanoemulsions. This indicated the suitability of the system to incorporate the drug. Hence, their results were not presented here.

Out of the nine combinations only six resulted in clear nanoemulsions. These six combinations were further screened with the help of ternary phase diagrams. Combinations containing Labrasol as the surfactant (VI – IX) did neither form a macroemulsion nor a nanoemulsion and hence were discarded. A ternary phase diagram is used to compare three different components at the same time. Since a SME mixture usually is a three component system comprising of a surfactant, cosurfactant and oil, ternary phase diagrams can be used to represent individual concentration ranges. The area

bound by the outer most points in the phase diagram shows the concentration range of each SME component that formed a clear nanoemulsion. The combinations enclosing a large area on the phase diagrams are preferable as they present a wider concentration range for nanoemulsion formation. Figure 4-4 and Figure 4-5 show the ternary phase diagrams for combinations I-VI that formed a clear nanoemulsion. As can be seen in Figure 4-4 (A) the combination comprising of Cremophor RH 40 – PEG 400 – Labrafil M 2125 CS occupied the largest region on phase diagrams. This formulation also exhibited the shortest emulsification times and thus was selected for drug loading. Further, the concentration of excipients used was within the common range for lipid based formulations and was very much below the toxic levels [67, 81].

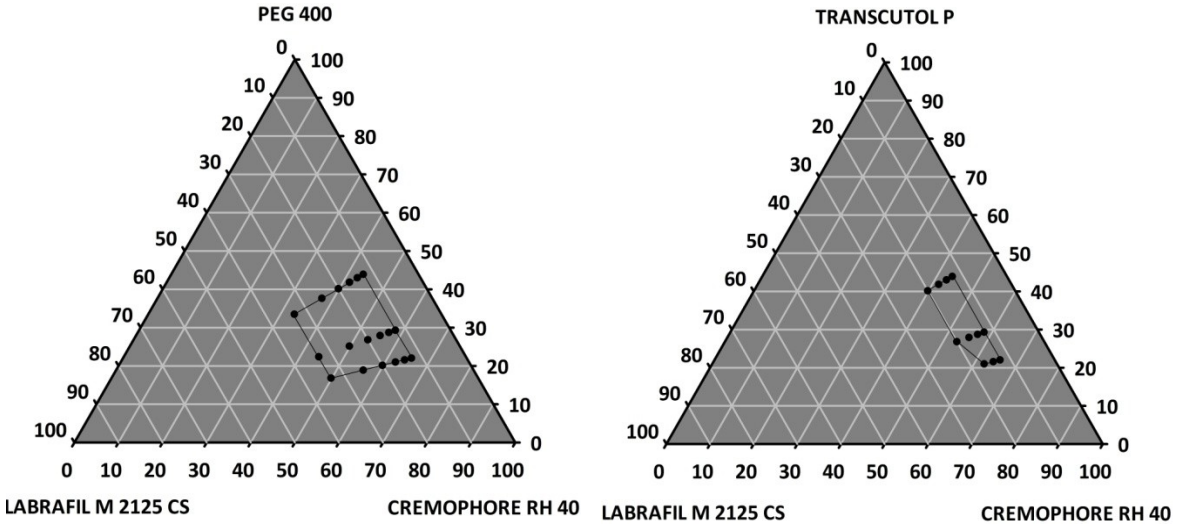

(A) (B)

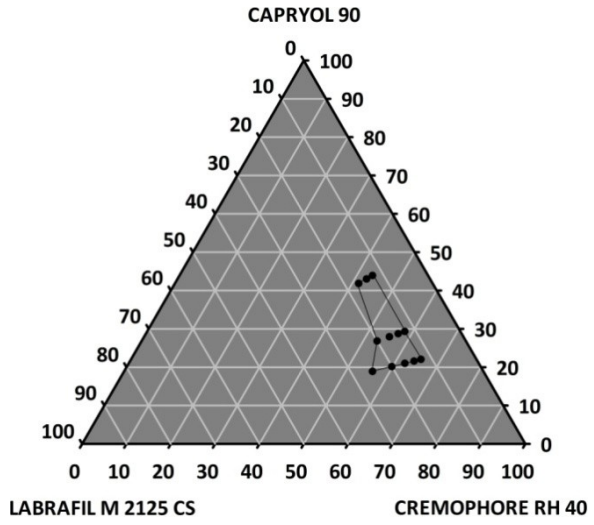

(C)

Figure 4-4: Ternary phase diagrams of combination (A) Cremophor RH 40 % - PEG 400 % - Labrafil M 2125 CS % (B) Cremophor RH 40 % - Transcutol P % - Labrafil M 2125 CS % and (C) Cremophor RH 40 % - Capyrol 90 % - Labrafil M 2125 CS %

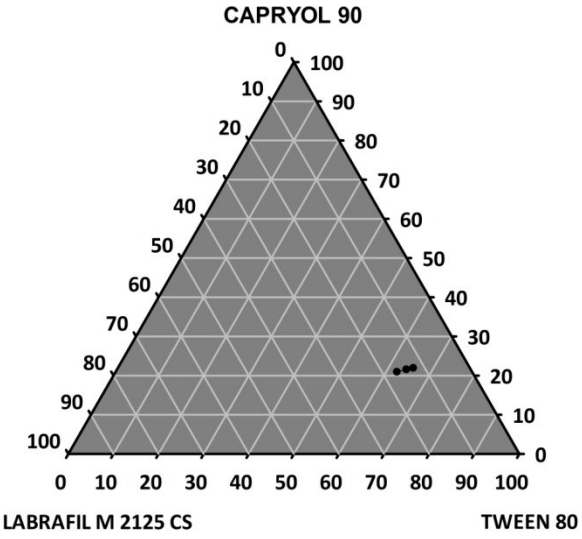

(A)

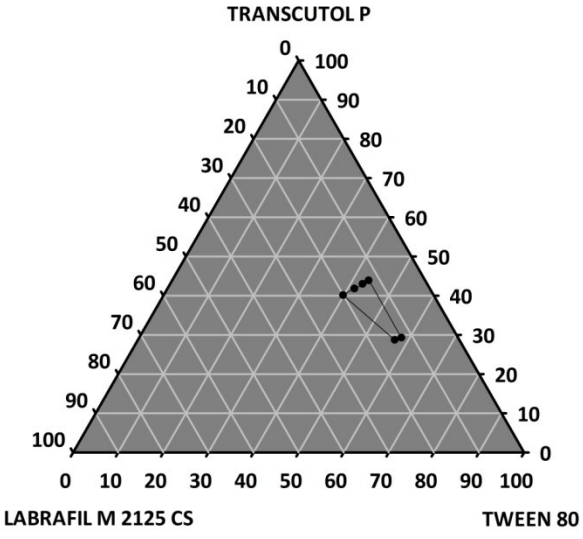

(B)

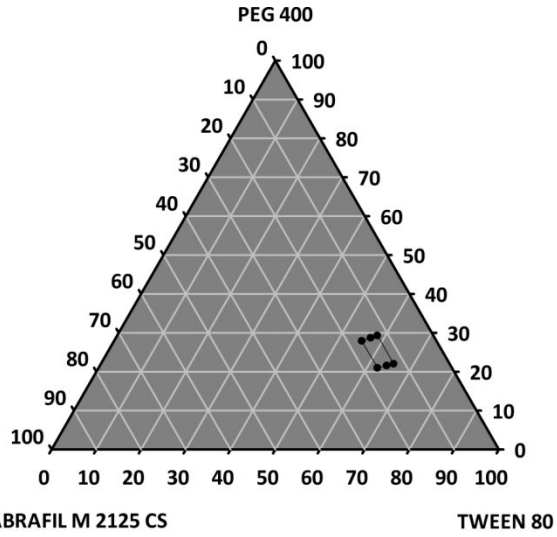

(C)

Figure 4-5: Ternary phase diagrams of combination (A) Tween 80 % - Capyrol 90 % - Labrafil M 2125 CS % (B) Tween 80 % - Transcutol P % - Labrafil M 2125 CS % and (C) Tween 80 % - PEG 400 % - Labrafil M 2125 CS %

4.3 Characterization of liquid SNEDDS

4.3.1 Droplet size determination

Nanoemulsion droplet size plays a very important role in predicting the rate and extent of drug absorption [87]. In W/O emulsions, droplet size refers to the size of the dispersed oil droplet in the water phase. Smaller oil droplets can assist in rapid breakdown of the triglycerides carrying the drug, leading to rapid drug release and drug absorption [88]. The results from the droplet size determination of blank and drug loaded SNEDDS are presented in table 4.3 The SNEDDS were passed through a 0.2 µm Nalgene® syringe filter and the diameter of the filtered SNEDDS were also determined (table 4.3).

Table 4.3: Droplet sizes obtained for drug loaded and blank SNEDDS

Formulation	**Scattering angle (degrees)**	**Droplet size (nm) (n = 3, ± S.D.)**
Cremophor RH 40 PEG 400 Oil	60	14.7 ± 0.8
	90	18.5 ± 0.6
	120	13.3 ± 0.5
Cremophor RH 40 PEG 400 Oil (Filtered through 0.2µm filter)	90	18.3 ± 0.7
Cremophor RH 40 PEG 400 Oil + Carbamazepine	90	18.6 ± 0.3

The blank nanoemulsion was measured at different scattering angles to predict the shape of the droplets. The droplet size distribution at scattering angles 60°, 90° and 120° is presented in Figure 4-6, 4.7 and 4.8, respectively. The droplet size distributions of filtered blank nanoemulsion and CBZ loaded nanoemulsion, both at scattering angle 90°, are presented in figures 4.9 and 4.10, respectively. No significant difference in the droplet size and size distribution between the blank and drug loaded formulations was observed. Furthermore, the Chi-square values were below the cut-off value (suggested by the instrument's manufacturer) indicating a unimodal population or monodispersity [89].

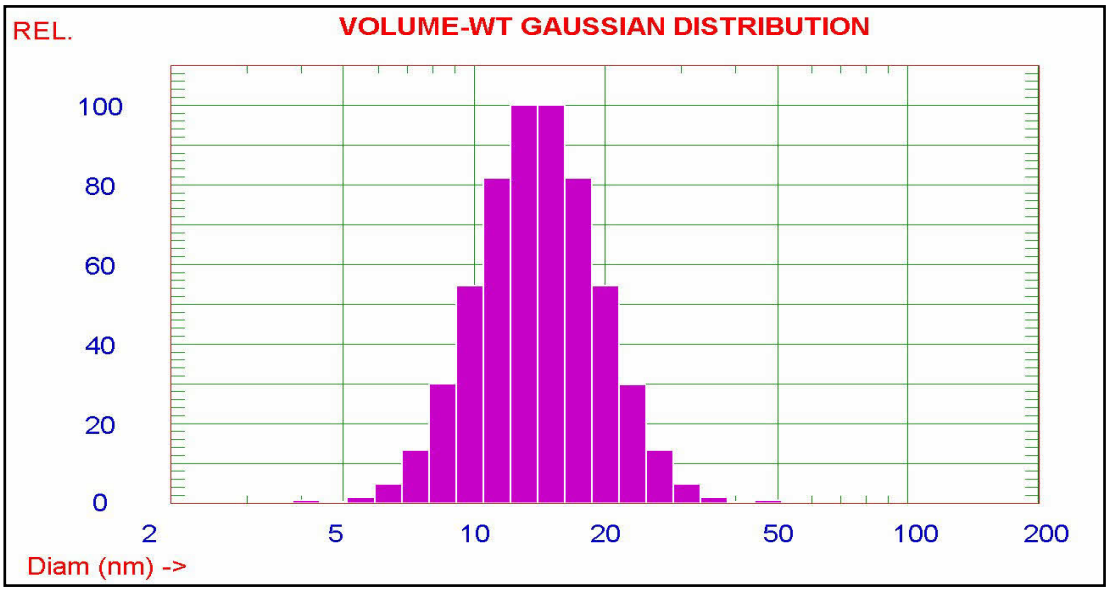

Figure 4-6: Droplet size distribution of blank nanoemulsion at 60^0 scattering angle

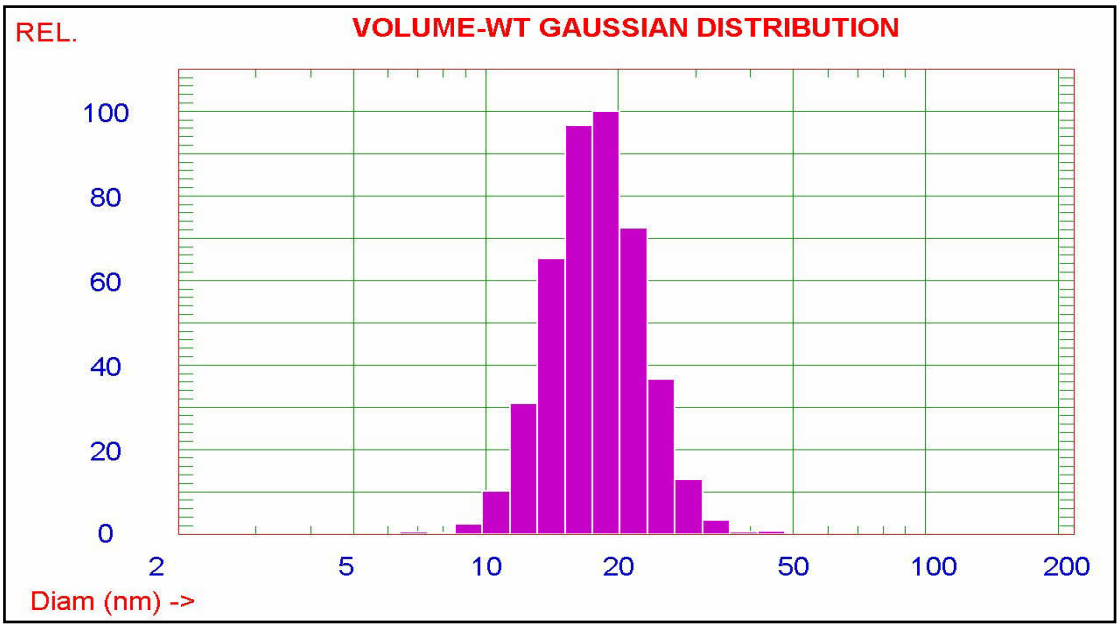

Figure 4-7: Droplet size distribution of blank nanoemulsion at 90^0 scattering angle

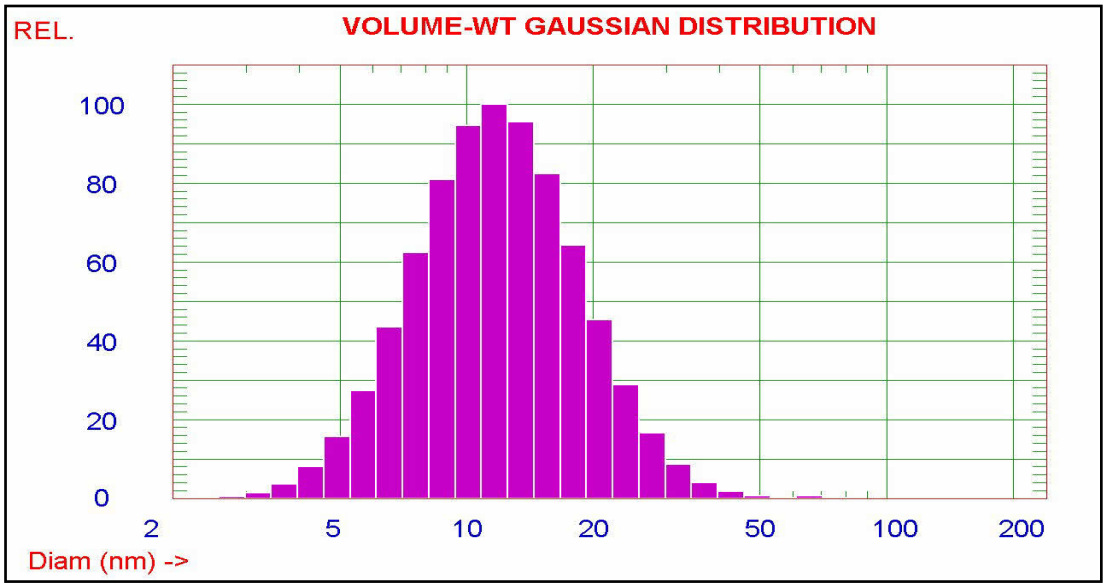
REL.
VOLUME-WT GAUSSIAN DISTRIBUTION
100
80
60
40
20
0
2
5
10
20
50
100
200
Diam (nm) ->
REL.
VOLUME-WT GAUSSIAN DISTRIBUTION
100
80
60
40
20
0
2
5
10
20
50
100
200
Diam (nm) ->
Figure 4-8: Droplet size distribution of blank nanoemulsion at 120^0 scattering angle
Figure 4-9: Droplet size distribution of blank nanoemulsion after filteration at 90^0 scattering angle

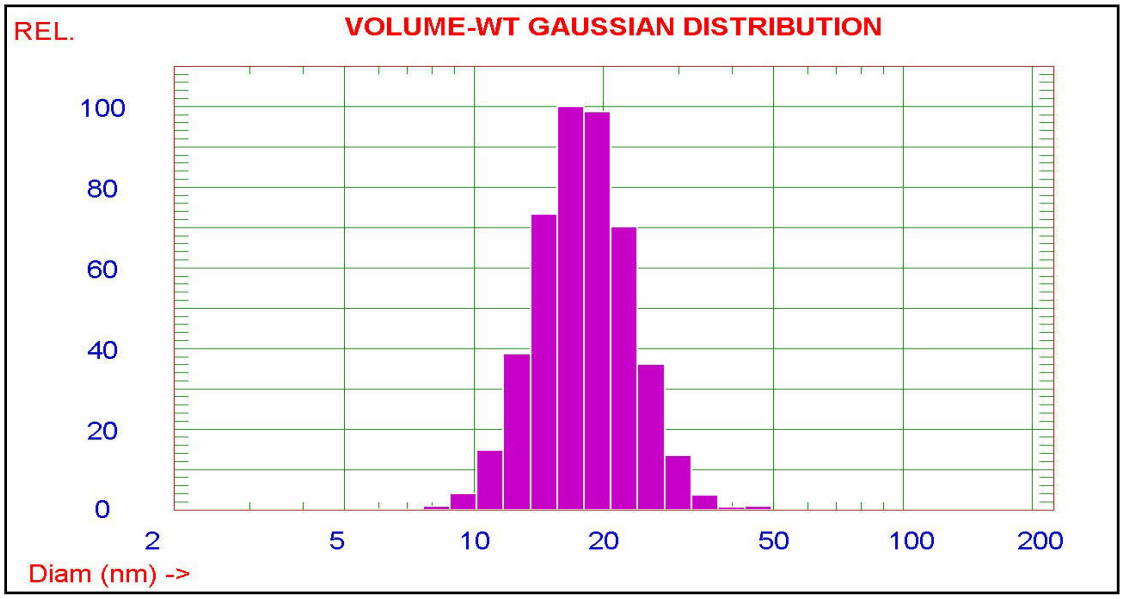

4.3.2 Zeta potential measurements

The zeta potential which is the charge on the surface of the droplets may affect its interaction with the cells in the RT. Therefore, the zeta potential can influence the bioavailability of the formulation. Positively charged droplets have been found to be more effective in delivering lipid drugs by enhancing the cellular binding [90]. In the present study, the zeta potential of the final formulation (without drug) was found to be zero indicating a neutral charge as all the excipients used were non-ionic (Figure 4-11). Zeta potential of the drug loaded nanoemulsion was also found to be zero indicating that drug loading did not result in change in zeta potential of droplets (Figure 4-12).

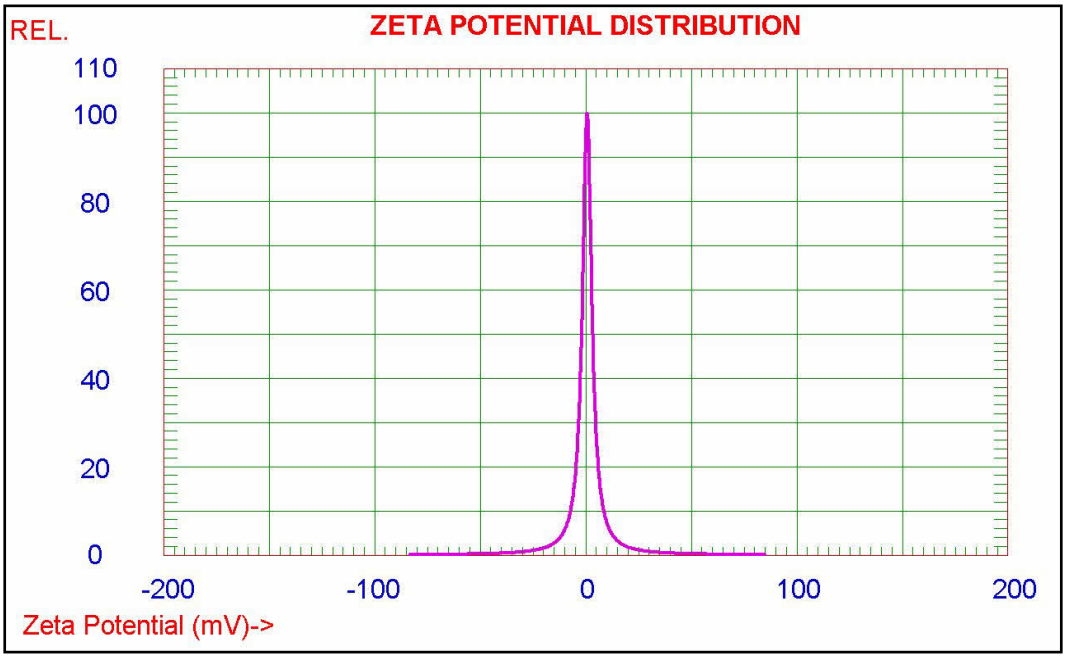

Figure 4-11: Zeta potential of blank nanoemulsion.

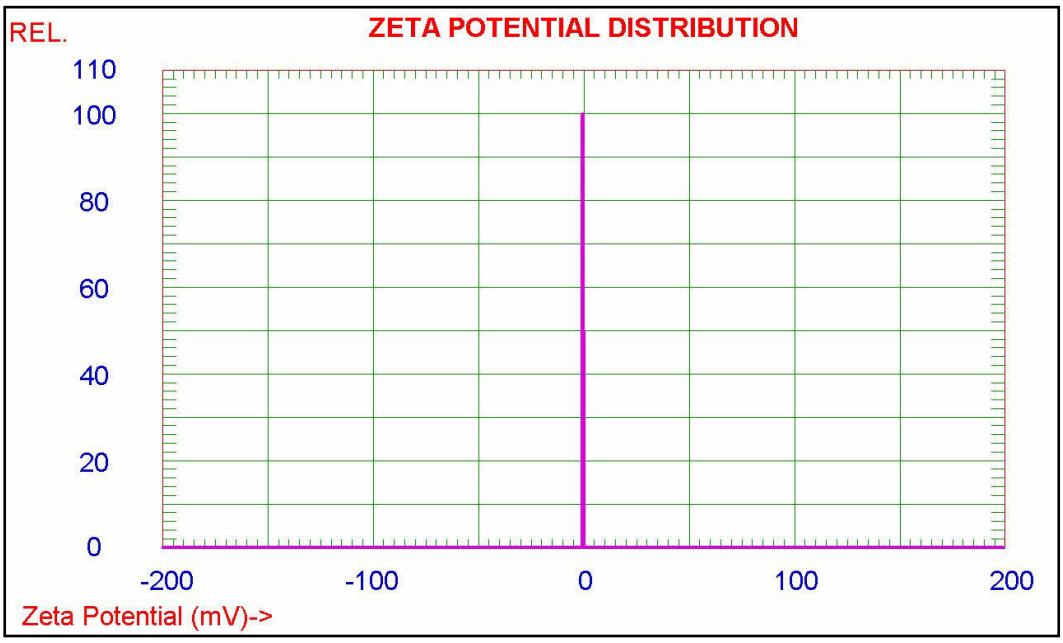

Figure 4-12: Zeta potential of CBZ containing nanoemulsion.

4.3.3 Thermodynamic properties

The crystalline nature of carbamazepine was confirmed by DSC thermograms (Figure 4-13). The drug exhibited a sharp melting endotherm at an onset temperature of 189^{0}C with a peak temperature of 192^{0}C. The heat of fusion was found to be 105.4348 J/g. The blank SNEDDS did not show any peak in the temperature range studied (Figure 4-14) and drug loaded SNEDDS (Figure 4-15) did not show any peaks under the temperature range studied indicating that CBZ was present in an amorphous or molecular dispersion form [91].

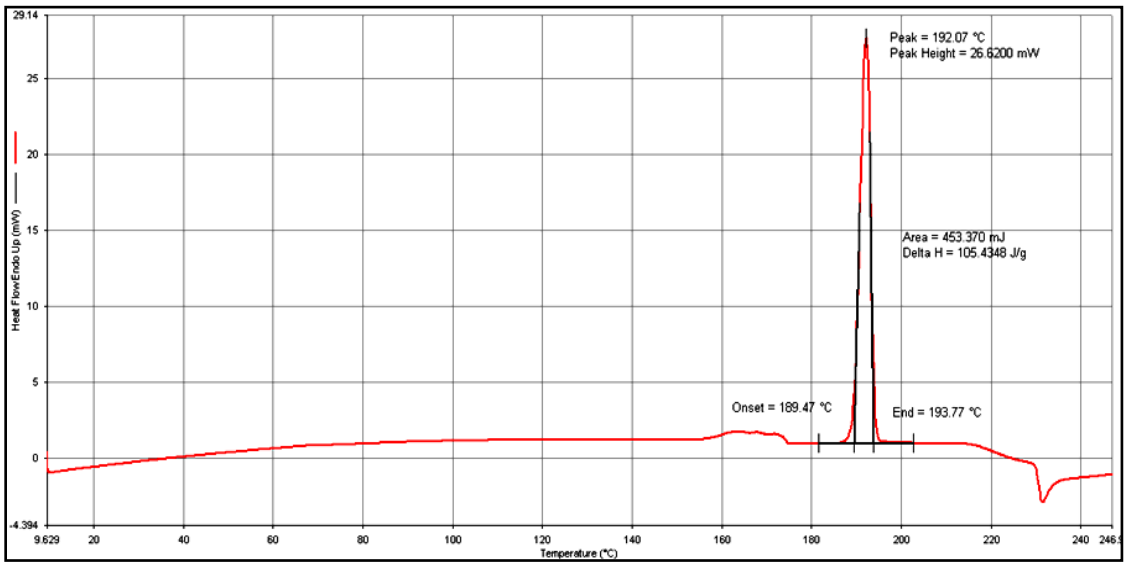

Figure 4-13: DSC thermogram of carbamazepine

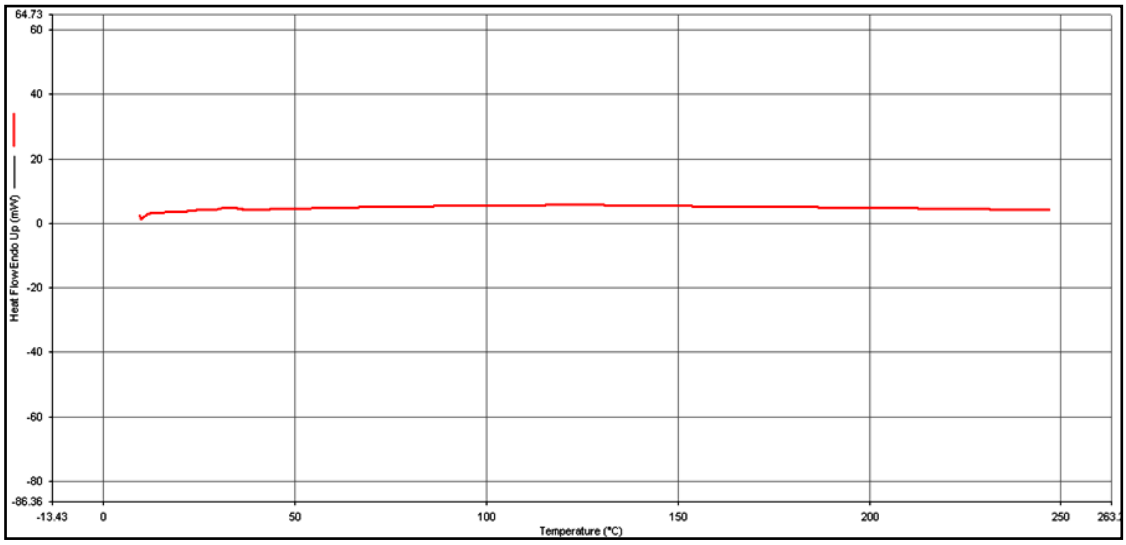

Figure 4-14: DSC of SME mixture devoid of drug

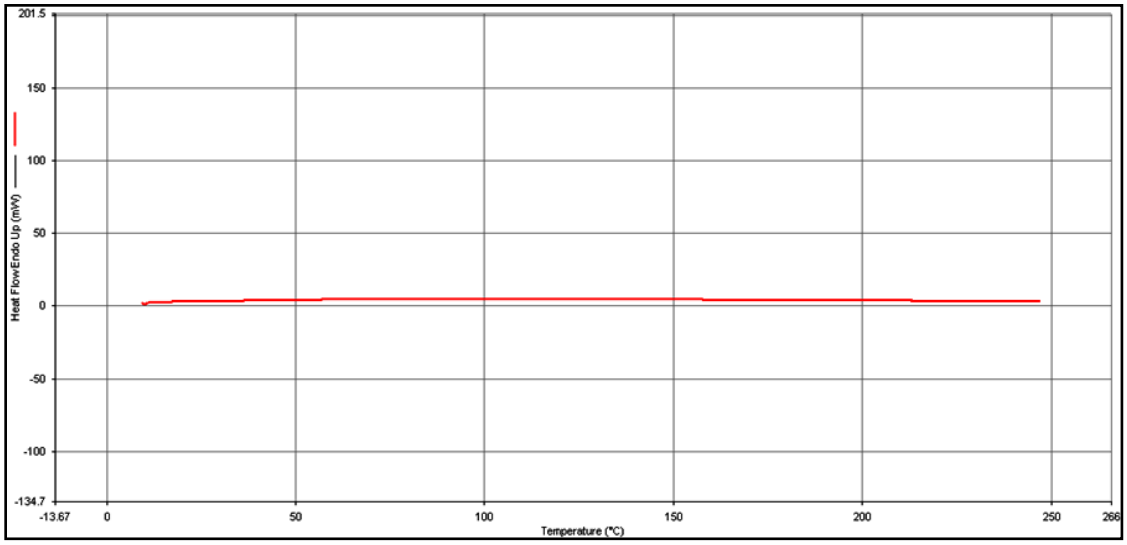

Figure 4-15: DSC of carbamazepine containing SME mixture

4.3.4 TEM images

Transmission electron microscopy (TEM) was used to study the morphology of the nanoemulsion droplets by visualizing the internal matrix and the shape of the individual droplets. The droplet size of both blank droplets without drug (Figure 4-16) and drug loaded droplets (Figure 4-17) was found to be larger than that determined using DLS. A possible reason for this could be spreading of the droplets on the grids when observed under TEM.

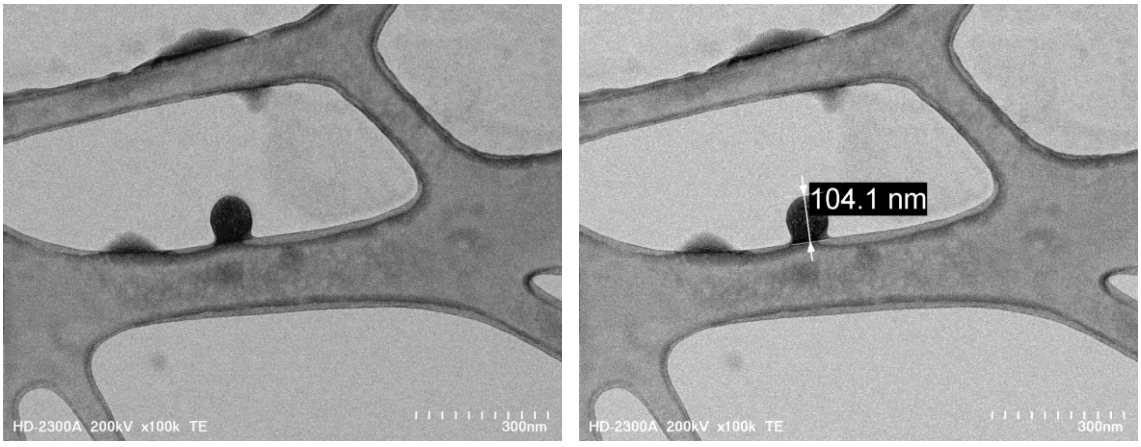

Figure 4-16: Representative TEM images of blank SNEDDS. Droplets appear black adsorbed on holey carbon support (white).

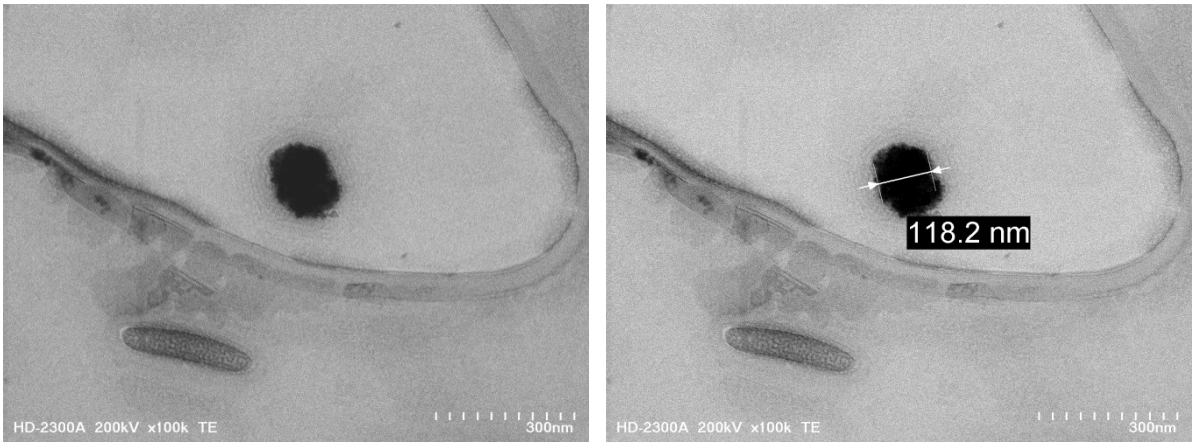

Figure 4-17: Representative TEM images of CBZ loaded SNEDDS. Droplets appear black adsorbed on holey carbon support (white).

4.4 Validation of sterility

Blank formulations were tested for sterility using direct inoculation as well as plate inoculation method. Fluid Thioglycollate Medium (FTM) was used for the detection of anaerobic bacteria while Soybean Casein Digest Medium (SCD) was used for the detection of fungi and aerobes [92]. All test tubes from the direct inoculation method remained clear throughout the 14 days test period, except for the positive controls and positive sample controls (Figure 4-18).

Figure 4-18: FTM tubes showing sample, positive sample control, positive control and negative control tubes, respectively after 24 hours of inoculation.

The samples were stored at 35^0C, which resembled body temperature and promoted the growth of aerobic and anaerobic bacteria. Growth of fungi was detected by storing the samples at 20^0C instead of 35^0C. Table 4.4 summarizes the presence or absence of microbial growth as observed in the plate method.

Table 4.4: The of presence (+) or absence (-) of growth in MH plates on day 0, 7 and 14

	Negative control	Positive control	Positive sample control	Sample
Day 0				
FTM	−	+	+	−
SCD 30-35°C	−	+	+	−
SCD 20°-25C.	−	+	+	−
Day 7				
FTM	−	+	+	−
SCD 30-35°C	−	+	+	−
SCD 20°-25C.	−	+	+	−
Day 14				
FTM	−	+	+	−
SCD 30-35°C	−	+	+	−
SCD 20°-25C.	−	+	+	−

Microbial growth was observed in all the positive and positive sample control plates as expected. Plates with the samples (nanoemulsion) did not show any growth on days 0, 7 and 14. These results confirmed that sterilfiltration and aseptic processing can be used to prepare sterile nanoemulsions.

4.5 Cell toxicity

MTT colorimetric assay was used to examine the *in vitro* toxicity of the optimal formulation in mouse embryonic fibroblast cells. The assay relies on the ability of viable cells to metabolize tetrazolium salt present in MTT reagent to purple formazan product [93]. The absorbance in the wells were measured to obtain quantifiable values. Higher absorbance value is directly related to the amount of formazan present in a particular well resulting in a more intense purple color. This indicates the presence of a higher number of viable cells in the well. Table 4.5 summarizes the results of one way ANOVA test which was used to compare the absorbance of sample containing wells against the control wells.

Table 4.5: Single factor ANOVA test for comparing cell viability of nanoemulsion containing wells against the control wells

Anova: Single Factor

Groups	*Count*	*Sum*	*Average*	*Variance*
Control	4	0.8963	0.2240	0.0004
11%	4	0.6068	0.1517	0.0002
5.5%	4	0.7724	0.1931	0.0004
0.50%	4	1.0928	0.2732	0.0003
0.25%	4	1.2144	0.3036	0.0008
0.125%	4	1.2140	0.3035	3.72E-05

ANOVA (11%)

Source of Variation	*SS*	*df*	*MS*	**F**	**P-value**	**F crit**
Between Groups	0.01048	1	0.01048	**32.3264**	**0.00128**	**5.98738**
Within Groups	0.00194	6	0.00032			
Total	0.01242	7				

ANOVA (5.5%)

Source of Variation	*SS*	*df*	*MS*	**F**	**P-value**	**F crit**
Between Groups	0.00192	1	0.00192	**4.86342**	**0.06959**	**5.98738**
Within Groups	0.00237	6	0.00039			
Total	0.00429	7				

ANOVA (0.5%)

Source of Variation	*SS*	*df*	*MS*	**F**	**P-value**	**F crit**
Between Groups	0.004827	1	0.004827	**12.89099**	**0.011498**	**5.987378**
Within Groups	0.002246	6	0.000374			
Total	0.007073	7				

ANOVA (0.25%)

Source of Variation	*SS*	*df*	*MS*	**F**	**P-value**	**F crit**
Between Groups	0.012648	1	0.012648	**21.74053**	**0.003458**	**5.987378**
Within Groups	0.003491	6	0.000582			
Total	0.016139	7				

ANOVA (0.125%)

Source of Variation	*SS*	*df*	*MS*	**F**	**P-value**	**F crit**
Between Groups	0.012617	1	0.012617	**55.99327**	**0.000294**	**5.987378**
Within Groups	0.001352	6	0.000225			
Total	0.013969	7				

Based on statistical F-test results, it was found that 11% nanoemulsion concentration was toxic to the cells. In all the other nanoemulsion containing wells the means did not significantly differ from the controls confirming that the optimal formulation was non-toxic to cells at a concentration of 0.5 % or lower.

The cell death and viability were also confirmed by microscopic examinations of the petri dishes containing positive control, 11% sample concentration and 0.5% sample concentration respectively (Figure 4-19).

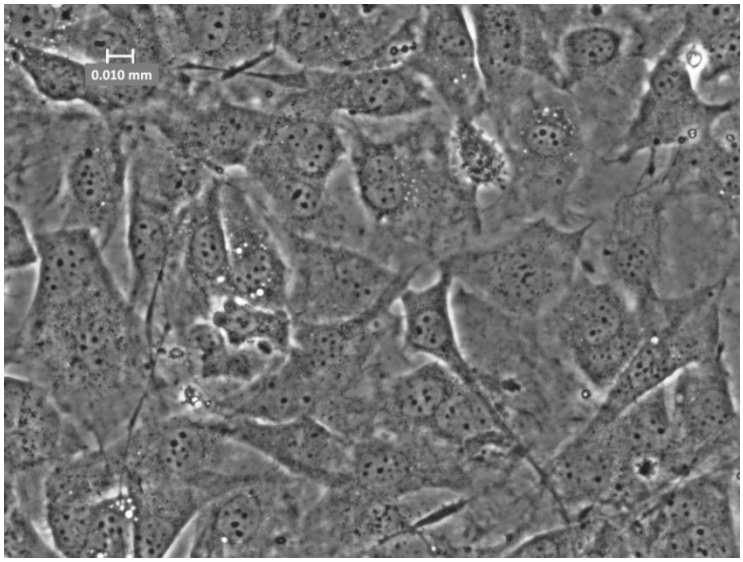

(A)

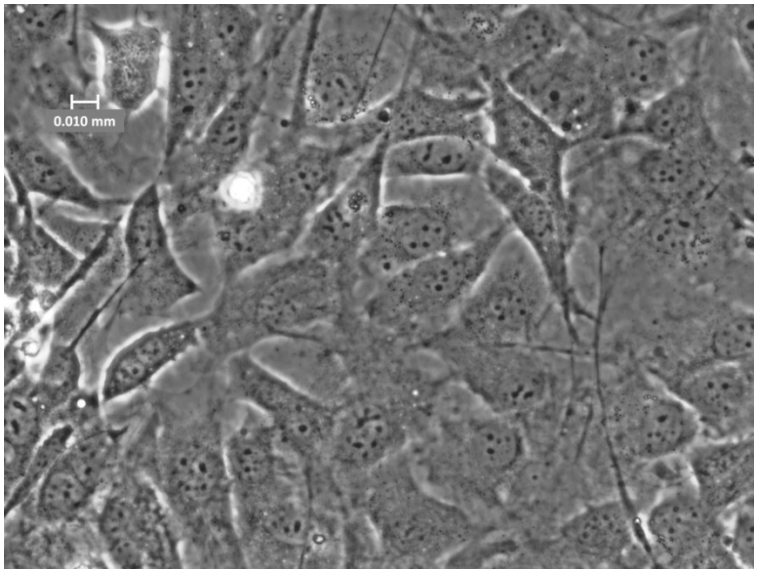

(B)

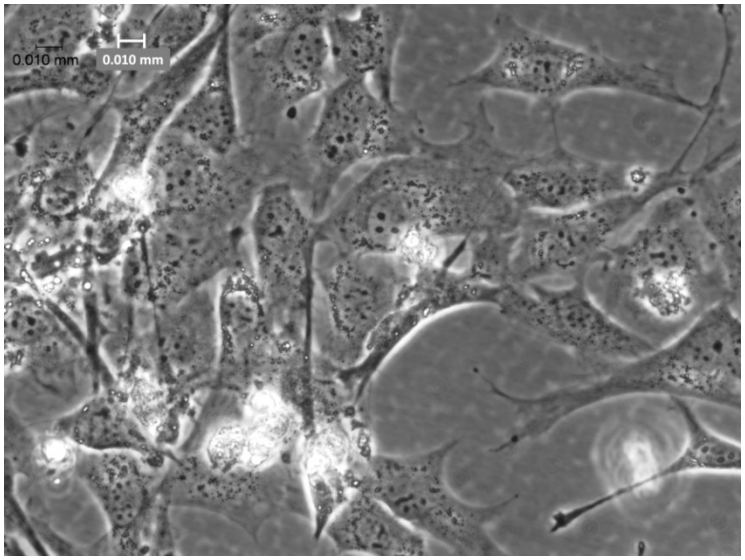

(C)

Figure 4-19: Petri dishes as observed under a light microscope: (A) positive control, (B)11% sample concentration, (C) 0.5% sample concentration

It can be seen from the microscopic images of the petri dishes that 11% sample concentration resulted in significant cell death as more cell debris and lesser cell density was observed. 0.5% sample concentration did not result in significant cell death since observed cell density appeared closer to the cell density of the untreated positive control.

4.6 Characterization of nebulized SNEDDS (mist)

4.6.1 Droplet size distribution of the mist

Droplets of size less than 5 µm have traditionally been used for alveolar delivery [94]. Normally, droplet size of ≤ 4.8 µm comes under the category of respirable range [25]. Thus, to avoid deposition of droplets in the upper airway and to ensure the delivery of the formulation to the desired site inside the lung, droplet size has to be < 5µm [95]. In the present study, mean diameter of the blank nanoemulsion mist devoid of drug was found to be 4.80µm (Figure 4-20) while that containing CBZ was found to be 4.0µm (Figure 4-21). Hence, the suitability of the formulation for pulmonary delivery was confirmed as the droplet sizes were found to be ≤ 4.8 µm

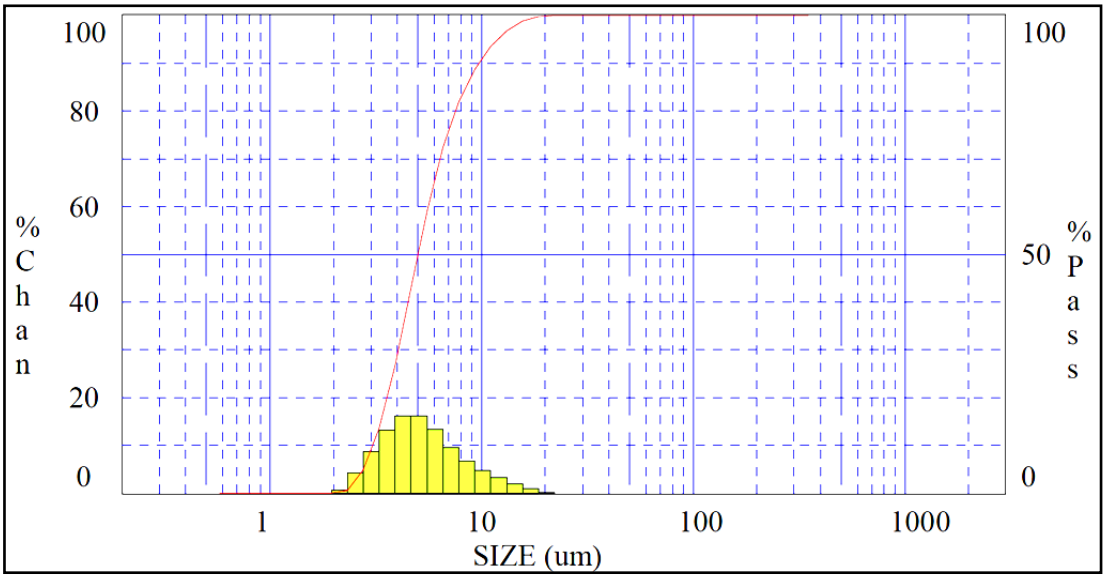

Figure 4-20: Droplet size distribution of blank nanoemulsion mist

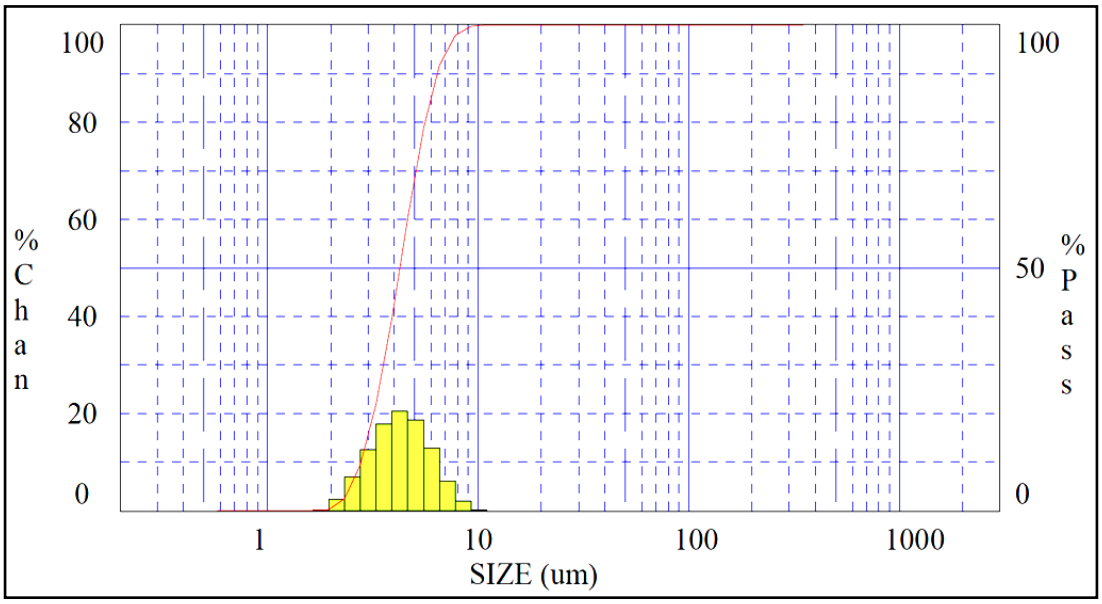

Figure 4-21: Droplet size distribution of CBZ loaded nanoemulsion mist

4.6.2 TEM images of the mist

The spreading of droplets on TEM grids observed in section 4.4.4 was again observed in the case of the SNEDDS mist. Figure 4-22 and Figure 4-23 shows the TEM picture of blank SNEDDS mist devoid of any drug and TEM picture of drug containing SNEDDS mist, respectively.

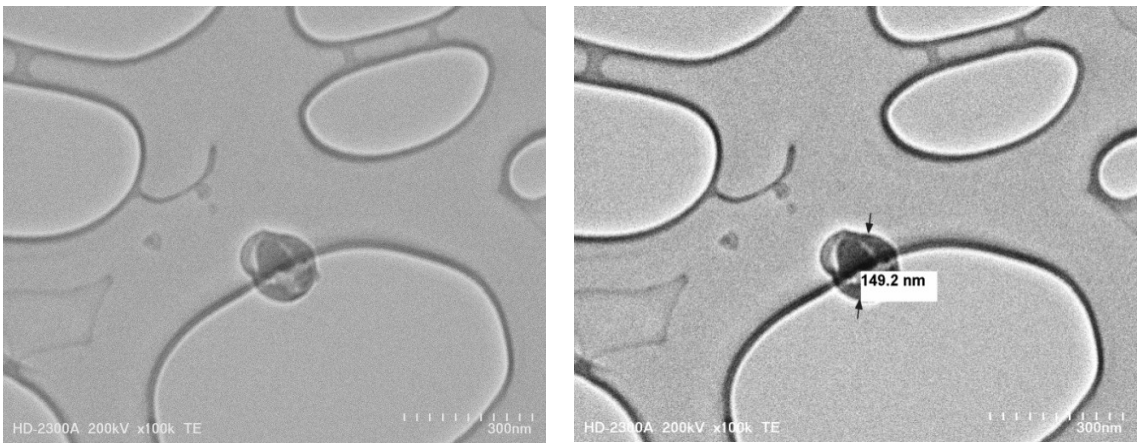

Figure 4-22: TEM images of blank SNEDDS mist

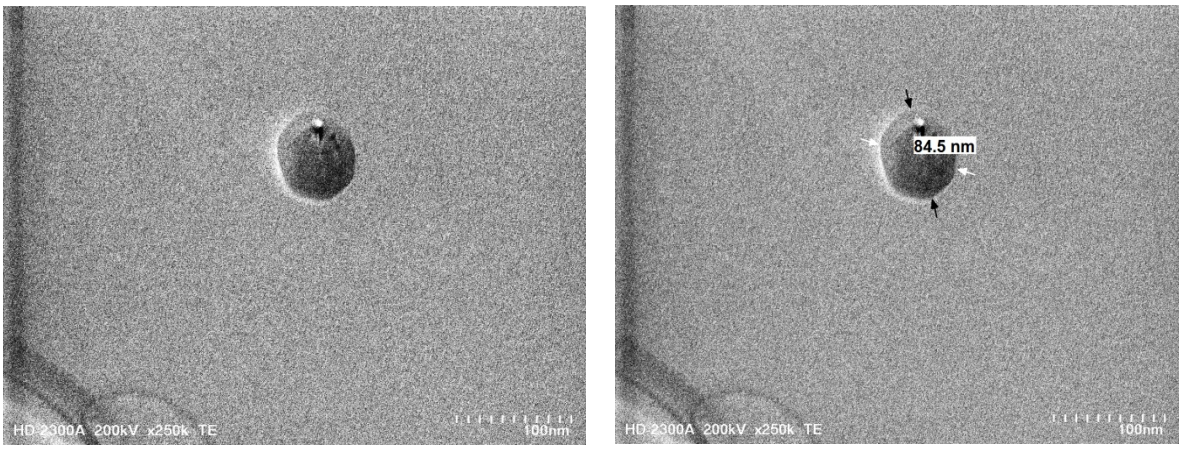

Figure 4-23: TEM images of drug loaded SNEDDS mist

Mist was deposited on the TEM grids as discussed in section 3.2.13. The overnight drying of grids evaporated deposited water and leaving behind only the dispersed oil droplets.

The spreading of droplets on TEM grid could be attributed to the surfactant and cosurfactant layer surrounding the droplet as the surfactants are good spreading and

wetting agents too. Nonetheless, the integrity of the SNEDDS droplets was confirmed by TEM as the droplet size and shape for liquid and nebulized nanoemulsions were found to be similar.

4.7 Histological analysis

Histology is the study of the microscopic anatomy of cells and tissues of plants and animals [96]. In the current study, the technique was used to examine the diffusion of the fluorescent dye labeled nanoemulsion through the porcine lung tissue. Sudan IV was incorporated in the nanoemulsion in order to make the nanoemulsion droplets fluoresce under a fluorescent microscope. Cryotome sections were carefully studied under a fluorescent microscope to detect the presence of nanoemulsion inside the tissue.

4.7.1 Dye solubility determination

The solubility of Sudan IV in individual excipients forming the nanoemulsion was determined using a UV-Vis spectrophotometer. The dye showed very good solubility in the oil and practically no solubility in water. Table 4.6 summarizes the solubility of Sudan IV in various excipients.

Table 4.6: Solubility of Sudan IV in excipients

Excipient	Solubility (mg/ml)
Cremophor RH 40	38.433 ± 3.4
Labrafil M 2125 CS	125.67 ± 11.2
PEG 400	178 ± 6.9
DMSO	497 ± 9.4
Water	Practically insoluble

Solubilities were determined by using a calibration curve of Sudan IV in DMSO plotted over a range of concentrations from 3 mg/ml to 20 mg/ml at 522 nm wavelength (Figure 4-24).

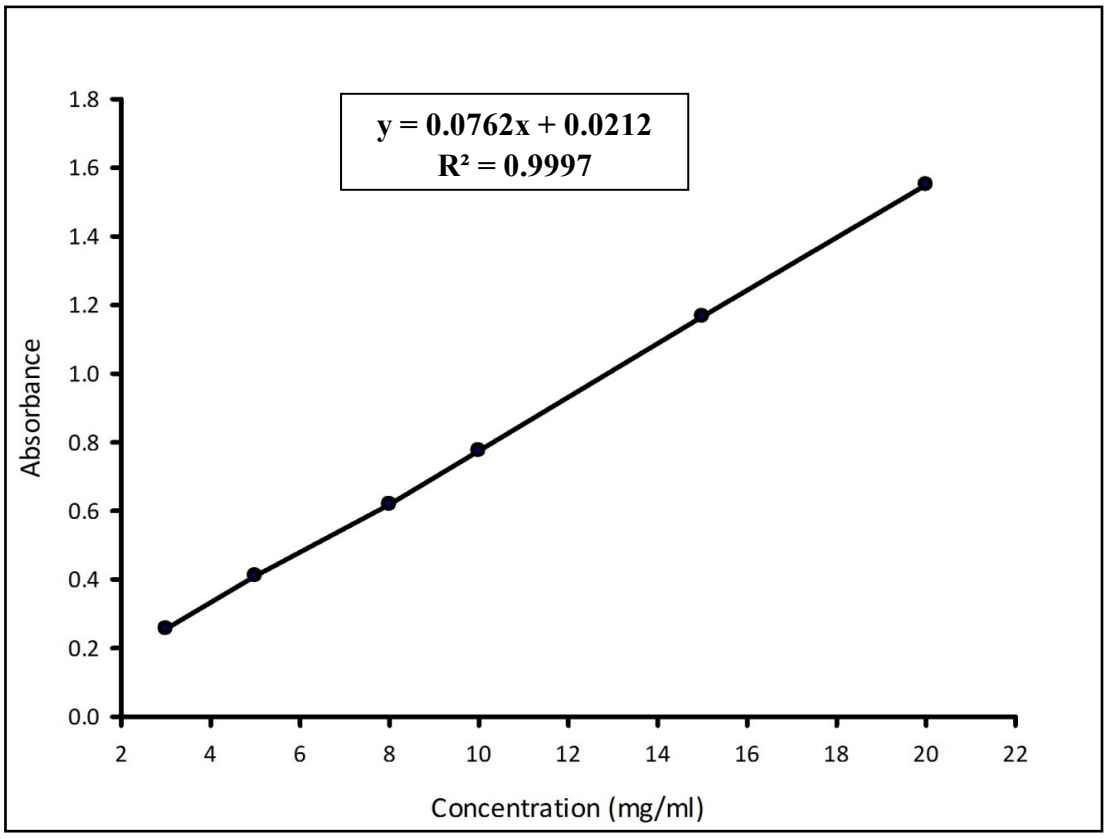

Figure 4-24: Calibration curve of Sudan IV in DMSO

4.7.2 Droplet size and zeta potential of dye loaded nanoemulsion

Droplet size and zeta potential determinations were used to characterize the dye loaded nanoemulsion.Droplet size was found to be 19 ± 2.1 nm (Figure 4-25) which was similar to the blank nanoemulsion devoid of drug (section 4.3.1). Zeta potential was found to be zero (Figure 4-26) as in the case of blank nanoemulsion indicating the absence of any free dye droplets. The incorporation of dye into the nanoemulsion did not alter the physicochemical properties (in terms of droplet size and zeta potential) of the nanoemulsion.

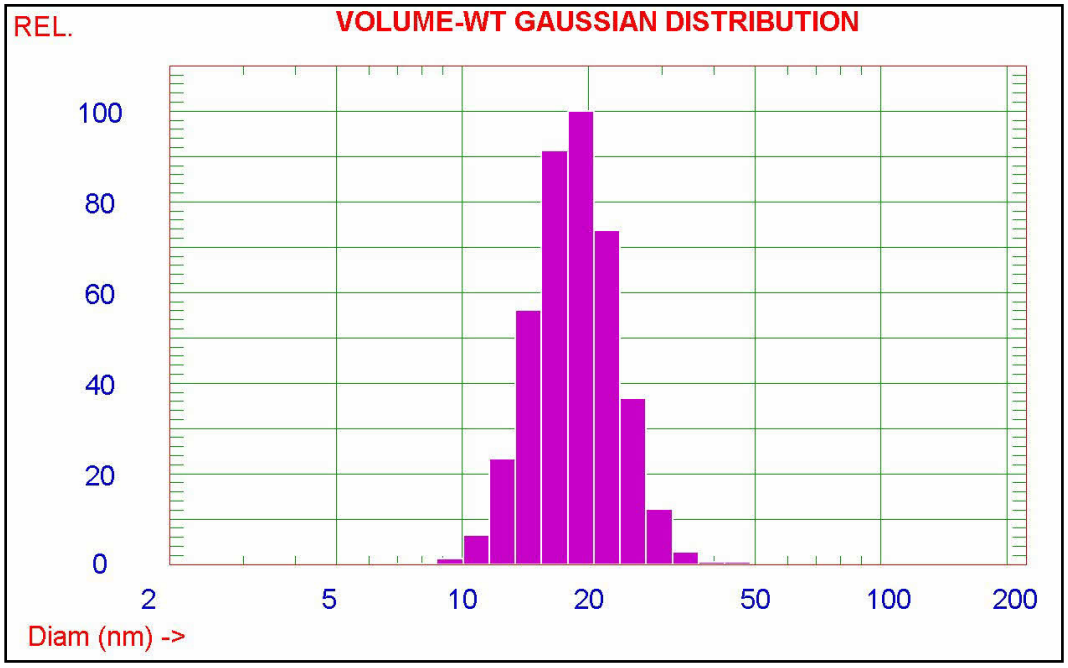

Figure 4-25: Droplet size distribution of Sudan IV containing SNEDDS

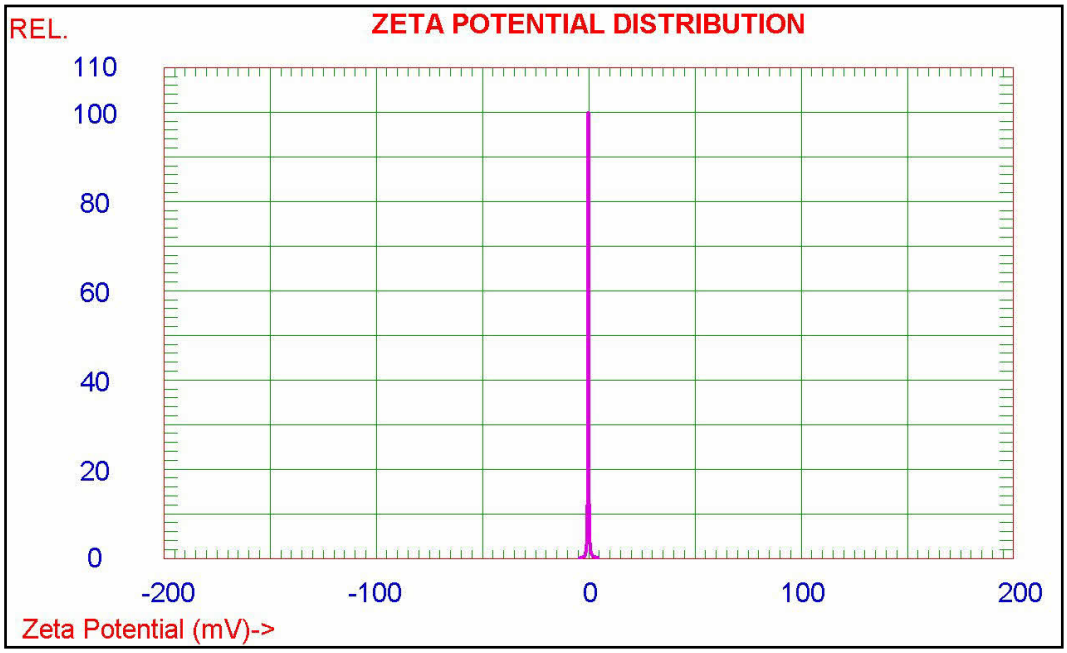

4.7.3 Microscopic examination of Cryosections

Thin sections of the tissue under study were mounted on a glass slide using DAPI. DAPI is a very specific stain for DNA and can stain nuclear and mitochondrial DNA [97]. When excited with a light of wavelength of around 390 nm, it fluoresces a bright blue color [98]. Since Sudan IV has a different fluorescent spectrum than DAPI it will exhibit a different fluorescent color (green) than DAPI under a fluorescent microscope. Tissue was exposed to PBS (negative control), blank nanoemulsion (i.e. without dye; positive control) and Sudan IV labeled nanoemulsion. Figure 4-27 – Figure 4-29 shows the tissues as observed under a fluorescent microscope.

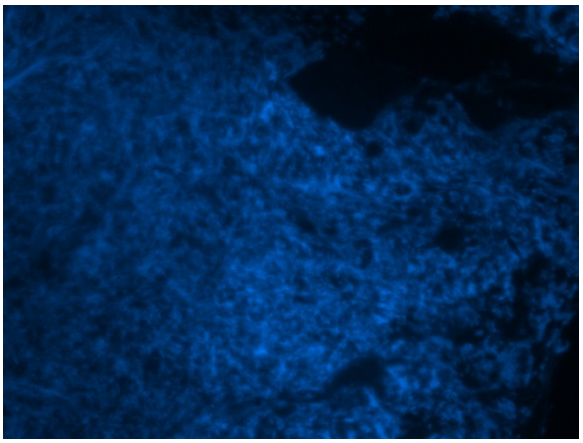

(A)

(B)

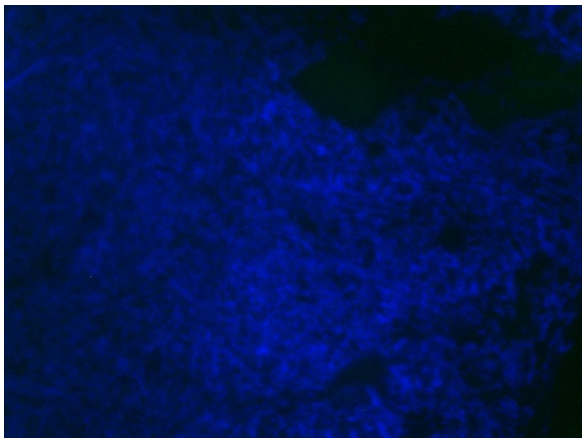

(C)

Figure 4-27: Negative control tissue under fluorescent microscope showing (A) Fluorescence by DAPI (B) absence of fluorescence in buffer (C) overlay spectra of DAPI and buffer

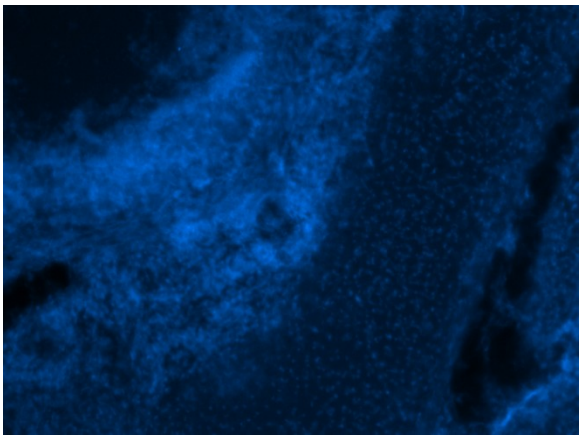

(A)

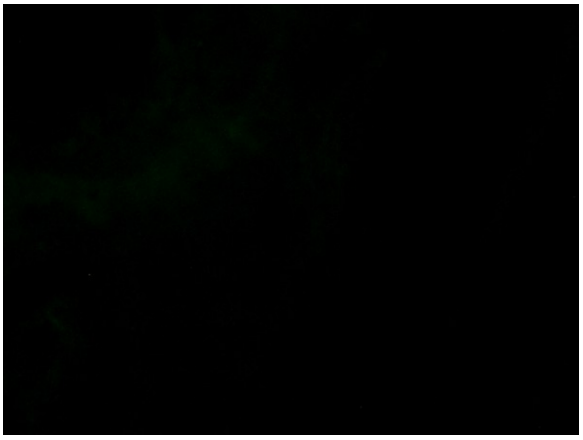

(B)

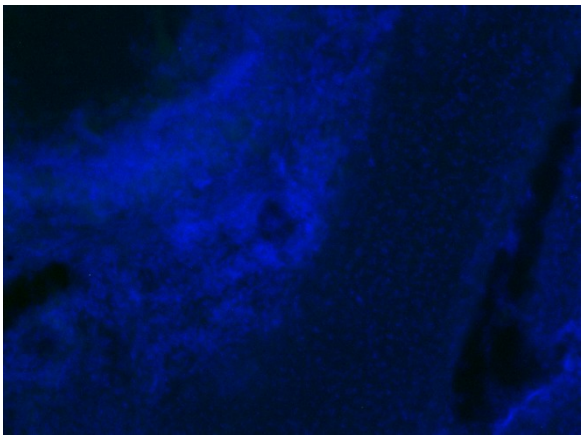

(C)

Figure 4-28: Positive control tissue under fluorescent microscope showing (A) fluorescence by DAPI (B) absence of fluorescence in blank nanoemulsion (C) overlay spectra of DAPI and blank nanoemulsion devoid of the dye

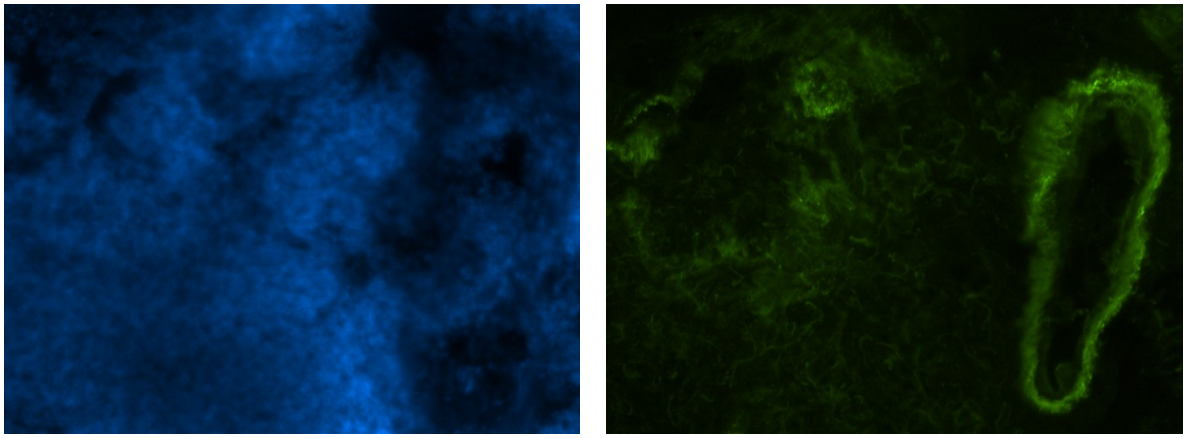

(A) (B)

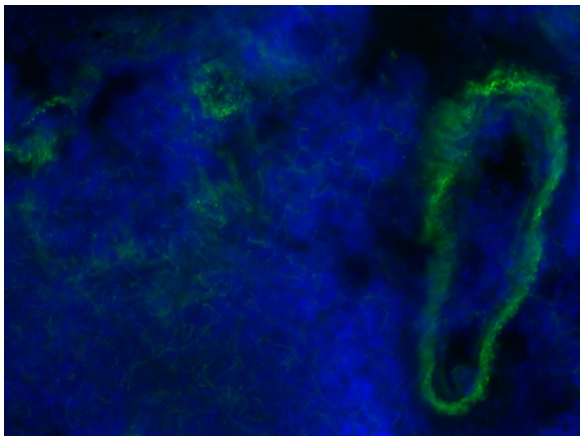

(C)

Figure 4-29: Sample tissue under microscope showing (A) fluorescence by DAPI (B) fluorescence by Sudan IV (C) overlay spectra of DAPI and Sudan IV containing nanoemulsion

The green fluorescence was only seen in tissues exposed to the Sudan IV contained nanoemulsions. Thus the presence of green fluorescence confirmed the penetration of dye inside the tissue and hence the nanoemulsion droplets containing them.

Chapter 5 – Conclusions

In this study, nanoemulsions were prepared using surfactant, cosurfactant and a long chain triglyceride. These self-nanoemulsifying systems were investigated for their potential for pulmonary drug delivery. Various lipid excipients in different combinations and amounts were evaluated for their self-nanoemulsifying properties based on emulsification times, droplets size and phase diagrams. The combination consisting of 50% Cremophor RH 40, 25% PEG 400 and 25% Labrafil M 2125 CS was selected as the optimal formmulation for drug incorporation. Nanoemulsions are known to improve the solubility of drugs included in class II of biopharmaceutical classification. Thus, carbamazepine was selected as a model drug for incorporation into the nanoemulsion as it possesses poor solubility characteristics. Carbamazepine (CBZ) loaded SNEDDS were prepared using the optimized formulation and were evaluated for self-nanoemulsification properties. Carbamazepine loaded SNEDDS were characterized using dynamic and electrophoretic light scattering, differential scanning calorimetry (DSC), and transmission electron microscopy (TEM). The droplet size of the nanoemulsion was found to be less than 20nm and a near zero zeta potential confirmed that drug incorporation did not have any effect on size and zeta potential of droplets. TEM pictures were used to study the nanoemulsion droplet morphology. The droplets were found to be spherical in shape with

a diameter of ~ 100nm. DSC confirmed that CBZ was present in a molecularly dissolved state. Sterility testing using *Staph. aureus* was conducted to confirm the ability to prepare sterile nanoemulsions. The toxicity of the formulation was evaluated on NIH 3T3 cell lines using MTT assay and biocompatibility of the formulation was evaluated.

The nanoemulsions were nebulized to check their potential for pulmonary drug delivery. Nanoemulsion mist was characterized using laser diffraction and TEM studies. Laser diffraction studies determined the droplet size of the mist to be ≤4.8µm, making them suitable for pulmonary delivery. TEM images confirmed the integrity of nanoemulsion droplet inside the mist. The droplets were able to retain the shape and size observed for liquid SNEDDS. SNEDDS were loaded with a fluorescent dye (Sudan IV) to visualize the permeation characteristics of the nanoemulsion through porcine lung tissue.

The objective of current study was to develop and optimize a novel SNEDDS to increase the solubility of poorly water soluble drugs. SNEDDS formed during current research showed good stability and showed potential for delivering poorly water soluble drugs belonging to BCS class II through pulmonary route.

Future studies would include establishing long term stability of the formulation and testing the formulation in animals to determine its suitability for clinical use.

References

1. Dahan, A. and A. Hoffman, *Rationalizing the selection of oral lipid based drug delivery systems by an in vitro dynamic lipolysis model for improved oral bioavailability of poorly water soluble drugs.* Journal of Controlled Release, 2008. **129**(1): p. 1-10.
2. Pouton, C.W., *Formulation of poorly water-soluble drugs for oral administration: Physicochemical and physiological issues and the lipid formulation classification system.* European Journal of Pharmaceutical Sciences, 2006. **29**(3-4): p. 278-287.
3. Pouton, C.W., *Formulation of self-emulsifying drug delivery systems.* Adv Drug Deliv Rev, 1997. **25**(1): p. 47-58.
4. Lawrence, M.J. and G.D. Rees, *Nanoemulsion-based media as novel drug delivery systems.* Adv Drug Deliv Rev, (0).
5. Lawrence, M.J. and G.D. Rees, *Nanoemulsion-based media as novel drug delivery systems.* Adv Drug Deliv Rev, 2000. **45**(1): p. 89-121.
6. Schulman, J.H., W. Stoeckenius, and L.M. Prince, *Mechanism of Formation and Structure of Micro Emulsions by Electron Microscopy.* The Journal of Physical Chemistry, 1959. **63**(10): p. 1677-1680.

7. Shinoda, K. and H. Kunieda, *Conditions to produce so-called nanoemulsions: Factors to increase the mutual solubility of oil and water by solubilizer.* Journal of Colloid And Interface Science, 1973. **42**(2): p. 381-387.

8. Ruckenstein, E. and R. Krishnan, *Effect of electrolytes and mixtures of surfactants on the oil-water interfacial tension and their role in formation of nanoemulsions.* Journal of Colloid And Interface Science, 1980. **76**(1): p. 201-211.

9. Constantinides, P.P., *Lipid nanoemulsions for improving drug dissolution and oral absorption: physical and biopharmaceutical aspects*. Pharm Res, 1995. **12**(11): p. 1561-72.

10. Kreuter, J., *Colloidal drug delivery systems*. Drugs and the pharmaceutical sciences. 1994, New York: M. Dekker. vii, 353 p.

11. Swenson, E.S., W.B. Milisen, and W. Curatolo, *Intestinal Permeability Enhancement: Efficacy, Acute Local Toxicity, and Reversibility.* Pharmaceutical Research, 1994. **11**(8): p. 1132-1142.

12. Kimura, M., et al., *Relationship between the Molecular Structures and Emulsification Properties of Edible Oils.* Bioscience, biotechnology, and biochemistry, 1994. **58**(7): p. 1258-1261.

13. Sekine, M., et al., *Improvement of bioavailability of poorly absorbed drugs. IV. Mechanism of the promoting effect of medium chain glyceride on the rectal absorption of water soluble drugs.* J Pharmacobiodyn, 1985. **8**(8): p. 645-52.

14. Amidon, G.L., et al., *A Theoretical Basis for a Biopharmaceutic Drug Classification: The Correlation of in Vitro Drug Product Dissolution and in Vivo Bioavailability.* Pharmaceutical Research, 1995. **12**(3): p. 413-420.

15. Kawashima, Y., et al., *Pulmonary delivery of insulin with nebulized DL-lactide/glycolide copolymer (PLGA) nanospheres to prolong hypoglycemic effect.* J Control Release, 1999. **62**(1-2): p. 279-87.

16. Harrison, L.I., et al., *Comparative absorption of inhaled and intramuscularly administered atropine.* Am Rev Respir Dis, 1986. **134**(2): p. 254-7.

17. Bouhuys, A., *The physiology of breathing: a textbook for medical students*. 1977: Grune & Stratton.

18. Patton, J.S. and R.M. Platz, *(D) Routes of delivery: Case studies.* Adv Drug Deliv Rev, 1992. **8**(2-3): p. 179-196.

19. Levitzky, M.G., *Pulmonary Physiology*. 1986: McGraw-Hill.

20. Medicine, U.S.N.L.o. *Module I: Introduction to Toxicology and Dose-Response*. 2010; Available from: http://toxlearn.nlm.nih.gov/htmlversion/images/5_4_lungs_labeled.jpg.

21. Schanker, L.S. and M.J. Less, *Lung pH and pulmonary absorption of nonvolatile drugs in the rat.* Drug Metab Dispos, 1977. **5**(2): p. 174-8.

22. Gonda, I., *STUDY OF THE EFFECTS OF POLYDISPERSITY OF AEROSOLS ON REGIONAL DEPOSITION IN THE RESPIRATORY TRACT.* Journal of Pharmacy and Pharmacology, 1981. **33**(S1): p. 52P-52P.

23. Byron, P.R., *Prediction of drug residence times in regions of the human respiratory tract following aerosol inhalation.* J Pharm Sci, 1986. **75**(5): p. 433-8.

24. Ganderton, D., et al., *Drug delivery to the respiratory tract*. 1987: VCH.

25. Gupta, P.K. and A.J. Hickey, *Contemporary approaches in aerosolized drug delivery to the lung.* Journal of Controlled Release, 1991. **17**(2): p. 127-147.

26. Kim, C.S., M.A. Eldridge, and M.A. Sackner, *Oropharyngeal deposition and delivery aspects of metered-dose inhaler aerosols.* Am Rev Respir Dis, 1987. **135**(1): p. 157-64.

27. Dalby, R. and J. Suman, *Inhalation therapy: technological milestones in asthma treatment.* Adv Drug Deliv Rev, 2003. **55**(7): p. 779-791.

28. Kleinstreuer, C., Z. Zhang, and J.F. Donohue, *Targeted drug-aerosol delivery in the human respiratory system.* Annu Rev Biomed Eng, 2008. **10**: p. 195-220.

29. Prokopovich, P., et al., *Friction in ultra-thin conjunction of valve seals of pressurised metered dose inhalers.* Wear, 2010. **268**(5-6): p. 845-852.

30. *United States Pharmacopeia 29- Natianal Formulary 24*, in *Pharmacopeial Forum: Vol no. 20(4)*. 1979, United States Pharmacopeial Convention, Inc.: Rockville, Md. p. v.

31. Bell, J.H., P.S. Hartley, and J.S.G. Cox, *Dry powder aerosols I: A new powder inhalation device.* Journal of Pharmaceutical Sciences, 1971. **60**(10): p. 1559-1564.

32. Wetterlin, K., *Turbuhaler: a new powder inhaler for administration of drugs to the airways.* Pharm Res, 1988. **5**(8): p. 506-8.

33. Pecora, R., *Dynamic light scattering : applications of photon correlation spectroscopy*. 1985, New York: Plenum Press. xiv, 420 p.

34. Gilman, A. and A. Lloyd, *Dynamic light scattering*, in *University of Minnesota, methods of experimental physics laboratory*. 2005.

35. Xu, R., *Particle Characterization: Light Scattering Methods*. 2000: Springer.

36. Merkus, H.G., *Particle Size Measurements: Fundamentals, Practice, Quality.*

37. Particle Sizing Systems, I. *Nicomp 380 DLS User Manual*. 2006; Available from: http://www.ims.uconn.edu/facilities/themal_pss-380-manual.pdf.

38. Koppel, D.E., *Analysis of Macromolecular Polydispersity in Intensity Correlation Spectroscopy: The Method of Cumulants.* The Journal of Chemical Physics, 1972. **57**(11): p. 4814-4820.

39. Sinko, P.J. and A.N. Martin, *Martin's physical pharmacy pharmaceutical sciences : physical chemical principles in the pharmaceutical sciences*. 2006, Philadelphia: Lippincott Williams & Wilkins.

40. Metzler, R. and J. Klafter, *Accelerating Brownian motion: A fractional dynamics approach to fast diffusion.* EPL (Europhysics Letters), 2000. **51**(5).

41. Optical Engineering Laboratories, U.o.W. *Laser Doppler Anemometry*. 2002; Available from: http://www.eng.warwick.ac.uk/oel/courses/turbine/LDA.htm.

42. Swarbrick, J. and J.C. Boylan, *Encyclopedia of pharmaceutical technology*. 1988, New York: M. Dekker.

43. Patil, S., et al., *Protein adsorption and cellular uptake of cerium oxide nanoparticles as a function of zeta potential.* Biomaterials, 2007. **28**(31): p. 4600-4607.

44. Egerton, R.F., *Physical Principles of Electron Microscopy: An Introduction to TEM, SEM, and AEM*. 2005: Springer.

45. Cosslett, V.E., *The electron microscope*. 1947, [London: Sigma.

46. JEOL. *Japan Electron Opticla Laboratories*. 200; Available from: http://www2.warwick.ac.uk/fac/sci/physics/current/postgraduate/regs/mpags/ex5/techniques/structural/tem/tem_ed.jpg.

47. Bozzola, J.J. and L.D. Russell, *Electron microscopy : principles and techniques for biologists*. 1999, Sudbury, Mass. [u.a.]: Jones and Bartlett.

48. Azonano. *Transmission Electron Microscope - A Basic Look How TEMs Work*. 2006; Available from: http://www.azonano.com/article.aspx?ArticleID=1723.

49. Pan, Z.W., Z.R. Dai, and Z.L. Wang, *Nanobelts of Semiconducting Oxides.* Science, 2001. **291**(5510): p. 1947-1949.

50. Skoog, D.A., S.R. Crouch, and F.J. Holler, *Principles of instrumental analysis*. 2007, Belmont, CA: Thomson Brooks/Cole.

51. Settle, F.A., *Handbook of instrumental techniques for analytical chemistry*. 1997, Upper Saddle River, NJ: Prentice Hall PTR.

52. Perkampus, H.-H., *UV-VIS spectroscopy and its applications*. 1992, Berlin; New York: Springer-Verlag.

53. Martin, A.E., *Difference and Derivative Spectra.* Nature, 1957. **180**(4579): p. 231-233.

54. Höhne, G., W. Hemminger, and H.J. Flammersheim, *Differential Scanning Calorimetry*. second ed. 2003: Springer.

55. Evitherm. *Calorimetric methods*. Available from: http://www.evitherm.org/Files/982/TherAna_Depository_MeasurementMethods_DiffPowerScanCalorimeter.jpg.

56. Coleman, N.J. and D.Q.M. Craig, *Modulated temperature differential scanning calorimetry: a novel approach to pharmaceutical thermal analysis.* International Journal of Pharmaceutics, 1996. **135**(1-2): p. 13-29.

57. Katz, E., et al., *Contributors*, in *Handbook of HPLC*. 1998, CRC Press. p. ix-xi.

58. Project, T.C.H. *High-Performance Liquid Chromatography (HPLC)*. 2000; Available from: http://www.files.chem.vt.edu/chem-ed/sep/lc/hplc.html.

59. Slack, G.C. and N.H. Snow, *ChemInform Abstract: HPLC Sample Preparation.* ChemInform, 2008. **39**(20): p. no-no.

60. BioImaging. *Fluorescence microscopy - a brief explanation*. 2008; Available from: http://www.scienceinyoureyes.com/uploads/pics/jablonski_eng.gif.

61. Jones, C., B. Mulloy, and A.H. Thomas, *Microscopy, optical spectroscopy, and macroscopic techniques*, ed. C. Jones, B. Mulloy, and A.H. Thomas. 1994, Totowa, N.J. :: Humana Press.

62. Burley, A., *Microscopy, optical spectroscopy and macroscopic techniques methods in molecular biology vol 22: Edited by C Jones, B Mulley and A H Thomas. pp 251. The Humana Press, Totowa, NJ. 1994. $49.50.* Biochemical Education, 1994. **22**(4): p. 219-219.

63. Spring, K.R., *Detectors for fluorescence microscopy.* Scanning Microsc, 1991. **5**(1): p. 63-9.

64. Spring, K.R. and M. Davidson, *Introduction to Fluorescence Microscopy*, in *Nikon MicroscopyU*. 2008.

65. Kobbert, C., et al., *Current concepts in neuroanatomical tracing.* Progress in Neurobiology, 2000. **62**(4): p. 327-351.

66. Panyam, J., et al., *Fluorescence and electron microscopy probes for cellular and tissue uptake of poly(d,l-lactide-co-glycolide) nanoparticles.* International Journal of Pharmaceutics, 2003. **262**(1-2): p. 1-11.

67. Rowe, R.C., P.J. Sheskey, and P.J. Weller, *Handbook of pharmaceutical excipients*. 4th ed. 2003: Pharmaceutical Press ;American Pharmaceutical Association. xxii, 776 p.

68. Rischin, D., et al., *Cremophor pharmacokinetics in patients receiving 3-, 6-, and 24-hour infusions of paclitaxel.* J Natl Cancer Inst, 1996. **88**(18): p. 1297-301.

69. Nerurkar, M.M., P.S. Burton, and R.T. Borchardt, *The Use of Surfactants to Enhance the Permeability of Peptides Through Caco-2 Cells by Inhibition of an Apically Polarized Efflux System.* Pharmaceutical Research, 1996. **13**(4): p. 528-534.

70. Miralles, M.J., J.W. McGinty, and A. Martin, *Combined water-soluble carriers for coprecipitates of tolbutamide.* J Pharm Sci, 1982. **71**(3): p. 302-4.

71. Gattefossé, *Capryol 90.* Technical literature, 2010.

72. Gattefossé. *PHARMACEUTICALS*. Available from: Labrafil® M2125CS.

73. Goodman, L.S., et al., *Goodman & Gilman's the pharmacological basis of therapeutics*. 10th ed. 2001, New York: McGraw-Hill. xxvii, 2148 p.

74. Macdonald, R.L. and M.J. McLean, *Anticonvulsant drugs: mechanisms of action.* Adv Neurol, 1986. **44**: p. 713-36.

75. Horobin, R.W., et al., *Conn's biological stains : a handbook of dyes, stains and fluorochromes for use in biology and medicine*. 10th ed. 2002, Oxford: Published for the Biological Stain Commission by BIOS. xv, 555 p.

76. Craig, D.Q.M., et al., *An investigation into the physico-chemical properties of self-emulsifying systems using low frequency dielectric spectroscopy, surface*

tension measurements and particle size analysis. International Journal of Pharmaceutics, 1993. **96**(1-3): p. 147-155.

77. El Maghraby, G.M., *Transdermal delivery of hydrocortisone from eucalyptus oil nanoemulsion: effects of cosurfactants.* Int J Pharm, 2008. **355**(1-2): p. 285-92.

78. Shakeel, F., et al., *Nanoemulsions as vehicles for transdermal delivery of aceclofenac.* AAPS PharmSciTech, 2007. **8**(4): p. 191-199.

79. http://www.devilbisshealthcare.com/images/products/pulmoneb-2.jpg.

80. Lipinski, C.A., et al., *Experimental and computational approaches to estimate solubility and permeability in drug discovery and development settings.* Adv Drug Deliv Rev, 2001. **46**(1-3): p. 3-26.

81. Pouton, C.W., *Lipid formulations for oral administration of drugs: non-emulsifying, self-emulsifying and ‘self-nanoemulsifying’ drug delivery systems.* European Journal of Pharmaceutical Sciences, 2000. **11**: p. S93-S98.

82. Sethia, S. and E. Squillante, *Solid dispersion of carbamazepine in PVP K30 by conventional solvent evaporation and supercritical methods.* Int J Pharm, 2004. **272**(1-2): p. 1-10.

83. Greiner, R.W. and D.F. Evans, *Spontaneous formation of a water-continuous emulsion from a w/o nanoemulsion*. Langmuir, 1990. **6**(12): p. 1793-1796.

84. Solans, C. and H. Kunieda, *Industrial applications of nanoemulsions*. Surfactant science series. 1997, New York: M. Dekker. ix, 404 p.

85. Malcolmson, C. and M.J. Lawrence, *A comparison of the incorporation of model steroids into non-ionic micellar and nanoemulsion systems.* Journal of Pharmacy and Pharmacology, 1993. **45**(2): p. 141-143.

86. Constantinides, P.P., *Lipid Nanoemulsions for Improving Drug Dissolution and Oral Absorption: Physical and Biopharmaceutical Aspects.* Pharmaceutical Research, 1995. **12**(11): p. 1561-1572.

87. Carrigan, P.J. and T.R. Bates, *Biopharmaceutics of drugs administered in lipid-containing dosage forms I: Gi absorption of griseofulvin from an oil-in-water emulsion in the rat.* J Pharm Sci, 1973. **62**(9): p. 1476-1479.

88. Tarr, B.D. and S.H. Yalkowsky, *Enhanced Intestinal Absorption of Cyclosporine in Rats Through the Reduction of Emulsion Droplet Size.* Pharmaceutical Research, 1989. **6**(1): p. 40-43.

89. Alleva, K., et al., *Analysis of the source of heterogeneity in the osmotic response of plant membrane vesicles.* European Biophysics Journal, 2009. **38**(2): p. 175-184.

90. Gershanik, T., et al., *Charge-dependent interaction of self-emulsifying oil formulations with Caco-2 cells monolayers: binding, effects on barrier function and cytotoxicity.* International Journal of Pharmaceutics, 2000. **211**(1-2): p. 29-36.

91. Vasconcelos, T., et al., *Solid dispersions as strategy to improve oral bioavailability of poor water soluble drugs.* Drug Discov Today, 2007. **12**(23-24): p. 1068-1075.

92. Swenson, C.E., et al., *Development and Validation of a Sterility Test Method for Large, Gentamicin-Containing Liposomes.* Journal of Liposome Research, 1992. **2**(1): p. 43-48.

93. Twentyman, P.R. and M. Luscombe, *A study of some variables in a tetrazolium dye (MTT) based assay for cell growth and chemosensitivity.* Br J Cancer, 1987. **56**(3): p. 279-285.

94. Elversson, J., et al., *Droplet and particle size relationship and shell thickness of inhalable lactose particles during spray drying.* Journal of Pharmaceutical Sciences, 2003. **92**(4): p. 900-910.

95. Adjei, A. and J. Garren, *Pulmonary Delivery of Peptide Drugs: Effect of Particle Size on Bioavailability of Leuprolide Acetate in Healthy Male Volunteers.* Pharmaceutical Research, 1990. **7**(6): p. 565-569.

96. *Merck Source (2002). Dorland's Medical Dictionary. Retrieved 2005-01-26.*

97. Williamson, D.H. and D.J. Fennell, *Chapter 16 The Use of Fluorescent DNA-Binding Agent for Detecting and Separating Yeast Mitochondrial DNA*, in *Methods Cell Biol*, M.P. David, Editor. 1975, Academic Press. p. 335-351.

98. Porter, K.G. and Y.S. Feig, *The Use of DAPI for Identifying and Counting Aquatic Microflora.* Limnology and Oceanography, 1980. **25**(5): p. 943-948.